

Ab initio Calculations of Optical Rotation

Mary C. Tam

Dissertation submitted to the Faculty of the
Virginia Polytechnic Institute and State University
in partial fulfillment of the requirements for the degree of

Doctor of Philosophy

in

Chemistry

T. Daniel Crawford, Chair

John R. Morris

James M. Tanko

Brian M. Tissue

Gordon T. Yee

April 18, 2006

Blacksburg, Virginia

Keywords: Coupled Cluster Theory, Optical Rotation

Copyright 2006, Mary C. Tam

Ab initio Calculations of Optical Rotation

Mary C. Tam

(ABSTRACT)

Coupled cluster (CC) and density functional theory (DFT) are highly regarded as robust quantum chemical methods for accurately predicting a wide variety of properties, such as molecular structures, thermochemical data, vibrational spectra, etc., but there has been little focus on the theoretical prediction of optical rotation. This property, also referred to as circular birefringence, is inherent to all chiral molecules and occurs because such samples exhibit different refractive indices for left- and right- circularly polarized light. This thesis focuses on the theoretical prediction of this chiroptic property using CC and DFT quantum chemical models. Several small chiral systems have been studied, including (*S*)-methyloxirane, (*R*)-epichlorohydrin, (*R*)-methylthiirane, and the conformationally flexible molecules, (*R*)-3-chloro-1-butene and (*R*)-2-chlorobutane. All predicted results have been compared to recently published gas-phase cavity ringdown polarimetry data. When applicable, well-converged Gibbs free energy differences among conformers were determined using complete-basis-set extrapolations of CC energies in order to obtain Boltzmann-averaged specific rotations. The overall results indicate that the theoretical rotation is highly dependent on the choice of optimized geometry and basis set (diffuse functions are shown to be extremely important), and that there is a large difference between the CC and DFT predicted values, with DFT usually predicting magnitudes that are larger than those of coupled cluster theory.

Dedication

Sir Isaac Newton once said, “If I have seen further than others, it is by standing upon the shoulders of giants”. This work is dedicated to my father, whose unconditional love, encouragement, and support have been my ‘giants’.

Acknowledgements

Above all, I thank God for His ultimate sacrifice, His saving graces, and His presense in my life. Without Him, my life would be be incomplete. This work would not have been possible without the help and guidance from my advisor, Dr. T. Daniel Crawford. His incredible scientific ability and vast amount of knowledge has been an inspiration throughout my pursuit of this degree. I would also like to thank my committee members, Dr. John R. Morris, Dr. James M. Tanko, Dr. Brian M. Tissue, and Dr. Gordon T. Yee for providing their beneficial insights concerning this research. Group members, Micah Abrams, Nicholas J. Russ, and Christopher E. Smith have enriched my work-life with their help in the laboratory, and simply with their encouragement, support, and friendship.

Through my parents, Francis and Margaret Tam, I have learned a love of God, an appreciation for life, and the desire to succeed. Their unselfless giving of love to family and friends, and their service to the community have made me realize the important aspects of life. Their involvement, even when unwelcomed, has made me a better person, and for that, I am eternally grateful. My brother, Peter, has taught me to take chances and enjoy the life that we are given, while my youngest brother, Matty, has shown me how important it is to develop your own sense of self.

I would especially like to thank two special ladies, Sheila Gradwell and Stephanie Hooper. Throughout our time at Virginia Tech, they have become my sisters. Their friendship and love are unfailing. The LifeTeen program at St. Mary's Catholic Church has been my home away from home. I am indebted to all involved, for their dedication to Christ, countless prayers, supportive moments, friendship, and the sheer joy that comes with being a part of something so wonderful.

Lastly, I would like to thank a very special person, Brent Cunningham. Through his love, encouragement, and support, he has taught me to be open to all that life has to offer. I am truly blessed to have him in my life and am counting the days until we are husband and wife. He forever has my heart. ♡

Contents

1	Introduction	1
1.1	Thesis Statement	1
1.2	Introduction and Motivation	1
1.3	The History of Optical Rotation	3
1.4	Circular Birefringence	4
1.5	The Electromagnetic Theory of Light	5
2	General Electronic Structure Theory	9
2.1	The Schrödinger Equation	9
2.2	The Born-Oppenheimer Approximation	10
2.3	Hartree-Fock Theory	11
2.4	Electron Correlation	15
2.5	Second Quantization	16

2.6	Coupled Cluster Theory	16
2.6.1	The Hausdorff Expansion	18
2.6.2	The Normal-Ordered Hamiltonian	18
2.6.3	Coupled Cluster Singles and Doubles	19
2.6.4	Higher Orders of CC Theory	21
2.7	Density Functional Theory	22
2.8	Basis Sets	26
3	Computing Chiroptic Properties	29
3.1	Introduction to Computing Optical Rotation	29
3.2	The Theory of Optical Rotation	30
3.2.1	The Electromagnetic Hamiltonian	30
3.2.2	The Time-Dependent Schrödinger Equation	32
3.2.3	Response to a Changing Magnetic Component of the Electromagnetic Field	32
3.3	Computing Optical Rotation with Coupled Cluster Theory	35
3.4	Computing Optical Rotation with Density Functional Theory	36
3.5	Origin Invariance in Optical Rotation Calculations	38
4	Coupled Cluster and Density Functional Theory Calculations of Optical Rotatory Dispersion of (<i>S</i>)-Methyloxirane	40

4.1	Introduction	41
4.2	Coupled Cluster Response Theory for Optical Rotation	44
4.3	Computational Details	46
4.4	Results and Discussion	48
4.5	Conclusions	60
5	<i>Ab Initio</i> Determination of Optical Rotatory Dispersion in the Conformationally Flexible Molecule (<i>R</i>)-Epichlorohydrin	62
5.1	Introduction	63
5.2	Computational Details	66
5.3	Results and Discussion	69
5.4	Conclusions	86
6	Coupled Cluster and Density Functional Theory Optical Rotatory Dispersion of the Conformationally Flexible Molecules (<i>R</i>)-3-chloro-1-butene and (<i>R</i>)-2-chlorobutane	88
6.1	Introduction	89
6.2	Computational Details	92
6.3	Results and Discussion	94
6.3.1	(<i>R</i>) – 3 – chloro – 1 – butene	94

6.3.2	<i>(R)</i> – 2 – chlorobutane	107
6.3.3	Comparison	116
6.4	Conclusions	117
7	Coupled Cluster and Density Functional Theory Calculations of Optical Rotation for (<i>R</i>)-Methylthiirane	118
7.1	Introduction	119
7.2	Computational Details	121
7.3	Results and Discussion	122
7.4	Conclusions	127
8	Conclusions	129
8.1	General Comments	129
8.2	<i>(S)</i> -Methyloxirane	130
8.3	<i>(R)</i> -Epichlorohydrin	130
8.4	<i>(R)</i> -3-chloro-1-butene and <i>(R)</i> -2-chlorobutane	132
8.5	<i>(R)</i> -Methylthiirane	133
8.6	Concluding Remarks	133
	Bibliography	136

List of Figures

4.1	Optimized geometries of (<i>S</i>)-methyloxirane using B3LYP and CCSD(T) methods with the 6-31G* and cc-pVTZ basis sets. Bond lengths are given in Å and bond angles in degrees.	49
4.2	Calculated optical rotary dispersion curve for (<i>S</i>)-2-methyloxirane using B3LYP and CCSD linear response methods with the Sadlej-pVTZ and aug-cc-pVDZ basis sets. .	57
5.1	Optimized geometries of the three minimum-energy conformers — <i>cis</i> , <i>gauche-I</i> , and <i>gauche-II</i> — of (<i>R</i>)-epichlorohydrin at the B3LYP/cc-pVTZ level of theory. Bond lengths are given in Å and bond angles in degrees.	70
6.1	Optimized geometries of the three minimum-energy conformers of (<i>R</i>)-3-chloro-1-butene at the B3LYP/cc-pVTZ level of theory. Bond lengths are given in Å and bond angles in degrees.	95
6.2	Optimized geometries of the three minimum-energy conformers of (<i>R</i>)-2-chlorobutane at the B3LYP/cc-pVTZ level of theory. Bond lengths are given in Å and bond angles in degrees.	108

7.1 Optimized geometry of (*R*)-methylthiirane at the B3LYP/cc-pVTZ level of theory.

Bond lengths are given in Å and bond angles in degrees. 124

List of Tables

4.1	B3LYP and CCSD specific rotation ($\text{deg dm}^{-1} (\text{g/mL})^{-1}$) for (<i>S</i>)-methyloxirane computed with various basis sets and optimized geometries at 589 nm. The center of mass is chosen to be the gauge origin.	51
4.2	B3LYP and CCSD specific rotation ($\text{deg dm}^{-1} (\text{g/mL})^{-1}$) for (<i>S</i>)-methyloxirane computed with various basis sets and optimized geometries at 355 nm. The center of mass is chosen to be the gauge origin.	52
4.3	CCSD specific rotation ($\text{deg dm}^{-1} (\text{g/mL})^{-1}$) for (<i>S</i>)-methyloxirane with the gauge origin placed at the center-of-mass (COM) or at the coordinates of the oxygen atom (O).	54
4.4	EOM-CCSD and B3LYP-TDDFT excitation energies for the two lowest Rydberg states of (<i>S</i>)-methyloxirane computed with various basis sets and optimized geometries.	59
5.1	Specific rotations (in $\text{deg}/[\text{dm} (\text{g/cm}^3)]$) of (<i>R</i>)-epichlorohydrin conformers at 355 nm. Computed at the B3LYP/cc-pVTZ optimized geometry.	72

5.2	Specific rotations (in deg/[dm (g/cm ³)] of (<i>R</i>)-epichlorohydrin conformers at 589 nm. Computed at the B3LYP/cc-pVTZ optimized geometry.	73
5.3	Specific rotations (in deg/[dm (g/cm ³)] of (<i>R</i>)-epichlorohydrin conformers at 633 nm. Computed at the B3LYP/cc-pVTZ optimized geometry.	74
5.4	EOM-CCSD and B3LYP-TDDFT excitation energies for (<i>R</i>)-epichlorohydrin computed with various basis sets at the B3LYP/cc-pVTZ optimized geometry.	76
5.5	Gas-phase conformer populations of (<i>R</i>)-epichlorohydrin.	79
5.6	Liquid-phase conformer populations for (<i>R</i>)-epichlorohydrin.	79
5.7	Specific rotations (in deg/[dm (g/cm ³)] for (<i>R</i>)-epichlorohydrin at 355 nm in gas- and liquid-phase environments. Computed at the B3LYP/cc-pVTZ optimized geometry.	82
5.8	Specific rotations (in deg/[dm (g/cm ³)] for (<i>R</i>)-epichlorohydrin at 589 nm in gas- and liquid-phase environments. Computed at the B3LYP/cc-pVTZ optimized geometry.	83
5.9	Specific rotations (in deg/[dm (g/cm ³)] for (<i>R</i>)-epichlorohydrin at 633 nm in gas- and liquid-phase environments. Computed at the B3LYP/cc-pVTZ optimized geometry.	84
6.1	Specific Rotations (in deg/[dm (g/cm ³)] of the individual conformers of (<i>R</i>)-3-chloro-1-butene at 355 nm. Computed at the B3LYP/cc-pVTZ optimized geometry.	97

6.2	Specific Rotations (in deg/[dm (g/cm ³)]) of the individual conformers of (<i>R</i>)-3-chloro-1-butene at 589 nm. Computed at the B3LYP/cc-pVTZ optimized geometry.	98
6.3	Specific Rotations (in deg/[dm (g/cm ³)]) of the individual conformers of (<i>R</i>)-3-chloro-1-butene at 633 nm. Computed at the B3LYP/cc-pVTZ optimized geometry.	99
6.4	Gas-Phase Conformer Populations	100
6.5	Specific Rotations (in deg/[dm (g/cm ³)]) for (<i>R</i>)-3-chloro-1-butene at 355 nm. Computed at the B3LYP/cc-pVTZ optimized geometry.	102
6.6	Specific Rotations (in deg/[dm (g/cm ³)]) for (<i>R</i>)-3-chloro-1-butene at 589 nm. Computed at the B3LYP/cc-pVTZ optimized geometry.	103
6.7	Specific Rotations (in deg/[dm (g/cm ³)]) for (<i>R</i>)-3-chloro-1-butene at 633 nm. Computed at the B3LYP/cc-pVTZ optimized geometry.	104
6.8	EOM-CCSD and B3LYP-TDDFT Excitation Energies Computed with Various Basis Sets at the B3LYP/cc-pVTZ Optimized Geometry.	106
6.9	Specific Rotations (in deg/[dm (g/cm ³)]) of the individual conformers of (<i>R</i>)-2-chlorobutane at 355 nm. Computed at the B3LYP/cc-pVTZ optimized geometry. . .	109
6.10	Specific Rotations (in deg/[dm (g/cm ³)]) of the individual conformers of (<i>R</i>)-2-chlorobutane at 589 nm. Computed at the B3LYP/cc-pVTZ optimized geometry. . .	110
6.11	Specific Rotations (in deg/[dm (g/cm ³)]) of the individual conformers of (<i>R</i>)-2-chlorobutane at 633 nm. Computed at the B3LYP/cc-pVTZ optimized geometry. . .	111

6.12	Specific Rotations (in deg/[dm (g/cm ³)]) for (<i>R</i>)-2-chlorobutane at 355 nm. Computed at the B3LYP/cc-pVTZ optimized geometry.	113
6.13	Specific Rotations (in deg/[dm (g/cm ³)]) for (<i>R</i>)-2-chlorobutane at 589 nm. Computed at the B3LYP/cc-pVTZ optimized geometry.	114
6.14	Specific Rotations (in deg/[dm (g/cm ³)]) for (<i>R</i>)-2-chlorobutane at 633 nm. Computed at the B3LYP/cc-pVTZ optimized geometry.	115
7.1	Specific Rotations (in deg/[dm (g/cm ³)]) for (<i>R</i>)-Methylthiirane at 355, 589, and 633 nm.	126
7.2	EOM-CCSD and B3LYP-TDDFT excitation energies for (<i>R</i>)-methylthiirane computed with various basis sets at the B3LYP/cc-pVTZ optimized geometry.	128

Chapter 1

Introduction

1.1 Thesis Statement

The purpose of the research described in this manuscript is to develop a deeper understanding of how the chiroptical property of optical rotation is computed using computational methods, specifically within coupled cluster theory. The methods described within have been applied to several small chiral systems to assess the quality of the theoretically computed optical rotation.

1.2 Introduction and Motivation

A molecule is chiral only if it has a non-superimposable mirror image. This means that the molecule and its mirror image are not identical, making up an enantiomeric pair. Each set of enantiomers has identical physical properties, such as boiling point, melting point, and density, but the way in

which they interact with other chiral molecules, e. g. active sites for enzymes in biological systems, can be totally different. For example, the left-handed enantiomer of the chiral molecule carvone smells like spearmint, while its right-handed counterpart smells like caraway.¹ (*R*)-limonene is found in orange peels, while the (*S*) enantiomer is present in lemons.² Often, one enantiomer produces a characteristic effect, while the other either produces no effect at all, or has a totally different effect. An example of this is ibuprofen, where the therapeutic effect is due to only one of its enantiomers, the (*S*) isomer.³ Although this drug is administered in a racemic mixture, some of the (*R*) enantiomer can be metabolically converted to its mirror image, increasing the therapeutic effect of the racemate.

Understanding and predicting the molecular properties of chiral molecules is a primary goal of organic chemistry. One of the focuses has been on the synthesis of these types of molecules, along with the ability to predict and control their properties. Chiral molecules are predominantly found in the pharmaceutical chemistry, where it is sometimes necessary to control the absolute configuration of the molecule. Experimentally, reliable determination of the absolute configuration of a chiral molecule is usually done by X-ray crystallography which can be very expensive and time consuming, and is not guaranteed to be successful.

The goal of this research is not to determine the absolute configuration of a chiral molecule through theoretical techniques, but to lay one small part of the foundation for doing so. Knowing the optical rotation can aid in the task of absolute configuration determination, and experimentally determining this property has become routine chemical technique. However, theoretical calculation of optical rotation has proved to be more challenging. It is the hope that the correct calculation of the optical rotation, along with the knowledge of other chiroptical properties and experimental

data, will lead to a more feasible route in determining the absolute configuration.

1.3 The History of Optical Rotation

The effect of optical activity was discovered in the early 1800s and has since been recognized as a useful tool in studying molecular structure. The first experiments relating to this phenomena were performed by Arago, who observed optical activity in quartz crystals in 1811.⁴ A year later, the French scientist, Biot passed polarized light through various concentrations of sucrose solutions and noted that the degree of rotation of light was directly related to the concentration of the solution, and inversely proportional to the square of the wavelength of light.⁵ Through his studies regarding the nature of light waves, Fresnel, discovered in 1825 that the superposition of left- and right-circularly polarized light with equal amplitudes and wavelength, resulted in linearly polarized light. Following this discovery, he related the optical activity of a chiral medium to a difference in velocities of the left- and right- components of the plane polarized light, causing a rotation of the plane of polarization.⁵

In 1847, Pasteur, a student of Biot's manually separated a sample of tartaric acid crystals, and recognized that separate solutions, with equal concentrations, rotated light in equal but opposite directions. Pasteur was also the first to suggest that a pair of enantiomers are mirror images of each other, and that a racemic mixture is optically inactive.⁴ van't Hoff and LeBel (1874) worked independently of each other, but both suggested that optical activity was due to an asymmetric arrangement of atoms in a molecule, and proposed the tetrahedral shape of some chiral molecules.⁶ Fisher's ability to identify many of the stereoisomers of the aldohexoses led to his development of the

Fischer projections, a cross figure representation used to distinguish the three dimensional structure of chiral molecules.⁴ And in 1966, Cahn, Ingold, and Prelog worked together to develop the (*R*) and (*S*) stereochemical distinctions used to identify mirror image configurations for molecules with stereogenic centers.⁴

Although the developmental understanding of optical activity has lasted over two hundred years, there is still a yearning to learn the elementary connection between optical rotation and molecular structure.

1.4 Circular Birefringence

Optical rotation, the rotation of plane-polarized light by chiral species, occurs because such samples exhibit differing refractive indices for left- and right-circularly polarized light.^{5,6} This phenomena is referred to as circular birefringence and is dependent on the propagation of plane polarized light through a chiral medium. Mathematically, the electric field vector for left- and right- circularly polarized light of frequency ω passing through a medium with refractive index η along the propagation direction (z) can be expressed by the following equations

$$\mathbf{E}_L = \varepsilon(\hat{\mathbf{i}} \cos \phi_L + \hat{\mathbf{j}} \sin \phi_L) \quad (1.1)$$

$$\mathbf{E}_R = \varepsilon(\hat{\mathbf{i}} \cos \phi_R - \hat{\mathbf{j}} \sin \phi_R) \quad (1.2)$$

where

$$\phi_L = \omega\left(t - \frac{\eta_L z}{c}\right) \quad (1.3)$$

$$\phi_R = \omega\left(t - \frac{\eta_R z}{c}\right). \quad (1.4)$$

When the medium interacting with the light wave does not exhibit circular birefringence, the refractive indices are identical for the left- and right-components, and the superposition of the left- and right- circularly polarized waves results in the electric vector,

$$\mathbf{E} = \mathbf{E}_L + \mathbf{E}_R = 2\epsilon\hat{\mathbf{i}} \cos \phi \quad (1.5)$$

giving a linear plane of polarized light, which oscillates in the plane along the unit vector $\hat{\mathbf{i}}$.

Because a chiral medium has different refractive indices for the left- and right- circular components of plane polarized light, one of the components will propagate faster than the other, causing a difference in their phases. When this happens, the superposition of the left- and right- circularly polarized waves is given by the following electric field vector

$$\mathbf{E} = \mathbf{E}_L + \mathbf{E}_R = 2\epsilon\left\{\hat{\mathbf{i}} \cos\left(\frac{z\omega\Delta\eta}{2c}\right) - \hat{\mathbf{j}} \sin\left(\frac{z\omega\Delta\eta}{2c}\right)\right\} \cos \phi \quad (1.6)$$

where $\Delta\eta$ is the difference between the left- and right- refractive indices and the plane polarized light has been rotated by a specific angle, $\Delta\theta$,

$$\Delta\theta = \frac{z\omega\Delta\eta}{2c}. \quad (1.7)$$

1.5 The Electromagnetic Theory of Light

The properties of an electromagnetic field are described by Maxwell's equations:⁷

$$\nabla \cdot \mathbf{D} = \rho \quad (1.8)$$

$$\nabla \cdot \mathbf{B} = 0 \quad (1.9)$$

$$\nabla \times \mathbf{E} = -\frac{\partial \mathbf{B}}{\partial t} \quad (1.10)$$

$$\nabla \times \mathbf{H} = \mathbf{J} + \frac{\partial \mathbf{D}}{\partial t} \quad (1.11)$$

where \mathbf{D} , ρ , \mathbf{H} , and \mathbf{J} represent the electric displacement, charge density, magnetic field strength, and current density, respectively.

When a chiral molecule is placed in an electromagnetic field, in the case of optical activity, there is a change in the spatial variation of the medium, causing a difference in polarizabilities of the electric field vectors, and in turn, different refractive indices for the left- and right- components of plane polarized light.⁵ From Maxwell's equation, Equation 1.10, where \mathbf{E} and \mathbf{B} represent the electric and magnetic field, respectively, the electric field is dependent on the time variation in the magnetic field. The spatial variation of the medium creates an induced electric dipole, or an electric polarization, \mathbf{P} , which is directly proportional to the change in the magnetic field with respect to time. When the spatial variation of the medium is considered, the total electric polarization is given by

$$\mathbf{P} = N\alpha\mathbf{E} - N\beta\frac{\partial\mathbf{B}}{\partial t} \quad (1.12)$$

where N is equal to the number density of molecules in the medium, α represents the polarizability, and β is a molecular characteristic unique to the medium.⁸ In an optically active medium, the relationship between the electric displacement, \mathbf{D} , and the polarization is expressed by:

$$\mathbf{D} = \epsilon_0\mathbf{E} + \mathbf{P} \quad (1.13)$$

and the magnetic flux density, \mathbf{B} is directly related to the magnetic field strength \mathbf{H} :

$$\mathbf{B} = \mu_0\mathbf{H} \quad (1.14)$$

where ϵ_0 is the permittivity and μ_0 is the permeability of free space.

These equations, along with Equation 1.12, can be used to derive a more compact expression for the difference in refractive indices for the left- and right- circular components of plane polarized light. Taking the curl of both sides of Equation 1.14, employing Maxwell's equation (Equation 1.11), and substituting the basic expression for the electric displacement (Equation 1.13), leads to

$$\nabla \times \mathbf{B} = \epsilon_0 \mu_0 \frac{\partial \mathbf{E}}{\partial t} + \mu_0 \alpha N \frac{\partial \mathbf{E}}{\partial t} - \mu_0 \beta N \frac{\partial^2 \mathbf{B}}{\partial t^2} \quad (1.15)$$

After taking the curl of both sides again, and using Maxwell's equations (Equation 1.10)

$$\nabla^2 \mathbf{B} = \epsilon_0 \mu_0 \left[1 + \frac{\alpha N}{\epsilon_0} \right] \frac{\partial^2 \mathbf{B}}{\partial t^2} + \mu_0 \beta N \left[\nabla \times \frac{\partial^2 \mathbf{B}}{\partial t^2} \right] \quad (1.16)$$

In an electromagnetic field, the magnetic component consists of left- and right- components which depend on the electric field:⁸

$$\mathbf{B}_L = \frac{\epsilon k_L}{\omega} \left[\hat{\mathbf{j}} \cos \phi_L - \hat{\mathbf{i}} \sin \phi_L \right] \quad (1.17)$$

$$\mathbf{B}_R = \frac{\epsilon k_R}{\omega} \left[\hat{\mathbf{j}} \cos \phi_R - \hat{\mathbf{i}} \sin \phi_R \right] \quad (1.18)$$

where k is the wave vector, related to difference in refractive indices for left- and right- circular components of the plane polarized light in a chiral medium,

$$\Delta k = \frac{\omega \eta_L}{c} - \frac{\omega \eta_R}{c} = \frac{\omega \Delta \eta}{c} \quad (1.19)$$

Using the previous form of \mathbf{B} , it can be shown that

$$\nabla^2 \mathbf{B}_{LR} = -\Delta k^2 \mathbf{B}_{LR} \quad (1.20)$$

$$\frac{\partial^2 \mathbf{B}_{LR}}{\partial t^2} = -\omega^2 \mathbf{B}_{LR} \quad (1.21)$$

and substituting these expressions into Equation 1.16, results in the final equation for $\Delta \eta$,⁸

$$\Delta \eta = 1 + \frac{\alpha N}{2\epsilon_0} \pm \frac{\omega \beta N}{2c\epsilon_0} = \frac{\omega \beta N}{c\epsilon_0}. \quad (1.22)$$

Inserting this equation in Equation 1.7 gives a new expression for $\Delta\theta$, the angle of rotation of plane polarized light through a chiral medium,

$$\Delta\theta = \frac{\omega^2\beta N}{2c^2\epsilon_0}. \quad (1.23)$$

It is this final relationship, in conjunction with quantum chemical techniques, that will be used to determine the optical rotation of chiral molecules.

Chapter 2

General Electronic Structure Theory

This chapter discusses the background and theory of the Hartree-Fock method, the most basic approximate method used to solve the Schrödinger equation. Advanced quantum chemical techniques, which aim to correct for the deficiencies of Hartree-Fock theory by taking into account electron correlation, are also described.

2.1 The Schrödinger Equation

In 1926, Erwin Schrödinger introduced the most fundamental equation in quantum mechanics:

$$H\Psi = E\Psi. \tag{2.1}$$

H is the Hamiltonian operator, Ψ is the wave function, whose square is a probability amplitude, and E is the energy. By finding a solution for the energy and wave functions (eigenvalues and eigenvectors of the Hamiltonian operator), it is possible to determine theoretically important molecular

properties, including optimized geometries, electric and magnetic dipole moments, harmonic vibrational frequencies, magnetizabilites, etc. For many-electron systems, the Hamiltonian includes terms that cause the Schrödinger equation to be completely inseparable for anything other than a hydrogen atom; therefore, it is impossible to find an exact solution. The main focus of this chapter is to describe Hartree-Fock theory the most basic route to determine approximate solutions to the Schrödinger equation, and also advanced computational methods which aim to correctly describe the electron correlation.

2.2 The Born-Oppenheimer Approximation

When considering a system that is composed of electrons and nuclei, the Hamiltonian (in atomic units) can be represented by:

$$\hat{H} = -\sum_i^N \frac{1}{2} \nabla_i^2 - \sum_A^M \frac{1}{2M_A} \nabla_A^2 - \sum_i^N \sum_A^M \frac{Z_A}{r_{iA}} + \sum_i^N \sum_{i<j}^N \frac{1}{r_{ij}} + \sum_A^M \sum_{A<B}^M \frac{Z_A Z_B}{R_{AB}} \quad (2.2)$$

These terms include the kinetic energy of the electrons, the kinetic energy of the nuclei, the attraction between the electrons and the nuclei, the electron-electron repulsion and the nuclear-nuclear repulsion, respectively. In 1927, Born and Oppenheimer, argued that the nuclei in the system move much slower than the electrons because they are more massive.⁹ From this, they assumed that the nuclei in the system are fixed, allowing the kinetic energy of the nuclei to be disregarded and the nuclear-nuclear repulsion term to be constant, and therefore added at a later time.⁹ After applying the Born-Oppenheimer approximation, the resulting Hamiltonian is referred to as the electronic Hamiltonian.¹⁰

$$\hat{H}_{elec} = \sum_i^N h_i(i) + \sum_i^N \sum_{i<j}^N \frac{1}{r_{ij}} = -\sum_i^N \frac{1}{2} \nabla_i^2 - \sum_i^N \sum_A^M \frac{Z_A}{r_{iA}} + \sum_i^N \sum_{i<j}^N \frac{1}{r_{ij}} \quad (2.3)$$

It is necessary to note that the total energy of the system must include the nuclear-nuclear repulsion.

$$\varepsilon_{tot} = \varepsilon_{elec} + \sum_A^M \sum_{A < B}^M \frac{Z_A Z_B}{R_{AB}} \quad (2.4)$$

Hereafter, only the electronic Hamiltonian and the resulting electronic wave functions will be considered.

2.3 Hartree-Fock Theory

In 1928, Hartree introduced his method for finding solutions to the Schrödinger equation.¹¹ Fock modified Hartree's method in 1930 by allowing the wave function to be represented by a Slater determinant.¹² This approach is commonly known as the Hartree-Fock (HF) method. The wave function, Ψ , has restrictions such that it is well-behaved and that it is antisymmetric with respect to the interchange of both spin and space coordinates of any two electrons. In the Slater determinant, exchanging the coordinates of two electrons is the same as exchanging two rows, with a resulting change in sign. Because of this property of a Slater determinant, the basic antisymmetric property of the wave function can be retained.

A Slater determinant for an N-electron system has the form¹³

$$|\Psi(x_1, x_2, \dots, x_N)\rangle = \left(\frac{1}{N!}\right)^{\frac{1}{2}} \begin{vmatrix} \chi_i(x_1) & \chi_j(x_1) & \dots & \chi_N(x_1) \\ \chi_i(x_2) & \chi_j(x_2) & \dots & \chi_N(x_2) \\ \vdots & \vdots & \ddots & \vdots \\ \chi_i(x_N) & \chi_j(x_N) & \dots & \chi_N(x_N) \end{vmatrix} \quad (2.5)$$

The χ_i represent the spin orbitals (both spin and spatial distribution), the x_N represent the coordinates of the electrons and the factor of $\left(\frac{1}{N!}\right)^{\frac{1}{2}}$ is included for normalization. The columns of

the Slater determinant refer to the spin orbitals while the rows refer to the electrons. A shortened version of writing the Slater determinant is with the normalization factor implied and only showing the diagonal elements of the determinant.

$$|\Psi(x_1, x_2, \dots, x_N)\rangle = \begin{vmatrix} \chi_i(x_1) & \chi_j(x_2) & \dots & \chi_N(x_N) \end{vmatrix} \quad (2.6)$$

The ground state Hartree-Fock energy is given by the energy expectation value,

$$E_{HF} = \langle \Psi_o | \hat{H} | \Psi_o \rangle \quad (2.7)$$

where Ψ_o is the ground state wave function and \hat{H} is the electronic Hamiltonian, which can be separated into its one-electron part, $h(i)$, and its two-electron part, r_{ij}^{-1} . The energy expression can be simplified using Slater's rules,¹³ an easy way to evaluate matrix elements between two Slater determinants. These rules are dependent on the operators between the two determinants, i.e. the one-electron part of the Hamiltonian or the two-electron part. Since the energy expression is dependent on two identical determinants for both the one-electron part and the two-electron part of the Hamiltonian, the energy expression for the ground state Hartree-Fock approximation is evaluated to be

$$E_{HF} = \sum_i^N \langle i|h|j \rangle + \frac{1}{2} \sum_i^N \sum_j^N \langle ij||ij \rangle \quad (2.8)$$

where i and j represent occupied spin orbitals.

Using Lagrange's method of undetermined multipliers, the energy can be minimized with respect to a linear variation of the spin orbitals while ensuring that the spin orbitals stay orthonormal, to find that the Hartree-Fock equations become an eigenvalue equation with the form:

$$\left[h(x_1) + \sum_{j \neq i} (\hat{J}_j(x_1) - \hat{K}_j(x_1)) \right] \chi_i(x_1) = \varepsilon_i \chi_i(x_1) \quad (2.9)$$

where \hat{J} is the coulomb operator which represents an average local potential at the position x_1 resulting from the electron contained in χ_i and \hat{K} is the exchange operator that involves the exchange of electron 1 and electron 2. The coulomb and exchange operators have the following form:

$$\hat{J}_j(x_1)\chi_i(x_1) = \left[\int dx_2 \chi_j^*(x_2) \frac{1}{r_{12}} \chi_j(x_2) \right] \chi_i(x_1) \quad (2.10)$$

$$\hat{K}_j(x_1)\chi_i(x_1) = \left[\int dx_2 \chi_j^*(x_2) \frac{1}{r_{12}} \chi_i(x_2) \right] \chi_j(x_1) \quad (2.11)$$

The result of applying Lagrange's method is the left hand side of Equation 2.9, the Fock operator. ε represents the orbital energies, the eigenvalues of the Fock operator.

The Hartree-Fock equations were usually solved numerically (only for atoms and simple diatomics) when this approximation was first developed. In 1951, Roothaan's paper entitled *New Developments in Molecular Orbital Theory*,¹⁴ suggested a method to solve these equations for general molecular systems using matrix techniques. He introduced the linear combinations of atomic orbitals to molecular orbitals (LCAO-MO) approximation. In Roothaan's procedure, the molecular orbitals have the form:

$$\psi_i = \sum_{\mu}^K C_{\mu i} \phi_{\mu} \quad (2.12)$$

where $i = 1, 2, 3 \dots K$. $C_{\mu i}$ is the matrix of the atomic orbital coefficients and ϕ_{μ} are the atomic orbitals. The atomic orbitals are given by the rows, and the columns of the matrix give the molecular orbitals. The final result is a set of matrix equations known as the Roothaan's equations:¹⁴

$$\mathbf{FC} = \mathbf{SC}\varepsilon \quad (2.13)$$

F is the Fock matrix, C is the expansion coefficient matrix, S is the overlap matrix, and ε is the diagonal matrix of the orbital energies. The overlap matrix consists of overlap integrals with the

form:

$$S_{\mu\nu} = \int dr_1 \phi_{\mu}^*(x_1) \phi_{\nu}(x_1) \quad (2.14)$$

They are a result of the fact that the basis functions are not orthogonal to each other and therefore the overlap integrals have values between zero and one. The Roothaan equations are nonlinear and therefore, must be solved iteratively until self-consistency is reached.

When implementing the Hartree-Fock theory approximation, the computational expense of the method is on the order of N^4 , where N is the number of basis functions.¹⁵ Spin may be included in Hartree-Fock theory by two common approaches: spin-restricted, which has closed-(RHF) and open-shell (ROHF) variants, and spin-unrestricted (UHF). Restricted Hartree-Fock theory assumes that each pair (α β) of spin orbitals has the same spatial orbitals associated with it. Unrestricted Hartree-Fock (UHF) allows the spatial part of the spin orbitals to be different for the α spin type and β spin type. The ROHF (restricted open-shell Hartree-Fock) wave function is an eigenfunction of the \hat{S}^2 and \hat{S}_z operator while UHF, on the other hand, is not an eigenfunction of \hat{S}^2 but is an eigenfunction of the \hat{S}_z operator.

At large internuclear separation, RHF does not correctly describe the fact that a molecule should dissociate, while UHF gives a more accurate description. Bartlett and Stanton mention that RHF is inadequate in this situation because “RHF uses equal orbitals for different spin at all internuclear separations, which does not allow the orbitals to localize on the individual atoms”.¹⁶ Cory and Zerner, in their 1999 paper,¹⁷ describe that the energy obtained from a UHF method is usually lower than the ROHF method because UHF allows for “greater variational freedom” than ROHF because of its different α and β spatial orbitals. Although UHF generally predicts the energy better, UHF sometimes has problems when predicting molecular properties. This is seen

by considering the bond length of Cr_2 . ROHF predicts the correct bond length, 1.64 Å, while UHF predicts the bond length to be 3.25 Å, which is considerably larger than the experimentally inferred value.¹⁷

2.4 Electron Correlation

In Hartree-Fock (HF) theory, the instantaneous coulombic interactions between the individual electrons is neglected because the model considers an average field produced by the electrons as a whole. This method disregards the fact that the motion of a single electron affects the motion of all other electrons in the systems. Therefore we say that Hartree-Fock theory lacks electron correlation, or the difference between the ‘real’ (total) energy of the system and the HF limit.

$$E_{CORR} = E_{total} - E_{HF} \quad (2.15)$$

Slater suggested that, in the Hartree-Fock approximation, the only electron correlation comes from the antisymmetric property of the wave function.¹⁸ \hat{J} , the coulomb operator accounts for the repulsion between two electrons, while the exchange operator, \hat{K} , only allows for correlation between electrons of parallel spin (exchange correlation); the motions of electrons with opposite spin are left uncorrelated.

Although Hartree-Fock theory can obtain approximately 95-98% of the total electronic energy, the remaining energy, E_{CORR} , is very important when predicting the properties of a molecule within chemical accuracy. Even though this method lacks electron correlation, one of its main benefits is its relative ease in providing a reference wave function for more advanced quantum chemical techniques.

2.5 Second Quantization

Second quantization, also known as occupation-number formalism, is an algebraic method that can be used as an alternative to Slater determinants that still keeps up with the antisymmetric nature of the wave function.¹³ Creation operators are defined by the fact that they can add orbitals to the determinant,

$$a_p^\dagger |\phi_q \dots \phi_s\rangle = |\phi_p \phi_q \dots \phi_s\rangle \quad (2.16)$$

Annihilation operators, the adjoint of the creation operators, remove orbitals when acting to the right

$$a_p |\phi_p \phi_q \dots \phi_s\rangle = |\phi_q \dots \phi_s\rangle \quad (2.17)$$

A series of creation and annihilation operators can be used to add or delete orbitals and electrons, in essence, to write Slater determinants. Pairs of creation and annihilation operators anticommute with each other and the combined creation and annihilation product give the Kronecker delta function. These relationships are useful when normal-ordering an operator. A more detailed explanation of second quantization can be found in Harris, Monkhorst and Freeman.¹⁹

2.6 Coupled Cluster Theory

Coupled cluster theory is one of the most reliable and popular computational methods to approximate the solutions to the Schrödinger equation in quantum chemistry. Developed in the 1960s by Čížek and Paldus,^{20,21} coupled cluster theory aims at correcting the problem of Hartree-Fock theory—the lack of electron correlation, by expanding the wave function as a series of cluster operators.

Cluster operators are used to represent the electronic correlation. A cluster operator involving n number of orbitals is defined by

$$\hat{T}_n = \left[\frac{1}{n!} \right]^2 \sum_{ij\dots ab\dots}^n t_{ij\dots}^{ab\dots} a^\dagger b^\dagger \dots ji \dots \quad (2.18)$$

The general wave function for formal coupled cluster theory, used to approximate the exact solution, is expressed as the series exponential of \hat{T} ,²²

$$\Psi_{CC} = e^{\hat{T}} \psi_o, \quad (2.19)$$

where ψ_o is the ground state wave function. Applying this wave function to the Schrödinger equation and multiplying on the left by the reference wave function, the coupled cluster energy can be obtained,

$$E_{CC} = \langle \psi_o | \hat{H} e^{\hat{T}} | \psi_o \rangle, \quad (2.20)$$

where \hat{T} is the cluster operator. The Hamiltonian in this energy expression is the basic electronic Hamiltonian expressed in second quantization form which is derived in Corson's 1946 paper²³

$$\hat{H} = \sum_{pq} = \langle p | \hat{h} | q \rangle p^\dagger q + \frac{1}{4} \sum_{pqrs} \langle pq || rs \rangle p^\dagger q^\dagger sr. \quad (2.21)$$

Expanding the exponential and distributing terms, the energy gives:

$$E_{CC} = \langle \psi_o | \hat{H} | \psi_o \rangle + \langle \psi_o | \hat{H} \hat{T} | \psi_o \rangle + \left\langle \psi_o | \hat{H} \frac{\hat{T}^2}{2!} | \psi_o \right\rangle + \left\langle \psi_o | \hat{H} \frac{\hat{T}^3}{3!} | \psi_o \right\rangle + \dots \quad (2.22)$$

From this expression, one can see that the coupled cluster energy is naturally truncated after the third term, a direct result of Slater's rules,¹³ and the fact that the Hamiltonian contains at most two-electron operators. Therefore, the higher terms in the energy equation include determinants that differ by more than two orbitals and have a zero result. The coupled cluster energy is thus:

$$E_{CC} = \langle \psi_o | \hat{H} | \psi_o \rangle + \langle \psi_o | \hat{H} \hat{T} | \psi_o \rangle + \left\langle \psi_o | \hat{H} \frac{\hat{T}^2}{2!} | \psi_o \right\rangle \quad (2.23)$$

no matter what the excitation level of \hat{T} is chosen to be.

2.6.1 The Hausdorff Expansion

In order to find a suitable programmable expression for the coupled cluster energy, the Hausdorff expansion may be used. This expansion multiplies the Schrödinger equation on the left by the reference wave function and the inverse of the exponential to give the energy expression of

$$E_{CC} = \langle \phi_o | e^{-\hat{T}} \hat{H} e^{\hat{T}} | \phi_o \rangle \quad (2.24)$$

Using the Campbell-Baker Hausdorff formula, $e^{-\hat{T}} \hat{H} e^{\hat{T}}$, also known as the similarity-transformed Hamiltonian, \bar{H} , can be expanded as

$$e^{-\hat{T}} \hat{H} e^{\hat{T}} = \hat{H} + [\hat{H}, \hat{T}] + \frac{1}{2!} [[\hat{H}, \hat{T}], \hat{T}] + \frac{1}{3!} [[[[\hat{H}, \hat{T}], \hat{T}], \hat{T}]] + \frac{1}{4!} [[[[[[\hat{H}, \hat{T}], \hat{T}], \hat{T}], \hat{T}], \hat{T}]] + \dots \quad (2.25)$$

Crawford and Schaefer explain that because the cluster operators commute with each other, and not the Hamiltonian, and the fact that the Hamiltonian is at most a two-electron operator with at most a total of four second quantization operators, this expansion will naturally truncate itself after the first five terms.²²

2.6.2 The Normal-Ordered Hamiltonian

Normal ordered second quantization operators can be used to evaluate each matrix element. This technique requires that all annihilation operators be placed to the right of all creation operators, relative to the Hartree-Fock determinant. Normal ordering of any operator is built so that its reference expectation value is zero. The anticommutation relations between the creation and annihilation operators can be applied to any operator to make it normal ordered. After each matrix element is normal-ordered, Wick's Theorem can be used. Wick's theorem allows for any string

of annihilation and creation operators to be written as the normal-ordered string plus all of the possible pairwise contractions.²⁴

After applying Wick's theorem to the similarity transformed Hamiltonian, the expression for the second quantized normally ordered electronic Hamiltonian²² is

$$\hat{H} = \sum_{pq} h_{pq} \{p^\dagger q\} + \sum_i h_{ii} + \frac{1}{4} \sum_{pqrs} \langle pq || rs \rangle \{p^\dagger q^\dagger sr\} + \sum_{ipq} \langle pi || qi \rangle \{p^\dagger q\} + \frac{1}{2} \sum_{ij} \langle ij || ij \rangle \quad (2.26)$$

This equation shows that the total electronic Hamiltonian for coupled cluster theory contains the Hartree-Fock energy (Equation 2.8). Therefore, the electronic Hamiltonian can be rewritten as the sum of the E_{SCF} and the normal ordered Hamiltonian, H_N :

$$\hat{H} = E_{SCF} + \sum_{pq} f_{pq} \{p^\dagger q\} + \frac{1}{4} \sum_{pqrs} p q r s \langle pq || rs \rangle \{p^\dagger q^\dagger sr\} \quad (2.27)$$

The non-correlated energy, E_{SCF} , has now been separated from the correlated part, H_N . This provides a way to find the coupled cluster correlation energy separately, and the Hartree-Fock energy can be added on later to compute the total energy of the system.

2.6.3 Coupled Cluster Singles and Doubles

The energy and amplitude equations for the formal coupled cluster single and doubles (CCSD) method are:

$$E_{CC} = \langle \psi_o | e^{-\hat{T}} \hat{H} e^{\hat{T}} | \psi_o \rangle \quad (2.28)$$

$$\langle \psi_i^a | e^{-\hat{T}} \hat{H} e^{\hat{T}} | \psi_o \rangle = E \langle \psi_i^a | e^{-\hat{T}} e^{\hat{T}} | \psi_o \rangle = 0 \quad (2.29)$$

$$\langle \psi_{ij}^{ab} | e^{-\hat{T}} \hat{H} e^{\hat{T}} | \psi_o \rangle = E \langle \psi_{ij}^{ab} | e^{-\hat{T}} e^{\hat{T}} | \psi_o \rangle = 0 \quad (2.30)$$

Using the CCSD case where the cluster operator is defined as $\hat{T} = \hat{T}_1 + \hat{T}_2$, the coupled cluster wave function becomes:

$$\Psi_{CC} = \{1 + \hat{T}_1 + \frac{1}{2!}\hat{T}_1^2 + \frac{1}{3!}\hat{T}_1^3 + \hat{T}_2 + \frac{1}{2!}\hat{T}_2^2 + \frac{1}{4!}\hat{T}_1^4 + \hat{T}_2\hat{T}_1 + \frac{1}{2!}\hat{T}_2\hat{T}_1^2\}\psi_o \quad (2.31)$$

where the definitions for the cluster operators are

$$\hat{T}_1 = \sum_{ia} t_i^a \{a^\dagger i\} \quad (2.32)$$

$$\hat{T}_2 = \frac{1}{4} \sum_{ijab} t_{ij}^{ab} \{a^\dagger b^\dagger ji\} \quad (2.33)$$

To find an expression for the CCSD energy, a generalized Wick's theorem can be applied. This new version of Wick's theorem gives only a non-zero result for the terms in the energy expression that have at least one contraction between the Hamiltonian operator and the cluster operator. This is the idea of a "connected cluster". Crawford and Schaefer derive the CCSD energy by using the fact that "the Hamiltonian must share at least one index with every cluster operator".²² The Hamiltonian only has the possibility of having no more than a total of four annihilation or creation operators, which can only connect to a total of at most four cluster operators at one time. After much tedious mathematics, the CCSD correlation energy is

$$E_{CCSD} = \langle \psi_o | \bar{H} | \psi_o \rangle = \sum_{ia} f_{ia} t_i^a + \frac{1}{4} \sum_{ijab} t_{ij}^{ab} \langle ij || ab \rangle + \frac{1}{2} \sum_{ijab} ijabt_i^a t_j^b \langle ij || ab \rangle \quad (2.34)$$

This energy expression will hold true even for higher approximate methods of coupled cluster theory, such as triples (CCSDT) and quadruples (CCSDTQ). The triple and quadruple excitations cannot contribute anything directly to the energy because it is impossible for them to produce any fully contracted terms with the Hamiltonian. \hat{T}_3 and \hat{T}_4 , the higher cluster operators in CCSDT and CCSDQ, can only contribute to the energy indirectly through their effect in the amplitude equations of t_i^a and t_{ij}^{ab} .

To completely solve the energy equation, it is necessary to determine the amplitude equations. For the CCSD method, there are only two types of cluster coefficients; one for the singles, the other for the doubles. The two sets of amplitude equations can be written as reference expectation values as follows:

$$\langle \psi_i^a | \bar{H} | \psi_o \rangle = \langle \psi_o | \{i^\dagger a\} \bar{H} | \psi_o \rangle = 0 \quad (2.35)$$

$$\langle \psi_{ij}^{ab} | \bar{H} | \psi_o \rangle = \langle \psi_o | \{i^\dagger j^\dagger ba\} \bar{H} | \psi_o \rangle = 0 \quad (2.36)$$

This is done so that it is possible to have fully contracted terms between the cluster operators and the Hamiltonian. After Wick's theorem is applied, a set of programmable equations can be found for both the singles cluster operator and the doubles cluster operator. These equations can be found in a paper written by Stanton *et al.*²⁵ and many others.^{22,26} This process is quite tedious and introduces many chances for error because of the large number of possible contractions. Diagrammatic techniques have been developed to avoid the mathematical tedium of Wick's theory.^{22,27,28} Diagrams allow the energy and amplitude equations to be derived quite easily and rapidly.

2.6.4 Higher Orders of CC Theory

Even though CCSD is a computationally expensive method (N^6) it has been shown that it is necessary to use higher levels of excitation in the coupled cluster method to provide accurate approximations of molecular properties. Full higher excitations such as triples, CCSDT (N^8) and quadruples, CCSDTQ (N^{10}) are too computationally expensive (in both memory and CPU time) to use for realistic systems. In an attempt to overcome this computational obstacle, Kucharski and Bartlett showed that there is a connection between the many body perturbation theory and coupled cluster theory through the use of diagrams.²⁷ Stanton and Gauss described this connection

by showing that the coupled cluster Hamiltonian can be expanded into small perturbations by the Hausdorff expansion.²⁹ The CCSD energy contains terms that are the same as MP2 and MP3, but it does not include the triple contributions from MP4. Therefore, a perturbative triples correction can be added to the CCSD energy. Although many different types of triples corrections have been developed, the most widely used method is the CCSD(T) method. This approach, developed by Raghavachari *et al.*,³⁰ involves a non-iterative N^7 computation. Stanton explained that the CCSD(T) method approximates the triples correction by using fourth and fifth order perturbation terms.³¹

2.7 Density Functional Theory

Density Functional Theory (DFT) was first used by solid-state physicists for the prediction of properties of large-sized solid systems. In the late 1990s, density functional theory became one of the more widely used quantum chemical techniques, and with W. Kohn's developmental work within DFT, for which he won the Nobel Prize in chemistry, this method can now be used to predict the chemical properties of molecules.³²

All of the wave function-based techniques described earlier are dependent on the spin and the three spatial coordinates of every electron within the system (a total of $4N$ coordinates for a N electron system). Density functional theory, on the other hand, reduces the complexity of the wave function methods by using the electron density to compute the energy,³³ which is only dependent on the number of electrons within the system. The mathematical expression for the energy in DFT becomes a 'function' of the electron density (or probability density), and contains the same terms

that are found in the electronic Hamiltonian.

In 1964, the Hohenberg-Kohn theorem proved that by knowing the electron density, it is possible to determine the ground-state energy and molecular properties for a given molecule.³³ Although this theorem confirmed that there is direct relationship between the two, the form of the functional representing the electron density remained unclear. A year later, Kohn and Sham, expressed the ground state energy in terms of the electron density, ρ , and a set of one-electron spatial orbitals,³⁴

$$E(\rho) = -\frac{\hbar^2}{2} \sum_i^N \int \psi_{KS}^*(\mathbf{r}_1) \nabla_1^2 \psi_{KS}(\mathbf{r}_1) d\mathbf{r}_1 - \sum_A^M \int \frac{Z_A}{r_{iA}} \rho(\mathbf{r}_1) d\mathbf{r}_1 + \frac{1}{2} \int \frac{\rho(\mathbf{r}_1)\rho(\mathbf{r}_2)}{r_{12}} d\mathbf{r}_1 d\mathbf{r}_2 + E_{XC}(\rho) \quad (2.37)$$

Here the first term represents the kinetic energy, followed by the electron-nuclei attraction, and the coulombic interaction term, where the electron density is dependent on the Kohn-Sham orbitals,

$$\rho(\mathbf{r}) = \sum_i^N |\psi_{KS}(\mathbf{r})|^2 \quad (2.38)$$

When the Kohn-Sham orbitals are used to determine the total energy, the result is an eigenvalue-like set of equations called the Kohn-Sham equations which are similar to Roothaan's equations in Hartree-Fock Theory. The last term, $E_{xc}(\rho)$, in Equation 2.37 is the exchange-correlation energy that consists of the exchange interaction, or the nonclassical interaction, between the electrons. The forms of the first three terms of the previous equation are known, but it is the form of final term that is still unclear. Since the exact functional that makes up the exchange-correlation energy is unknown, approximations must be made to compute it.

The main goal of density functional theory is to design "functionals", or mathematical expressions to correctly compute the electron density.³⁵ One of the most basic ways to approach the electron density is with the local density approximation (LDA) where the exchange correlation

energy is,³⁶

$$E_{xc} = \int \rho(\mathbf{r}) \varepsilon_{xc}[\rho(\mathbf{r})] d\mathbf{r} \quad (2.39)$$

which can be further separated into different contributions for exchange and correlation interactions,

$$\varepsilon_{xc}(\rho) = \varepsilon_x(\rho) + \varepsilon_c(\rho) \quad (2.40)$$

This method is based on the assumption of a uniform gas, which is clearly not appropriate, because it is unrealistic to consider the electronic charge of a molecule equally distributed. Although this method provides a route to compute the energy of a molecule through the electron density, it tends to overestimate the electron density, and therefore, does not provide results that are within chemical accuracy.³⁵

Other steps have been taken to rectify the problems associated with the uniform gas approximation of LDA, by accounting for the fluctuations in density. In the Generalized Gradient Approximation (GGA), E_{xc} is not only dependent on the electron density, but also its derivatives which considers the inhomogeneity of the real electron density.³⁷ Most GGA functionals are developed by adding a correction term to the LDA functional:

$$E_{xc}^{GGA}(\rho) = E_{xc}^{LDA}(\rho) + F \left[\frac{|\nabla\rho(\mathbf{r})|}{\rho^{\frac{4}{3}}(\mathbf{r})} \right] \quad (2.41)$$

where F is a functional of the gradient of the density, and can be divided into separate exchange and correlation functionals.³⁸ One of the most popular exchange functionals was developed in 1998 by Becke,³⁹ to correctly describe the asymptotic behavior of the electronic density. This functional, often referred to as “B”, has the form:³⁵

$$F_B = -\beta\rho^{\frac{1}{3}} \frac{\left[\frac{|\nabla\rho(\mathbf{r})|}{\rho^{\frac{4}{3}}(\mathbf{r})} \right]^2}{1 + 6\beta \left[\frac{|\nabla\rho(\mathbf{r})|}{\rho^{\frac{4}{3}}(\mathbf{r})} \right] \sinh^{-1} \left[\frac{|\nabla\rho(\mathbf{r})|}{\rho^{\frac{4}{3}}(\mathbf{r})} \right]} \quad (2.42)$$

where the β parameter is determined by an optimized fit of known exact exchange energies of the noble gases. Although the Becke functional provides somewhat accurate results,⁴⁰ improvements have led to the hybrid functionals, such as the B3–Becke’s 3 parameter functional—which takes into account the exact exchange energy, that can be calculated through the Hartree-Fock technique.³⁵ Becke determined the values of his three parameters by data fitting to atomization energies, ionization potentials, proton affinities, and atomic energies of the G1 molecule set.^{40–42}

While the B3 functional only focuses on the exchange contributions of the energy, it is also necessary to account for the correlation effects, even though these effects are significantly smaller than the exchange. The LYP correlation functional developed by Lee, Yang, and Parr,⁴³ is based on the work of Colle and Salvette,⁴⁴ and has the form:

$$\begin{aligned}
 E_{xc}^{LYP} = & -a \frac{\gamma}{(1 + d\rho^{-\frac{1}{3}})} - \\
 & \left[ab \frac{\gamma e^{-c\rho^{-\frac{1}{3}}}}{9(1 + d\rho^{-\frac{1}{3}})\rho^{\frac{8}{3}}} \right] \times \left[18(2^{\frac{2}{3}})\left(\frac{3}{10}\right)(3\pi^2)^{\frac{2}{3}}(\rho_{\alpha}^{\frac{8}{3}} + \rho_{\beta}^{\frac{8}{3}}) - 18\rho t_W \right] - \\
 & \left[ab \frac{\gamma e^{-c\rho^{-\frac{1}{3}}}}{9(1 + d\rho^{-\frac{1}{3}})\rho^{\frac{8}{3}}} \right] \times \left[\rho_{\alpha}(2t_W^{\alpha} + \nabla^2 \rho_{\alpha}) + \rho_{\beta}(2t_W^{\beta} + \nabla^2 \rho_{\beta}) \right] \quad (2.43)
 \end{aligned}$$

where a, b, c, and d are parameters found by fitting to helium atom data, the γ factor is based on the separate electron density for α and β spin, and t_W^{σ} is a kinetic energy function, known as the local Weizsacker density,^{35,45}

$$\gamma = 2 \left[1 - \frac{\rho_{\alpha}^2 + \rho_{\beta}^2}{\rho^2} \right] \quad (2.44)$$

$$t_W^{\sigma} = \frac{1}{8} \left[\frac{|\nabla \rho_{\sigma}|^2}{\rho_{\sigma}} - \nabla^2 \rho_{\sigma} \right] \quad (2.45)$$

When the B3 exchange functional is used in conjunction with the LYP correlation, the result is the B3LYP functional, the most popular and (arguably) robust functional used in density functional theory.

There are many similarities between DFT and HF theory, but there is one extreme difference. With all wave function based techniques, there is a clear route to the exact solution of the Schrödinger equation; express the wave function as a linear combination of all possible excited determinants and choose an infinite basis set, and the exact energy of the system is obtainable. With DFT, there is no clear cut path to the exact answer. If the exact form of the functional representing the electron density was known, then DFT would provide the total energy of the system, including electron correlation. Although there is some ambiguity surrounding the choice of “functional” for the electron density, density functional theory is advantageous because it has the possibility of predicting more accurate results than HF theory with a similar computational expense.

2.8 Basis Sets

Basis sets are a group of functions used to represent atomic orbitals in the LCAO-MO approach. There are two main types of atomic orbitals used in basis sets: Slater type orbitals and Gaussian type orbitals. A Slater type orbital has the form

$$\chi_{\zeta,n,l,m}(r, \theta, \phi) = NY_{l,m}(\theta, \phi)r^{(n-1)}e^{-\zeta r} \quad (2.46)$$

while the form for a Gaussian type orbital is

$$\chi_{\zeta,n,l,m}(r, \theta, \phi) = NY_{l,m}(\theta, \phi)r^{(2n-2-l)}e^{-\zeta r^2} \quad (2.47)$$

where N is the normalization constant and $Y_{l,m}$ are spherical harmonic functions. The major difference between the two types of orbitals comes from their r-dependence. Because of the square power of the Gaussian orbital, it decays much more quickly than the Slater function.¹³ Also, Slater

functions have a finite slope (i.e. a cusp) while Gaussian functions have a zero slope at the nucleus. Davidson and Feller explained that the Gaussian functions do not correctly approximate the exact solution because they have the wrong behavior close and far away from the nucleus.⁴⁶ Therefore, it would take many more Gaussian functions to obtain correct solutions to the Schrödinger equation than Slater functions. In spite of this, one is more likely to choose Gaussian functions over Slater functions because the integral evaluation with Slater functions is much more difficult and also, Slater functions are more computationally expensive.

Basis sets, such as 6-31G are split valence basis sets that use sums of Gaussian orbitals for each core shell and multiple sums for each valence shell. Polarization functions, an additional set of angular momentum functions for each atom, are represented by a *. These functions are important when predicting the molecular properties because they account for the distortion of the orbital in a molecular environment.⁴⁷ For example, the 6-31G* basis set adds a set of d-type functions for first row atoms and the 6-31G** basis set adds the d-type functions along with a set of uncontracted p-type functions for hydrogen.

Dunning developed a set of Gaussian basis sets to be used in correlated methods, the correlation consistent basis sets (cc-pVXZ), designed to contain “all of the correlating functions which lower the correlation energy by similar amounts as well as all correlating functions which lower the energy by larger amounts”.⁴⁸ These basis sets can be used to add *d*, *f*, and *g*-type polarization functions. Dunning’s calculations on the first row atoms showed that the correlation consistent basis sets provide a set of functions that accurately describe the molecular correlation effects. Additional diffuse functions can be added to these types of functions, giving the aug-cc-pVXZ basis sets. The main advantage of the cc-pVXZ and aug-cc-pVXZ type basis sets is that they provide a series of

basis sets which converge to the basis set limit.

Chapter 3

Computing Chiroptic Properties

3.1 Introduction to Computing Optical Rotation

Ab initio calculation of optical rotation is of relatively new interest, but since its implementation in density functional theory in 2000,^{49–55} and more recently in coupled cluster theory,^{53,56–60} it has been successfully used to determine the absolute configuration for a variety of molecules.^{54,61,62} When using the optical rotation to determine the absolute configuration of a chiral molecule, the theory must correctly predict both the sign and magnitude of the specific rotation. These types of calculations inherently contain several sources of error as a consequence of electron correlation effects and basis set dependence.

In 1982, Amos developed the static limit electric-dipole magnetic-dipole linear response polarizability tensor which marked the pathway to the calculation of optical rotation.⁶³ *Ab initio* calculations for computing optical rotation were first implemented in the Hartree-Fock method by

Polavarapu and Kondru.⁶⁴⁻⁶⁶ They were able to predict optical rotation values for small molecules using the Hartree-Fock (HF) method with small basis sets. More recently, optical rotation calculations were carried out using methods which include electron correlation. Stephens *et al.* has examined the use of density functional theory (DFT) to compute optical rotation values for small molecules, showing that there is a large deviation between theoretical and experimental values.⁵¹ The few coupled cluster (CC) calculations that have been reported show the same deviations, and also, the theoretical values for CC and DFT theories are not consistent with each other.^{53,56}

3.2 The Theory of Optical Rotation

An excellent resource describing the fundamental theory behind optical rotation can be found in texts by Caldwell and Eyring⁶⁷ and by Barron.⁵ Here, only a brief overview of the theory is presented.

3.2.1 The Electromagnetic Hamiltonian

Before we can compute the optical rotation, it is necessary to derive the energy expression for the chiral system in the presence of electric and magnetic fields. In an electromagnetic field, the charged particle undergoes a Lorentz force:⁷

$$\mathbf{F} = e \left[\mathbf{E} + \left(\frac{\mathbf{v}}{c} \right) \times \mathbf{B} \right] \quad (3.1)$$

where e is the charge of the electron, moving with a velocity, \mathbf{v} . According to the Euler-Lagrange equation,

$$\nabla L = \frac{d}{dt} \frac{\partial L}{\partial \mathbf{v}} \quad (3.2)$$

which leads to the following Lagrangian, comprised of the kinetic and potential energy

$$L = \frac{1}{2}mv^2 - e\phi + \frac{e}{c}\mathbf{A} \cdot \mathbf{v} \quad (3.3)$$

where ϕ and \mathbf{A} are scalar and vector potentials.⁵ The Hamiltonian is related to the Lagrangian function through

$$\hat{H} = \mathbf{v} \cdot \frac{\partial L}{\partial \mathbf{v}} - L \quad (3.4)$$

which leads to the following form of the electromagnetic Hamiltonian, explicitly dependent on \mathbf{p} and \mathbf{r} ⁵

$$\hat{H} = \frac{1}{2m} \left[\mathbf{p} - \frac{e}{c}\mathbf{A} \right]^2 + e\phi \quad (3.5)$$

By substituting $-i\hbar\nabla$ for the momentum and assuming that the vector potential is unvarying,

$$\hat{H} = \frac{-\hbar^2\nabla^2}{2m} + \frac{e^2}{2mc^2}\mathbf{A}^2 + e\phi \quad (3.6)$$

The Hamiltonian describing a system in the presence of an electromagnetic field can be divided into two terms, a reference Hamiltonian and a perturbed part, $\hat{H} = \hat{H}_o + \hat{H}'(t)$ where

$$\hat{H}'(t) = -\frac{e}{mc} \sum_i \mathbf{A}(\mathbf{r}_i) \cdot \mathbf{p}_i \quad (3.7)$$

When using the following form of the vector potential,

$$\mathbf{A}(\mathbf{r}) = \mathbf{A}(0) + (\mathbf{r} \cdot \nabla_0)\mathbf{A}(0) \quad (3.8)$$

the complete interaction Hamiltonian evaluated to the first order is⁶⁷

$$\begin{aligned} \hat{H}'(t) = & -\frac{e}{mc} \left[\sum_i \mathbf{A}(0) \cdot \mathbf{p}_i + \frac{1}{2} (\nabla_0 \times \mathbf{A}(0)) \cdot (\mathbf{r}_i \times \mathbf{p}_i) \right] \\ & + \left[\frac{im}{2\hbar} \right] \left[-\frac{e}{mc} \right] \{ H_o(\mathbf{r} \cdot \nabla_0)(\mathbf{A}(0) \cdot \mathbf{r}) - (\mathbf{r} \cdot \nabla_0)(\mathbf{A}(0) \cdot \mathbf{r} H_o) \} \end{aligned} \quad (3.9)$$

3.2.2 The Time-Dependent Schrödinger Equation

Because there is a realistic time dependence of the applied electromagnetic field (the perturbed part of the total Hamiltonian is time dependent), the molecular wave functions cannot be solved using the regular Schrödinger equation discussed in the first chapter. Instead, the perturbed wave functions can be solved using the time- dependent Schrödinger equation:⁶⁷

$$\hat{H}\Psi = [\hat{H}_o + \hat{H}'(t)] = i\hbar \frac{\partial \Psi}{\partial t} \quad (3.10)$$

where the wave function has the following form

$$\Psi(t) = \Psi_o e^{-\frac{iE_o t}{\hbar}} + \sum_n a_n(t) \Psi_n e^{\frac{iE_n t}{\hbar}} \quad (3.11)$$

and the coefficients for the perturbed wave function are

$$a_n(t) = \frac{1}{i\hbar} \int_0^t H'(t) e^{i\omega_{no}t} dt \quad (3.12)$$

3.2.3 Response to a Changing Magnetic Component of the Electromagnetic Field

In order to calculate the optical rotation of a chiral molecule, it is necessary to determine the polarization of the medium, due to the changing magnetic component of the electromagnetic field.

To do this, the perturbed Hamiltonian is expressed as:⁸

$$H'(t) = -\boldsymbol{\mu} \cdot \mathbf{E}(t) - \mathbf{m} \cdot \mathbf{B}(t) \quad (3.13)$$

where $\boldsymbol{\mu}$ and \mathbf{m} are the electric-dipole and magnetic-dipole and \mathbf{E} and \mathbf{B} are dependent on the separate left- and right- components of circularly polarized light (represented by \pm)

$$\mathbf{E}^\pm(t) = \varepsilon(\hat{\mathbf{i}} \cos \omega t \pm \hat{\mathbf{j}} \sin \omega t) \quad (3.14)$$

$$\mathbf{B}^\pm(t) = \beta \pm \hat{\mathbf{i}} \sin \omega t - \hat{\mathbf{j}} \cos \omega t \quad (3.15)$$

After substituting the previous equations into Equation 3.13, along with the Euler's identities for $\sin \omega t$ and $\cos \omega t$, and including the term, $(1 - e^{-\frac{t}{\tau}})$, for switching on the field, the perturbed Hamiltonian has the form:⁸

$$\begin{aligned} \hat{H}'(t) = & -\frac{1}{2}\varepsilon(1 - e^{-\frac{t}{\tau}}) \left[\boldsymbol{\mu}_x(e^{i\omega t} + e^{-i\omega t}) \mp \boldsymbol{\mu}_y i(e^{i\omega t} - e^{-i\omega t}) \right] \\ & -\frac{1}{2}\beta(1 - e^{-\frac{t}{\tau}}) \left[-\mathbf{m}_x(e^{i\omega t} + e^{-i\omega t}) \mp i\mathbf{m}_y(e^{i\omega t} - e^{-i\omega t}) \right] \end{aligned} \quad (3.16)$$

The response of an observable quantity to the applied electromagnetic field is found by its expectation value,⁶⁷

$$\langle Q \rangle_{nn} = \int \Psi_n'^* Q \Psi_n' d\tau \quad (3.17)$$

For the electric-dipole (using Equation 3.11 for the wave function)

$$\langle \boldsymbol{\mu}^\pm \rangle = \langle 0 | \boldsymbol{\mu} | 0 \rangle + \sum_n a_n^\pm(t) \langle 0 | \boldsymbol{\mu} | n \rangle e^{i\omega_{0n}t} + \sum_n a_n^{\pm*}(t) \langle n | \boldsymbol{\mu} | 0 \rangle e^{-i\omega_{0n}t} \quad (3.18)$$

This equation can be further simplified by using the previous expressions for the perturbed Hamiltonian and the coefficients for the perturbed wavefunction (Equations 3.13 and 3.12)

$$\begin{aligned} \langle \boldsymbol{\mu}^\pm \rangle = & \frac{2}{\hbar} \text{Re} \sum_n \left[\frac{\omega_{n0}}{\omega_{n0}^2 - \omega^2} \right] \langle 0 | \boldsymbol{\mu} | n \rangle \langle n | \boldsymbol{\mu} | 0 \rangle \mathbf{E}^\pm(t) - \\ & \frac{2}{\hbar} \text{Im} \sum_n \left[\frac{1}{\omega_{n0}^2 - \omega^2} \right] \langle 0 | \boldsymbol{\mu} | n \rangle \langle n | \mathbf{m} | 0 \rangle \mathbf{B}^\pm(t) \end{aligned} \quad (3.19)$$

($\mathbf{B}^\pm(t)$ is directly related to the vector potential, \mathbf{A} , which in turn is related to the derivative of the magnetic field through Maxwell's equations)

Another approach to determining the response of the electric-dipole to the electromagnetic field is through the Hellman-Feynman theorem⁸

$$\frac{dE}{dP} = \left\langle \frac{\partial \hat{H}}{\partial P} \right\rangle \quad (3.20)$$

where E is the energy and P is the chosen parameter (in this case, P is the electric field, ϵ). When the partial derivative of the perturbed Hamiltonian (Equation 3.13) with respect to the electric field is taken, the result is $-\mu$ which is equivalent to the derivative of the energy with respect to the electric field. If the energy is expressed as a Taylor series expansion, its connection to the electric-dipole results in

$$\langle \boldsymbol{\mu} \rangle = - \left[\frac{dE}{d\epsilon} \right] \Big|_0 - \left[\frac{d^2 E}{d\epsilon^2} \right] \Big|_0 \epsilon - \frac{1}{2} \left[\frac{d^3 E}{d\epsilon^3} \right] \Big|_0 \epsilon^2 - \dots \quad (3.21)$$

$$\langle \boldsymbol{\mu} \rangle = \mu_0 + \alpha \epsilon + \frac{1}{2} \beta \epsilon^2 + \dots \quad (3.22)$$

where μ_0 is the permanent dipole, and α and β are the polarizability and hyperpolarizability, respectively (in Equation 3.22, β is not the same as the β tensor or the Rosenfeld polarizability tensor, it is only used here as the hyperpolarizability). When the case of an electric field with an induced magnetic field is considered, the previous equation can be compared to Equation 3.19, and the result is an expression for the beta tensor⁸ (Rosenfeld Polarizability Tensor)⁶⁷

$$\boldsymbol{\beta} = \frac{2}{\hbar} \text{Im} \sum_n \frac{\langle 0 | \boldsymbol{\mu} | n \rangle \langle n | \mathbf{m} | 0 \rangle}{\omega_{n0}^2 - \omega^2} \quad (3.23)$$

which consists of three components averaged in solution

$$\beta_{xx} + \beta_{yy} + \beta_{zz} \longrightarrow \beta = \frac{2}{3\hbar} \text{Im} \sum_n \frac{\langle 0 | \boldsymbol{\mu} | n \rangle \cdot \langle n | \mathbf{m} | 0 \rangle}{\omega_{n0}^2 - \omega^2} \quad (3.24)$$

This leads us to our final expression of the angle of rotation of plane polarized light through a chiral medium (from Equation 1.23):

$$\Delta\theta = \frac{\omega^2 N}{c^2 \epsilon_0 \hbar} \text{Im} \sum_n \frac{\langle 0 | \boldsymbol{\mu} | n \rangle \langle n | \mathbf{m} | 0 \rangle}{\omega_{n0}^2 - \omega^2} \quad (3.25)$$

3.3 Computing Optical Rotation with Coupled Cluster Theory

Coupled cluster linear response theory allows for the calculation of molecular response properties, such as optical rotation.^{68–73} This technique requires taking the second derivative of the time-averaged coupled cluster Lagrangian function:⁷²

$$\beta_\omega \longleftarrow \frac{d^2 L_{CC}}{d\boldsymbol{\mu} d\mathbf{m}} \quad (3.26)$$

which leads to the following linear response function, which is essentially equivalent to the beta tensor

$$\langle\langle \boldsymbol{\mu}; \mathbf{m} \rangle\rangle_\omega = \frac{1}{2} \hat{C}^{\pm\omega} \hat{P}(\boldsymbol{\mu}(-\omega), \mathbf{m}(\omega)) \left[\langle 0 | \hat{\Lambda} [\bar{\boldsymbol{\mu}}, \hat{X}^\omega_{\mathbf{m}}] | 0 \rangle + \frac{1}{2} \langle 0 | \hat{\Lambda} [[\bar{H}, \hat{X}^\omega_{\boldsymbol{\mu}}], \hat{X}^{-\omega}_{\mathbf{m}}] | 0 \rangle \right] \quad (3.27)$$

where $|0\rangle$ is the Hartree-Fock reference state, the overbar denotes the similarity transformation of the given operator [*e.g.*, $\bar{H} = \exp(-\hat{T})\hat{H}\exp(\hat{T})$], and $\hat{\Lambda}$ is a cluster operator parametrizing the coupled cluster “left-hand” ground-state wave function. The permutation operator $\hat{C}^{\pm\omega}$ simultaneously changes signs of the the chosen field frequency, ω , and takes the complex conjugate of the equation, while $\hat{P}(\boldsymbol{\mu}, \mathbf{m})$ permutes the property operators $\boldsymbol{\mu}$ and \mathbf{m} . This previous expression for $\langle\langle \boldsymbol{\mu}; \mathbf{m} \rangle\rangle_\omega$ is analogous to the Rosenfeld polarizability tensor, where the specific rotation is directly

related the trace of β :

$$[\alpha]_\omega = \frac{(7.20 \times 10^6)h^2 N_A \omega}{c^2 m_e^2 M} \times \left[\frac{1}{3} \text{Tr}(\beta) \right] \quad (3.28)$$

In Equation 3.27, \hat{X}_μ and \hat{X}_m represent the perturbed wave functions, or the response of the wave function to the applied electromagnetic field. These are determined by solving the following system of linear equations, which is dependent on Φ_i , the excited determinants

$$\langle \Phi_i | (\bar{H} - \omega) | \Phi_j \rangle \langle \Phi_j | \hat{X}_\mu^\omega | 0 \rangle = -\langle \Phi_i | \bar{\mu} | 0 \rangle \quad (3.29)$$

$$\langle \Phi_i | (\bar{H} - \omega) | \Phi_j \rangle \langle \Phi_j | \hat{X}_m^\omega | 0 \rangle = -\langle \Phi_i | \bar{m} | 0 \rangle \quad (3.30)$$

The following sequence lists the steps needed for evaluation of the linear response function.⁷⁴

1. Use ground state coupled cluster theory to determine the cluster operators, \hat{T} .
2. Compute \bar{H} , $\bar{\mu}$ and \bar{m} .
3. Determine $\hat{\Lambda}$, the left-hand ground-state wave function.
4. Solve the previous system of linear equations (Equation 3.29 and 3.30) to obtain the perturbed wave functions.
5. Combine all parameters to solve for $\langle\langle \mu; m \rangle\rangle_\omega$.

3.4 Computing Optical Rotation with Density Functional Theory

In density functional theory, the time-dependence of the applied electromagnetic field is treated using time-dependent DFT (TD-DFT),⁷⁵⁻⁷⁷ where the linear response function that represents the

beta tensor has the form⁷⁸

$$\langle\langle\mu_x; m_y\rangle\rangle_\omega = \boldsymbol{\mu}_x^+(\boldsymbol{\Gamma} - \omega\boldsymbol{\Delta})^{-1}\mathbf{m}_y \quad (3.31)$$

where $\boldsymbol{\Gamma}$ and $\boldsymbol{\Delta}$ are matrices that contain all the single excitations and de-excitations of the Kohn-Sham orbitals,⁷⁹

$$\boldsymbol{\Gamma} = \begin{pmatrix} \mathbf{A} & \mathbf{B} \\ \mathbf{B} & \mathbf{A} \end{pmatrix} \quad (3.32)$$

$$\boldsymbol{\Delta} = \begin{pmatrix} \mathbf{1} & \mathbf{0} \\ \mathbf{0} & -\mathbf{1} \end{pmatrix}, \quad (3.33)$$

The \mathbf{A} and \mathbf{B} submatrices of Equation 3.32 contain the molecular orbitals, orbital energies and antisymmetrized electron repulsion integrals.⁷⁴

In actuality, density functional calculations of optical rotation do not explicitly compute the inverse matrix in Equation 3.31. Instead, the perturbed wave function is determined from the following system of linear equations:

$$(\boldsymbol{\Gamma} - \omega\boldsymbol{\Delta})\mathbf{Z}_x = \boldsymbol{\mu}_x \quad (3.34)$$

$$(\boldsymbol{\Gamma} - \omega\boldsymbol{\Delta})\mathbf{Z}_x = \mathbf{m}_x \quad (3.35)$$

The following sequence lists the steps required for a density functional theory calculation of optical rotation.⁷⁴

1. Use density functional theory to obtain the Kohn-Sham orbitals.
2. Use the previously described equations to compute the matrices \mathbf{A} and \mathbf{B} .
3. Use \mathbf{A} and \mathbf{B} to determine the form of $\boldsymbol{\Gamma}$ (Equation 3.32).

4. Iteratively solve Equations 3.34 and 3.35.
5. Combine all previously solved items, to obtain an expression for the β tensor (Equation 3.31) which can be used to calculate the specific rotation through Equation 3.28.

3.5 Origin Invariance in Optical Rotation Calculations

One of the main problems with optical rotation calculations is the result of origin dependence, meaning that the computed value is contingent on the position of the molecule, which is clearly unrealistic. This origin dependence is caused by translation of the coordinate origin along a vector, \mathbf{a} , which in turn causes a shift in the linear response function:

$$\langle\langle \mathbf{r}'; \mathbf{r}' \times \mathbf{p}' \rangle\rangle_{\omega} = \langle\langle \mathbf{r}; \mathbf{r} \times \mathbf{p} \rangle\rangle_{\omega} - \langle\langle \mathbf{r}; \mathbf{a} \times \mathbf{p} \rangle\rangle_{\omega} \quad (3.36)$$

It is the last term that specifically causes the lack of origin independence through its relationship to $\langle\langle \mathbf{r}; \mathbf{p} \rangle\rangle_{\omega}$:

$$\begin{aligned} \langle\langle \mathbf{r}; \mathbf{a} \times \mathbf{p} \rangle\rangle_{\omega} &= a_x [\langle\langle r_z; p_y \rangle\rangle_{\omega} - \langle\langle r_y; p_z \rangle\rangle_{\omega}] + a_y [\langle\langle r_x; p_z \rangle\rangle_{\omega} - \langle\langle r_z; p_x \rangle\rangle_{\omega}] + \\ & a_z [\langle\langle r_y; p_x \rangle\rangle_{\omega} - \langle\langle r_x; p_y \rangle\rangle_{\omega}] \end{aligned} \quad (3.37)$$

When computing optical rotation with density functional theory and GIAOs (gauge invariant atomic orbitals), the following equation-of-motion response function is satisfied⁷⁴

$$\omega \langle\langle \mathbf{r}; \mathbf{r} \rangle\rangle_{\omega} = \langle\psi_0 | [\mathbf{r}, \mathbf{r}] | \psi_0 \rangle + \langle\langle \mathbf{r}; [\mathbf{r}, \hat{H}] \rangle\rangle_{\omega} \quad (3.38)$$

Since $[\mathbf{r}, \hat{H}] = i\mathbf{p}$, through substitution Equation 3.38 becomes

$$\omega \langle\langle \mathbf{r}; \mathbf{r} \rangle\rangle_{\omega} = \langle\psi_0 | [\mathbf{r}, \mathbf{r}] | \psi_0 \rangle + \langle\langle \mathbf{r}; i\mathbf{p} \rangle\rangle_{\omega} \quad (3.39)$$

When this relationship for $\langle\langle\mathbf{r}; i\mathbf{p}\rangle\rangle_\omega$ is used in Equation 3.37, it becomes zero through symmetry relations, providing origin invariance in density functional theory optical rotation calculations.

When coupled cluster theory is used to calculate optical rotations, its equation-of-motion response function does not satisfy the conditions of Equation 3.38, leading to origin dependent results (length-gauge). An alternate method is to perform optical rotation calculations within coupled cluster theory using the “velocity gauge” developed by Pedersen *et al.*⁵⁸ In this method, an alternate form of the Rosenfeld tensor is used, and with exact wave functions,

$$Tr \langle\langle\mathbf{r}; \mathbf{r} \times \mathbf{p}\rangle\rangle_\omega = \frac{1}{\omega} Tr \langle\langle\mathbf{p}; \mathbf{r} \times \mathbf{p}\rangle\rangle_\omega \quad (3.40)$$

which causes the last term in Equation 3.36 to go to zero, resulting in origin independence. One major difference between “length-gauge” and “velocity-gauge” results, is that the response function for the former decays to zero in the static limit, whereas the “velocity-gauge” response function does not because of the factor of $1/\omega$, which cancels with the ω in the numerator of Equation 3.28. Pedersen *et al.* account for this unrealistic result by shifting $\langle\langle\mathbf{p}; \mathbf{r} \times \mathbf{p}\rangle\rangle_\omega$ by the static limit value $\langle\langle\mathbf{p}; \mathbf{r} \times \mathbf{p}\rangle\rangle_0$.

Chapter 4

Coupled Cluster and Density

Functional Theory Calculations of

Optical Rotatory Dispersion of

(*S*)-Methyloxirane

Reproduced in part with permission from Mary C. Tam, Nicholas J. Russ and T. Daniel Crawford,

J. Chem. Phys. **112**, 3550-3557, 2004.

4.1 Introduction

A long-standing problem in natural products chemistry is the determination of the absolute configuration of newly isolated compounds. Although the assessment of the enantiomeric purity of such chiral species is routinely achieved by measuring optical rotation angles or integrating chiral GC/HPLC traces, determining the absolute configuration is more difficult.^{6,80} The most convincing analyses rely on X-ray crystallographic data of the compound itself (using anomalous dispersion) or of a derivative that incorporates a known stereocenter. In the case of a non-crystalline compound, asymmetric synthesis — or total synthesis from starting materials of known absolute configuration — must be performed. When these methods fail, less secure chiroptical and NMR methods are used. All of these approaches are time-consuming, and none are guaranteed to be successful.

An alternative approach is to compute directly the chiroptical properties of selected molecular structures and compare the results with the associated properties [optical rotation angles, optical rotatory dispersion (ORD) spectra, or circular dichroism (CD) spectra] of the original natural product isolate.^{49,64,65,81–84} The quantum mechanical foundation for such computations has been known since the work of Rosenfeld in 1928.⁸⁵ Using time-dependent perturbation theory, one may show that the angle of rotation, $[\alpha]_\omega$, of plane-polarized light of frequency ω in a chiral medium is related to the trace of the frequency-dependent electric-dipole magnetic-dipole polarizability tensor,

$$\beta(\omega) = \frac{c}{3\pi h} \text{Im} \sum_{n \neq 0} \frac{\langle 0 | \boldsymbol{\mu} | n \rangle \langle n | \mathbf{m} | 0 \rangle}{\omega_{n0}^2 - \omega^2}, \quad (4.1)$$

where $\boldsymbol{\mu}$ and \mathbf{m} are the electric and magnetic dipole operators, respectively, and the summation runs over excited electronic (unperturbed) wave functions, $|n\rangle$. This tack has been taken with both semiempirical^{86–88} and *ab initio* quantum chemical techniques,^{63,81,89,90} most recently with

density functional theory^{49,84,91,92} and coupled cluster theory^{53,56,93} and several applications have appeared in the literature.^{64,82,94–101} Unfortunately, the quality of such theoretical predictions is often difficult to assess because fair comparisons with experimental data are not straightforward. First, the theoretical approach may contain many sources of error, such as choice of one-electron basis set, dynamic electron correlation effects, etc. Second, experimental data are often obtained under widely varying conditions, and solvent and/or temperature effects, as well as conformational averaging, may have a significant impact on measured chiroptical spectra.

A recent breakthrough in the development of cavity ring-down polarimetry (CRDP) by Müller, Wiberg, and Vaccaro has allowed ultrasensitive gas-phase measurements of optical rotation of a number of small chiral molecules, thus opening the door to more systematic comparisons between theory and experiment.^{102,103} Müller *et al.* reported that, contrary to conventional wisdom, solvent effects can indeed be significant, perhaps leading to dramatic differences in both magnitude and sign of optical rotation angles relative to gas-phase results. For example, among the molecules studied by Müller *et al.* is propylene oxide (also known as methyloxirane), a potentially ideal test case for higher-level theoretical models because it is conformationally rigid and contains only four non-hydrogen atoms. Müller *et al.* measured a 355 nm specific rotation of the (*S*) enantiomer of methyloxirane of $+10.2 \text{ deg dm}^{-1} (\text{g/mL})^{-1}$ in the gas-phase and $-26.4 \text{ deg dm}^{-1} (\text{g/mL})^{-1}$ in cyclohexane. These results agree qualitatively with those of Kumata *et al.*, who reported a wide variation of sodium D-line (589 nm) specific rotation of (*S*)-methyloxirane in benzene ($-30.6 \text{ deg dm}^{-1} (\text{g/mL})^{-1}$) *vs* water ($+4.3 \text{ deg dm}^{-1} (\text{g/mL})^{-1}$).¹⁰⁴

In the only theoretical comparison to these new experimental results to date, Giorgio *et al.* recently reported density-functional theory (DFT) specific rotation data for (*S*)-methyloxirane using

a variety of basis sets.¹⁰⁵ They found that the B3LYP functional was capable of predicting the correct sign for the optical rotation with the use of high-angular-momentum correlation-consistent basis sets¹⁰⁶ or specially tailored Sadlej basis sets,^{107,108} but the magnitude of the rotation was overestimated by a factor of two. In addition, they reported that large-basis-set Hartree-Fock optical rotation calculations disagreed qualitatively with the results of Müller *et al.*, a point recently made in several systematic studies by Cheeseman, Frisch, Devlin, and Stephens.^{49,84} Giorgio *et al.* also indicated that the anomalously large frequency dispersion observed in (*S*)-methyloxirane is related to the lowest energy Cotton effect, even though the corresponding absorption occurs at only 174.1 nm (7.12 eV)¹⁰⁹ some distance from the wavelength of the CRDP radiation source at 355 nm (3.49 eV) used by Müller and co-workers.¹⁰²

Given the apparent need for higher-level theoretical calculations of optical rotation in (*S*)-methyloxirane, we have applied coupled cluster linear response theory to this problem. Coupled cluster is widely regarded as the most reliable quantum chemical approach for computing a variety of properties of small molecules, including molecular structure, vibrational spectra, NMR chemical shieldings, UV/Vis spectra, and thermochemical properties.^{110–113} Thus, we seek to extend its applicability to optical rotation and to benchmark its accuracy relative to experiment. In particular, using a new implementation of the coupled cluster singles and doubles (CCSD) model for frequency-dependent properties, described in the next section, we have considered the effect of basis set, optimized geometry, and gauge origin on the computed rotation angles of (*S*)-methyloxirane for comparison to both DFT data and the experimental results of Müller and co-workers. We find that: (1) the quality of both the DFT and coupled cluster predictions vary widely with basis set and choice of optimized structure; (2) DFT benefits from an incorrect prediction of the lowest energy

Rydberg transition in methyloxirane; and (3) coupled cluster, while correct in its determination of the energy of the lowest Rydberg state, instead fails to predict the width of the pole surrounding the resonance.

4.2 Coupled Cluster Response Theory for Optical Rotation

The Rosenfeld β tensor in Eq. (4.1) may be computed within the coupled cluster model using response theory,^{114–118} in which β is related to the linear response function,

$$\beta(\omega) = \langle\langle \boldsymbol{\mu}; \mathbf{m} \rangle\rangle_\omega = \frac{d^2 \{L_{CC}\}_T}{d\boldsymbol{\mu} d\mathbf{m}}, \quad (4.2)$$

where $\{L_{CC}\}_T$ represents the time-averaged coupled cluster Lagrangian.¹¹⁷ Evaluating the derivative above leads to an operator form of the linear response function,

$$\langle\langle \boldsymbol{\mu}; \mathbf{m} \rangle\rangle_\omega = \frac{1}{2} \hat{C}^{\pm\omega} \hat{P}(\boldsymbol{\mu}(-\omega), \mathbf{m}(\omega)) \left[\langle 0 | \hat{\Lambda} [\bar{\boldsymbol{\mu}}, \hat{X}_{\mathbf{m}}^\omega] | 0 \rangle + \frac{1}{2} \langle 0 | \hat{\Lambda} \left[[\bar{H}, \hat{X}_{\boldsymbol{\mu}}^\omega], \hat{X}_{\mathbf{m}}^{-\omega} \right] | 0 \rangle \right] \quad (4.3)$$

where $|0\rangle$ is the Hartree-Fock reference state, the overbar denotes the similarity transformation of the given operator [*e.g.*, $\bar{H} = \exp(-\hat{T})\hat{H}\exp(\hat{T})$], and $\hat{\Lambda}$ is a cluster operator parametrizing the coupled cluster “left-hand” ground-state wave function (developed also in coupled cluster analytic energy gradient theory).^{119–123} The permutation operator $\hat{C}^{\pm\omega}$ simultaneously changes signs on the chosen field frequency, ω , and takes the complex conjugate of the equation, while $\hat{P}(\hat{A}, \hat{B})$ permutes the property operators \hat{A} and \hat{B} . The perturbed wave functions, $\hat{X}_{\boldsymbol{\mu}}^\omega$, are determined by solving the system of linear equations

$$\langle \Phi_i | (\bar{H} - \omega) | \Phi_j \rangle \langle \Phi_j | \hat{X}_{\boldsymbol{\mu}}^\omega | 0 \rangle = -\langle \Phi_i | \bar{\boldsymbol{\mu}} | 0 \rangle, \quad (4.4)$$

where the Φ_i represent excited determinants. It is worth noting that the eigenvalues of the response matrix on the left-hand side of the above equation (sometimes referred to in the literature as the coupled cluster Jacobian matrix) are related to the excitation energies of the system, an approach to UV/Vis spectra known as the equation-of-motion coupled cluster (EOM-CC) method.^{115,124}

One may therefore evaluate the above linear response function by the following steps:

1. Solve the ground-state coupled cluster equations for the cluster operators, \hat{T} .^{125,126}
2. Compute the similarity-transforms of the Hamiltonian, \bar{H} , and other operators required for the response function, *i.e.*, $\bar{\mu}$ and \bar{m} .¹²⁴
3. Solve the left-hand ground-state wave function equations for $\hat{\Lambda}$.¹²³
4. Solve the system of linear equations in Eq. (4.4) for each component of each perturbation for both positive and negative values of the field frequency, ω . For the optical rotation function, this leads to twelve sets of perturbed wave function equations which must be solved.
5. Compute the contributions to the total linear response function given in Eq. (4.3).^{115,118}

We have derived and implemented the linear response function for the Rosenfeld β tensor at the coupled-cluster singles and doubles (CCSD) level of theory within the program package PSI3.¹²⁷ We have adopted a factorization strategy of the many diagrams appearing implicitly in Eqs. (4.4) and (4.3) similar to that used in efficient ground-state coupled cluster energy and analytic gradient implementations, such that no single term scales worse than $\mathcal{O}(N^6)$.^{128,129} The program makes full use of Abelian point-group symmetry when available for efficiency, though for (*S*)-methyloxirane, no such symmetry is present.

An important failing of the above approach to coupled cluster frequency-dependent properties, as noted by Pedersen and Koch,^{93,130–132} is its lack of origin independence for magnetic-field-dependent properties, such as optical rotation. Although this problem can be circumvented for Hartree-Fock and DFT response methods using gauge-including atomic orbitals (GIAOs, also known as London orbitals),^{49,89,133–135} this technique will not ensure origin invariance for conventional coupled cluster or perturbation methods due their lack of orbital optimization. On the other hand, GIAOs can substantially improve the basis-set dependence of magnetic-field dependent properties,¹³⁶ a point we will address below.

4.3 Computational Details

The optimized geometry of (*S*)-methyloxirane was determined using analytic energy gradients at the B3LYP^{137–139} and CCSD(T)^{122,125,140–143} levels of theory with two different basis sets: the standard 6-31G* split-valence basis set of Pople *et al.*¹⁴⁴ and the correlation-consistent triple-zeta (cc-pVTZ) basis set of Dunning.¹⁰⁶ These four optimized structures were confirmed to be minima on the potential energy surface *via* harmonic vibrational frequency calculations, carried out using analytic energy second derivative methods.^{145,146}

Optical rotation calculations for a variety of wavelengths were carried out using the coupled cluster singles and doubles (CCSD) linear response approach described in the previous section and using time-dependent density-functional theory (TDDFT) with the B3LYP functional.^{49,82} The molecular center of mass was chosen as the origin for most of the calculations reported here, though the coordinates of the oxygen atom were used for additional analysis. The B3LYP data

were obtained both with and without GIAOs for comparison to the CCSD results (*vide supra*). In addition, the positions of poles in the values of $[\alpha]$ (i.e., excitation energies) were computed using EOM-CCSD¹²⁴ and TDDFT/B3LYP approaches.^{147,148}

In addition, several different basis sets were employed for the optical rotation calculations: (1) the split-valence basis sets, 6-31G*, 6-31++G**, and 6-311++G(2d,2p);¹⁴⁴ (2) the correlation-consistent basis sets, cc-pVDZ, cc-pVTZ, aug-cc-pVDZ, d-aug-cc-pVDZ, and a mixed basis consisting of the aug-cc-pVTZ basis for carbon and oxygen and the aug-cc-pVDZ basis for hydrogen (238 contracted Gaussian functions);^{106,149,150} and (2) the Sadlej-pVTZ basis set, which was developed specifically for computations of electric properties, including dipole polarizabilities.^{107,108} Pure angular momentum polarization functions were used for the 6-311++G(2d,2p), correlation-consistent, and Sadlej basis sets, while Cartesian polarization functions were used with all other basis sets. All electrons were correlated for the geometry and frequency calculations, but the core electrons were held frozen for all of the CCSD optical rotation and excitation energy calculations. (The only reason for this choice is a program limitation in the ACESII system, which was used for the structural optimizations. Coupled cluster geometries determined using frozen core orbitals differ negligibly — at most 0.001 Å in bond lengths and less than 0.1 degrees in bond and dihedral angles at the CCSD(T)/6-31G* level — from the all-electron data used here.) Basis sets were obtained from the Extensible Computational Chemistry Environment Basis Set Database.¹⁵¹

All coupled cluster optical rotation calculations were carried out with the PSI3 program package,¹²⁷ while B3LYP optical rotation calculations were carried out using Gaussian03.¹⁵² Coupled cluster geometry optimizations, harmonic vibrational frequency calculations, and excitation energy calculations were carried out with the ACESII program package,¹⁵³ while B3LYP optimized geome-

tries, harmonic vibrational frequencies, and excitation energies were computed with the Gaussian suite.¹⁵²

4.4 Results and Discussion

Fig. 4.1 reports the optimized geometry of (*S*)-methyloxirane at the B3LYP/6-31G*, B3LYP/cc-pVTZ, CCSD(T)/6-31G*, and CCSD(T)/cc-pVTZ levels of theory. Although the CCSD(T)/cc-pVTZ results are reasonably expected to be the most accurate, the rigid structure of this molecule depends very little on the choice of method, and all four structures agree very well with the experimentally inferred geometry of Creswell and Schwendeman.¹⁵⁴ Bond lengths vary among the four methods only slightly — all within ca. 0.01 Å — and the variation in the bond angles is, at most, a few tenths of a degree. Most importantly, the angle of the methyl group out of the plane formed by the oxirane ring, which one might expect to be the most important structural feature influencing the computed rotations,^{90,99} varies by less than a degree (54.95 degrees at the B3LYP/cc-pVTZ level *vs* 55.89 degrees at the CCSD(T)/cc-pVTZ level). Nevertheless, as we show below, the choice of optimized structure still has a significant impact on the computed optical rotation.

Tables 4.1 and 4.2 report the computed values of $[\alpha]_{\lambda}$ (in $\text{deg dm}^{-1} (\text{g/mL})^{-1}$) at the B3LYP and CCSD levels of theory using a variety of basis sets at the two key wavelengths: 589 and 355 nm, respectively. Nearly all choices of basis set and optimized geometry for both methods predict a negative value of $[\alpha]_{589}$, in qualitative agreement with the CCl_4 -solvent-dependent experimental result of $-18.7 \text{ deg dm}^{-1} (\text{g/mL})^{-1}$ of Kumata *et al.*,¹⁰⁴ though, as noted earlier, the influence

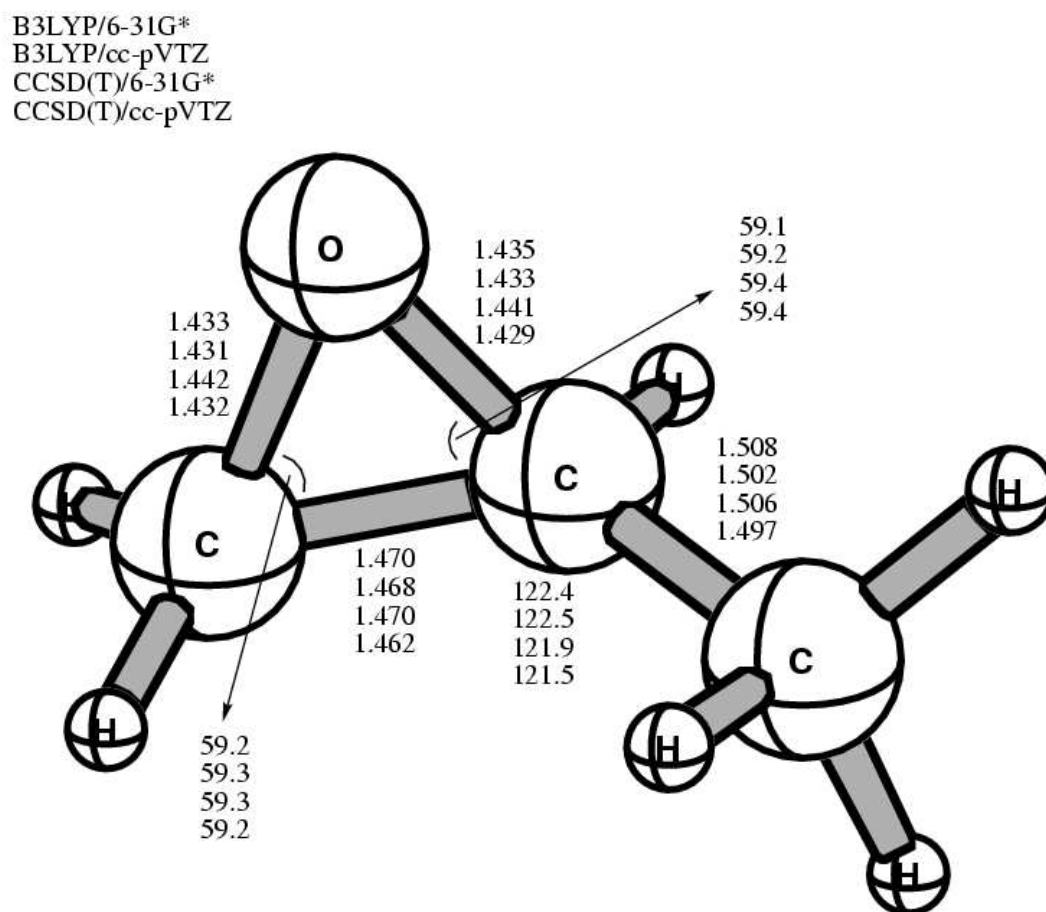


Figure 4.1: Optimized geometries of (*S*)-methyloxirane using B3LYP and CCSD(T) methods with the 6-31G* and cc-pVTZ basis sets. Bond lengths are given in Å and bond angles in degrees.

of solvent may be considerable. On the other hand, the variation of the results with respect to basis set — even for the GIAO-based B3LYP method — is striking. We find that the effect of diffuse functions in the basis set is particularly important, in agreement with previous studies by Cheeseman *et al.*^{49,84} and by Wiberg *et al.*¹⁰⁰ While the 6-31G*, cc-pVDZ, and cc-pVTZ basis sets, which lack diffuse functions, give values of $[\alpha]_{589}$ that are too large in magnitude, even the 6-31++G** basis set, which includes diffuse *s* and *p* functions for the heavy atoms and diffuse *s* functions on the hydrogens, produces angles around $-35 \text{ deg dm}^{-1} (\text{g/mL})^{-1}$ for B3LYP and near $-50 \text{ deg dm}^{-1} (\text{g/mL})^{-1}$ for CCSD. The aug-cc-pVDZ basis set, which also includes diffuse *d* functions on the heavy atoms and diffuse *p* functions on the hydrogens, performs well for B3LYP, but poorly for CCSD, while the d-aug-cc-pVDZ basis set, which includes two sets of diffuse functions for each atom, reverses this behavior. Finally, the Sadlej-pVTZ basis, which is optimized for computing electrical response properties, gives essentially the same CCSD $[\alpha]_{589}$ as d-aug-cc-pVDZ, but B3LYP values that are near zero (and even positive with the B3LYP/cc-pVTZ geometry).

Table 4.1: B3LYP and CCSD specific rotation ($\text{deg dm}^{-1} (\text{g/mL})^{-1}$) for (*S*)-methyloxirane computed with various basis sets and optimized geometries at 589 nm. The center of mass is chosen to be the gauge origin.

Geometry Type	6-31G*	6-31++G**	6-311++G(2d,2p)	cc-pVDZ	cc-pVTZ	aug-cc-pVDZ	d-aug-cc-pVDZ	mixed-cc-pVTZ ¹	aug-cc-pVTZ	Sadlej-pVTZ
B3LYP (GIAO)										
B3LYP/6-31G*	-22.6	-37.0	-14.9	-49.5	-24.5	-19.4	-11.8	-14.56	-12.7	-1.27
B3LYP/cc-pVTZ	-23.8	-37.0	-13.1	-49.0	-23.3	-16.8	-9.26	-11.93	-10.0	2.17
CCSD(T)/6-31G*	-27.8	-38.7	-16.7	-53.9	-27.5	-21.0	-12.9	-16.49	-14.2	-3.02
CCSD(T)/cc-pVTZ	-30.4	-38.8	-14.2	-55.2	-26.7	-18.1	-9.07	-13.47	-11.1	0.58
B3LYP(non-GIAO)										
B3LYP/6-31G*	-29.3	-36.0	-3.83	-44.8	-28.1	-21.0	-9.19	-11.56	-11.3	-10.4
B3LYP/cc-pVTZ	-28.1	-34.0	-1.94	-44.1	-27.4	-18.5	-6.58	-8.70	-8.49	-7.45
CCSD(T)/6-31G*	-33.9	-37.2	-5.28	-48.9	-31.6	-22.6	-10.8	-13.14	-12.0	-12.0
CCSD(T)/cc-pVTZ	-34.6	-34.8	-2.63	-49.7	-30.5	-19.5	-7.70	-9.74	-9.49	-8.69
CCSD										
B3LYP/6-31G*	-24.1	-49.8	-17.6	-38.2	-29.6	-29.2	-18.6	-20.02	—	-18.8
B3LYP/cc-pVTZ	-23.7	-47.4	-15.8	-37.4	-28.5	-26.9	-16.4	-17.56	—	-16.4
CCSD(T)/6-31G*	-28.5	-50.8	-19.0	-42.2	-32.6	-30.6	-20.1	-21.66	—	-20.3
CCSD(T)/cc-pVTZ	-28.9	-48.0	-16.5	-42.6	-31.5	-27.6	-17.3	-18.60	—	-17.3

¹aug-cc-pVTZ(C,O) + aug-cc-pVDZ(H)

Table 4.2: B3LYP and CCSD specific rotation ($\text{deg dm}^{-1} (\text{g/mL})^{-1}$) for (*S*)-methyloxirane computed with various basis sets and optimized geometries at 355 nm. The center of mass is chosen to be the gauge origin.

Geometry Type	6-31G*	6-31++G**	6-311++G(2d,2p)	cc-pVDZ	cc-pVTZ	aug-cc-pVDZ	d-aug-cc-pVDZ	mixed-cc-pVTZ ²	aug-cc-pVTZ	Sadlej-pVTZ
B3LYP (GIAO)										
B3LYP/6-31G*	-51.9	-57.2	9.36	-122	-40.4	-5.19	20.3	6.29	11.4	46.8
B3LYP/cc-pVTZ	-51.5	-56.7	14.8	-119	-36.1	2.80	27.8	14.28	19.5	57.1
CCSD(T)/6-31G*	-67.7	-61.7	4.60	-135	-49.5	-9.87	17.3	0.68	6.97	41.8
CCSD(T)/cc-pVTZ	-73.9	-61.3	12.5	-138	-46.4	-0.52	28.9	10.08	16.6	52.6
B3LYP (non-GIAO)										
B3LYP/6-31G*	-76.0	-53.2	41.7	-117	-59.1	-11.7	25.4	14.69	15.7	19.4
B3LYP/cc-pVTZ	-74.1	-46.4	47.5	-114	-54.7	-4.01	33.2	23.44	24.1	25.5
CCSD(T)/6-31G*	-90.0	-58.2	37.8	-129	-68.3	-15.9	20.9	10.23	11.2	15.1
CCSD(T)/cc-pVTZ	-90.8	-47.9	46.3	-130	-63.9	-6.54	30.3	20.86	21.6	25.3
CCSD										
B3LYP/6-31G*	-65.0	-118	-22.4	-102	-71.0	-56.8	-24.3	-32.84	—	-24.9
B3LYP/cc-pVTZ	-63.1	-110	-17.0	-98.6	-67.4	-49.9	-17.8	-25.50	—	-17.7
CCSD(T)/6-31G*	-78.5	-120	-26.2	-114	-80.1	-60.6	-28.5	-37.59	—	-29.0
CCSD(T)/cc-pVTZ	-78.5	-111	-18.6	-114	-76.4	-51.4	-20.1	-28.17	—	-20.0

²aug-cc-pVTZ(C,O) + aug-cc-pVDZ(H)

The variation in the values of $[\alpha]_{355}$ (Table 4.2) with respect to basis set is even greater than that of $[\alpha]_{589}$. For the basis sets lacking diffuse functions, strong negative rotation angles are computed for all methods — even greater than $100 \text{ deg dm}^{-1} (\text{g/mL})^{-1}$ for CCSD/cc-pVDZ — in dramatic disagreement with the gas-phase CRDP result of $[\alpha]_{355} = +10.2 \text{ deg dm}^{-1} (\text{g/mL})^{-1}$ of Müller and co-workers. For the larger basis sets that include diffuse functions, the B3LYP predictions of $[\alpha]_{355}$ are positive, in qualitative to semi-quantitative agreement with experiment, while the CCSD results remain negative for all the basis sets used here. Furthermore, the B3LYP results show the correct direction of the dispersion in $[\alpha]_{\lambda}$ (more positive for 355 nm than for 589 nm) for several of the more diffuse basis sets, while CCSD rotation angles are consistently more negative at 355 nm than their 589 nm counterparts. In short, none of the coupled cluster calculations of $[\alpha]_{355}$ carried out in this work are in even qualitative agreement with the experimental data by Müller *et al.*

In addition, Tables 4.1 and 4.2 also reveal a surprisingly strong dependence of the computed values of $[\alpha]_{\lambda}$ on the choice of optimized geometry. Although computed values of $[\alpha]_{589}$ vary with structure by only a few $\text{deg dm}^{-1} (\text{g/mL})^{-1}$ for a given method and basis set, for the $[\alpha]_{355}$ data, the variation can be greater than $15 \text{ deg dm}^{-1} (\text{g/mL})^{-1}$, as observed for the B3LYP/Sadlej-pVTZ and CCSD/6-31G* levels of theory. This disparity occurs in spite of the rather small structural differences among the four optimized geometries shown in Fig. 4.1.

Optical rotation calculations were also carried out to assess the origin dependence of the CCSD results and the effect of using London orbitals/GIAOs with DFT. Tables 4.1 and 4.2 therefore include B3LYP optical rotation data both with and without GIAOs for the 355 and 589 nm wavelengths. For most basis sets, the non-GIAO B3LYP results differ little (usually less than $5 \text{ deg dm}^{-1} (\text{g/mL})^{-1}$) from their GIAO-based counterparts. Two notable exceptions are the Sadlej-pVTZ and

Table 4.3: CCSD specific rotation ($\text{deg dm}^{-1} (\text{g/mL})^{-1}$) for (*S*)-methyloxirane with the gauge origin placed at the center-of-mass (COM) or at the coordinates of the oxygen atom (O).

Geometry Type	CCSD/aug-cc-pVDZ				CCSD/d-aug-cc-pVDZ			
	355 nm		589 nm		355 nm		589 nm	
	COM	O	COM	O	COM	O	COM	O
B3LYP/6-31G*	-56.8	-77.8	-29.2	-36.2	-24.4	-55.7	-18.6	-28.9
B3LYP/cc-pVTZ	-49.9	-69.7	-26.9	-33.5	-17.8	-47.6	-16.4	-26.2
CCSD(T)/6-31G*	-60.6	-81.5	-30.6	-37.6	-28.5	-60.1	-20.1	-30.4
CCSD(T)/cc-pVTZ	-51.4	-71.1	-27.6	-34.2	-20.0	-50.0	-17.3	-27.1

the mixed aug-cc-pVTZ/aug-cc-pVDZ basis set results for $[\alpha]_{355}$: without GIAO's the B3LYP data shift by more than $25 \text{ deg dm}^{-1} (\text{g/mL})^{-1}$ towards the experimental result for the former and nearly $20 \text{ deg dm}^{-1} (\text{g/mL})^{-1}$ away from the experimental result for the latter. Table 4.3 reports CCSD/aug-cc-pVDZ and CCSD/d-aug-cc-pVDZ optical rotation data for 355 and 589 nm wavelengths for the four optimized structures computed at two choices of gauge origin: the molecular center-of-mass and the coordinates of the oxygen atom. In every case, the rotation becomes more negative as the origin shifts away from the center-of-mass — by as much as $30 \text{ deg dm}^{-1} (\text{g/mL})^{-1}$ for the d-aug-cc-pVDZ basis set — and the results are again much more sensitive for $[\alpha]_{355}$ than for $[\alpha]_{589}$.

The above results beg an important question: why does B3LYP appear to perform somewhat better for the 355 nm optical rotation than CCSD, giving rotation angles that are at least in qualitative agreement with the experimental result of Müller and co-workers? The answer lies in the ability of each method, B3LYP and CCSD, to describe the first-order pole structure (the Cotton effect) in $[\alpha]_\lambda$ implied by Eq. (4.1) as the frequency of the incident radiation approaches resonance with an electronic excitation. In CC response theory, the occurrence and shape of such a pole depends both on the structure of the perturbed wave functions, \hat{X}_μ^ω , determined in Eq. (4.4), and the dependence of the linear response function in Eq. (4.3) on these functions. The appearance of the EOM-CC response matrix, $\langle \Phi_i | (\bar{H} - \omega) | \Phi_j \rangle$ in Eq. (4.4) indicates that, as ω approaches an eigenvalue of \bar{H} (an excitation energy) the perturbed wave function components will become infinitely large (with variable sign). However, as noted previously by Christiansen *et al.*,¹¹⁷ although the CC linear response function contains terms that depend *quadratically* on the perturbed wave functions (*i.e.*, the second term on the right-hand side of Eq. (4.3), this does not obviate the ability of coupled cluster response theory to produce a correct first-order pole structure in $[\alpha]_\lambda$. (It is worth noting that this point is closely related to the ability of coupled cluster methods to describe correctly the first-order pole structure of vibrational force constants in pseudo-Jahn-Teller theory, a topic pertinent to studies of real and artifactual symmetry-breaking in polyatomic molecules.^{155–157})

Density-functional response theory, on the other hand, benefits from variational optimization of the component Kohn-Sham orbitals, and a linear response function that closely resembles that of the random-phase approximation (RPA):⁹²

$$\langle\langle \boldsymbol{\mu}; \mathbf{m} \rangle\rangle_\omega = \begin{pmatrix} \boldsymbol{\mu}_S & \boldsymbol{\mu}_{S^+} \end{pmatrix} \begin{pmatrix} \mathbf{A} - \omega \mathbf{I} & \mathbf{B} \\ -\mathbf{B} & -\mathbf{A} + \omega \mathbf{I} \end{pmatrix}^{-1} \begin{pmatrix} \mathbf{m}_S \\ \mathbf{m}_{S^+} \end{pmatrix} \quad (4.5)$$

where the submatrices \mathbf{A} and \mathbf{B} represent matrix elements of the Kohn-Sham effective Hamiltonian between excited determinants, and the property vectors include single excitations (subscript S) and single de-excitations (subscript S^+). The eigenvalues of the inverted response matrix appearing in Eq. (4.5) represent excitation energies, but because the TDDFT linear response function depends at most linearly on the (implicit) perturbed wave functions, the method will give a correct first-order pole at resonance.

Thus, two questions remain: (1) How well do CCSD and B3LYP methods predict the *position* of the pole in $[\alpha]_\lambda$, *i.e.*, the excitation energies of the system, and (2) how well do they reproduce the *shape* of the pole? Fig. 4.2 plots the optical rotatory dispersion spectrum of (*S*)-methyloxirane for the B3LYP/Sadlej-pVTZ, B3LYP/aug-cc-pVDZ, CCSD/Sadlej-pVTZ, and CCSD/aug-cc-pVDZ methods at the CCSD(T)/cc-pVTZ optimized geometry. As the radiation wavelength becomes shorter, all four methods predict an increase in $[\alpha]_\lambda$, as expected. However, the B3LYP method clearly rises more rapidly than its CCSD counterpart, in apparent agreement with the experimental data.

However, this behavior of the B3LYP linear response function stems from an *incorrect* prediction of the position of the pole. Table 4.4 reports vertical excitation energies for the lowest two excited states of (*S*)-methyloxirane — both of which are Rydberg transitions — using TDDFT/B3LYP and the EOM-CCSD method with several different basis sets that include diffuse functions, all using the CCSD(T)/cc-pVTZ optimized geometry. The corresponding experimental excitations reported by Cohen *et al.* are 7.12 eV (174.1 nm) and 7.75 eV (160.0 nm).¹⁰⁹ As can be seen from the table, the B3LYP method is in error by 0.5-0.6 eV *too low*. (Such errors of TDDFT with current

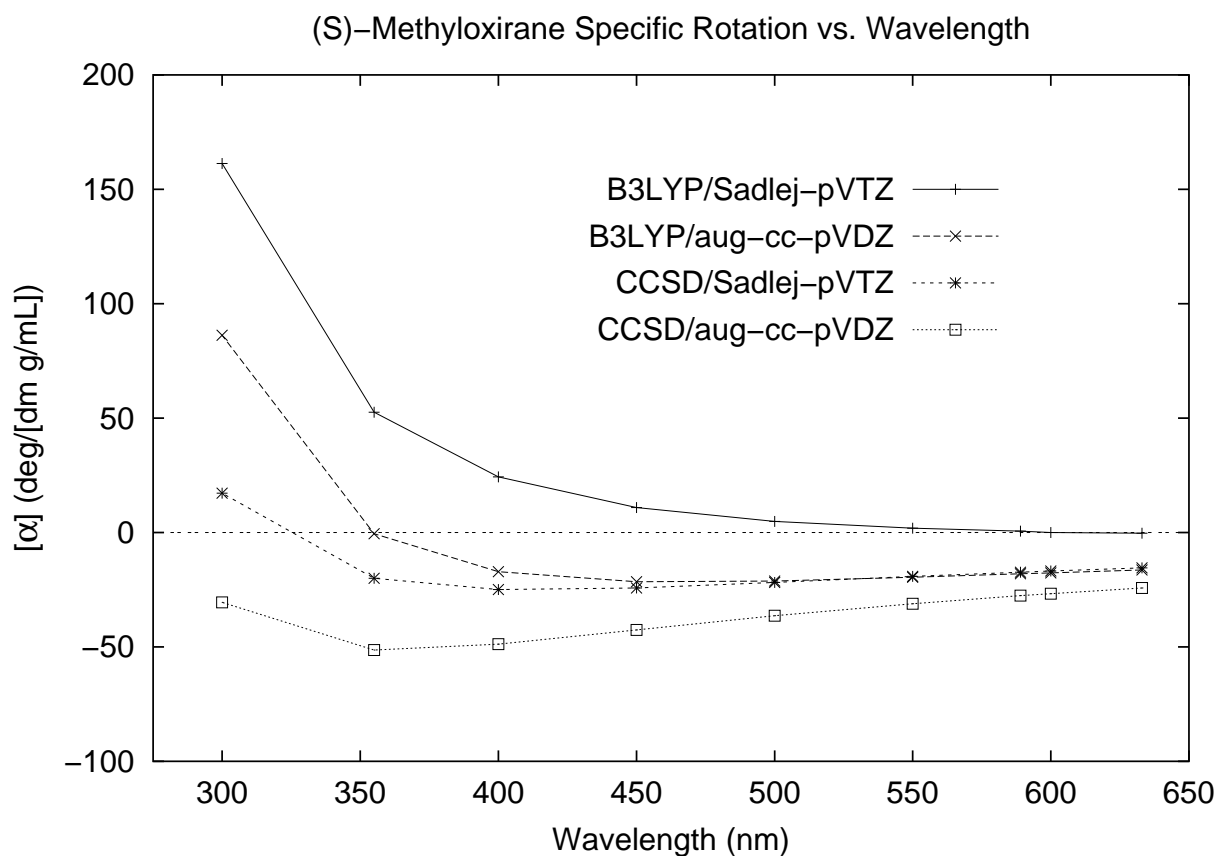


Figure 4.2: Calculated optical rotary dispersion curve for (*S*)-2-methyloxirane using B3LYP and CCSD linear response methods with the Sadlej-pVTZ and aug-cc-pVDZ basis sets.

functionals are common for Rydberg-type excitations.) Thus, the position of the B3LYP pole in $[\alpha]_{\lambda}$ is shifted *closer* to the 355 nm wavelength of the incident radiation, resulting in a faster rise in the rotation angle, and apparently fortuitously agreement with the experimental result of Müller and co-workers.

Table 4.4: EOM-CCSD and B3LYP-TDDFT excitation energies for the two lowest Rydberg states of (*S*)-methyloxirane computed with various basis sets and optimized geometries.

Geometry Type	EOM-CCSD						B3LYP/TDDFT					
	aug-cc-pVDZ		d-aug-cc-pVDZ		Sadlej-pVTZ		aug-cc-pVDZ		d-aug-cc-pVDZ		Sadlej-pVTZ	
	eV	nm	eV	nm	eV	nm	eV	nm	eV	nm	eV	nm
B3LYP/6-31G*	7.17	173	7.14	174	7.14	174	6.54	190	6.48	191	6.58	188
	7.63	162	7.38	166	7.42	167	6.98	176	6.89	180	7.03	176
B3LYP/cc-pVTZ	7.18	173	7.14	174	7.14	174	6.54	190	6.48	191	6.58	188
	7.48	166	7.39	168	7.60	163	6.99	178	6.89	180	7.03	176
CCSD(T)/6-31G*	7.16	173	7.13	174	7.13	174	6.53	190	6.48	191	6.57	189
	7.43	167	7.56	164	7.39	168	6.97	178	6.88	180	7.01	177
CCSD(T)/cc-pVTZ	7.19	172	7.15	173	7.16	173	6.55	189	6.49	191	6.59	188
	7.49	166	7.59	163	7.44	168	6.99	177	6.89	180	7.04	176

On the other hand, Table 4.4 shows that the EOM-CCSD method gives a lowest-energy excitation that is essentially identical to the experimental result (within only 0.05 eV). However, while the CCSD method clearly predicts a correct *position* of the pole, the width and curvature of the pole are clearly underestimated, resulting in poor agreement with the experimental value of $[\alpha]_{355}$ experimental value.

4.5 Conclusions

We have presented theoretical calculations of optical rotation angles for the difficult case of (*S*)-methyloxirane using TDDFT/B3LYP and coupled cluster linear response theories. We find that both methods are exquisitely sensitive to the choice of one-electron basis set and that diffuse functions have a particularly large impact on the computed values of $[\alpha]_{\lambda}$. Furthermore, both methods show a surprising sensitivity to the choice of optimized geometry, with $[\alpha]_{355}$ values varying by as much as $15 \text{ deg dm}^{-1} (\text{g/mL})^{-1}$ among structures that appear to differ only negligibly.

At first glance, the DFT optical rotation angles appear to be superior to those of the CCSD method. For example, the B3LYP $[\alpha]_{355}$ values computed with large, diffuse basis sets agree reasonably well with the experimental gas-phase results of Müller and co-workers, while those from CCSD are qualitatively incorrect. However, the success of DFT in this case may actually stem from a cancellation of errors. Specifically, the B3LYP functional underestimates the lowest electronic excitation energy of (*S*)-methyloxirane by 0.5-0.6 eV, thus shifting the first-order pole (the Cotton effect) in $[\alpha]_{\lambda}$ towards the experimentally chosen incident radiation lines, resulting in a fortuitous positive shift in the value of $[\alpha]_{355}$ towards the experimental result. On the other hand, while the

CCSD method correctly predicts the position of the pole, with a lowest excitation energy within only 0.05 eV of experiment, the shape/curvature of the ORD region near $\lambda = 355$ nm is still significantly in error.

We agree wholeheartedly with the assessment of Giorgio *et al.*¹⁰⁵ that the optical rotation of (*S*)-methyloxirane is one of the most difficult cases to be treated to date. In order to eventually resolve these discrepancies between theory and experiment, we are working to extend our coupled cluster response programs in two important directions: (1) implementation of GIAOs for CC optical rotation in an effort improve the dramatic basis set dependence of the computed rotation angles; and (2) inclusion of triple excitations in the CC ansatz [*e.g.*, the CC3 or EOM-CCSD(T) methods] to determine the importance of residual dynamic electron correlation effects. We will report on these developments in future publications.

Chapter 5

Ab Initio Determination of Optical Rotatory Dispersion in the Conformationally Flexible Molecule (*R*)-Epichlorohydrin

Reproduced in part with permission from Mary C. Tam and T. Daniel Crawford, *J. Phys. Chem. A.*, **110**, 2290-2298, 2006.

5.1 Introduction

Optical rotation — the rotation of plane-polarized light by samples of chiral species — occurs because such samples exhibit differing refractive indices for left- and right-circularly polarized light due to the dissymmetric electronic distributions inherent in chiral structures.^{5,6} For decades organic chemists have sought a deeper understanding of the various factors influencing optical rotation due to its intimate connection to absolute configuration, a property of great interest to the pharmaceutical industry, for example. *Ab initio* calculation of optical rotation¹⁵⁸ is of relatively new interest, beginning with the work of Polavarapu in 1997 at the Hartree-Fock level of theory,⁶⁴ and since its implementation in density functional theory (DFT)¹³⁷ in 2000,^{49,53,55,84,91,159} and more recently in coupled cluster (CC) theory,^{53,56,160–163} it has been used successfully to determine the absolute configurations of a variety of molecules.^{61,62} The development of ever more advanced theoretical techniques will improve our fundamental understanding of the relationship between molecular structure and optical rotation and help to design more robust tools for determining absolute configuration.^{55,164,165}

In order for theoretical predictions of properties such as optical rotation to be reliable in the determination of the absolute configurations of chiral molecules, they must correctly predict both the sign and magnitude of the specific rotation [*i.e.*, the total rotation, normalized for path length (dm) and concentration (g/mL)]. Such calculations naturally contain several “internal” sources of error, including those arising from truncation of the *N*-electron and one-electron spaces — electron correlation and basis set effects, respectively — as well as difficulties arising from zero-point vibrational motion.^{53,166–168} The comparison to experiment is further complicated by the wide variety of conditions under which optical rotation is measured in the laboratory, and “external”

factors such as solvation and temperature provide strong perturbations in many cases.¹⁰⁴

This work focuses specifically on the impact of conformational flexibility on theoretical determinations of optical rotation.^{99,169–172} When several conformers are present in a given sample at a specified temperature, the observed specific rotation may be approximated as a weighted average of the rotations of the individual conformers. In 2003, Polavarapu *et al.* addressed this issue for the small molecule, (*R*)-epichlorohydrin, both experimentally and using DFT,¹⁷⁰ and obtained its intrinsic rotation (*i.e.*, the limiting value of the specific rotation at zero concentration) in several solvents at 589 nm. Using the B3LYP^{138,139} functional and a variety of basis sets, they found that the optical rotation varied greatly (and antagonistically) with the C–C–C–Cl dihedral angle among the three minimum-energy conformations, referred to as *cis*, *gauche-I* and *gauche-II* (Fig. 5.1). Nevertheless, using conformer populations in several solvents (determined in a previous study,¹⁷³ where theoretical infrared absorption spectra were compared to those of experiment) and the B3LYP $[\alpha]_D$ values, they reported population-weighted specific rotations that compared reasonably well with the experimental solvent-phase data. For example, the observed intrinsic $[\alpha]_D$ for (*R*)-epichlorohydrin in CHCl₃ was $+3.2 \pm 1.5 \text{ deg dm}^{-1} (\text{g/mL})^{-1}$ as compared to the conformationally averaged B3LYP value of $+4 \pm 3 \text{ deg dm}^{-1} (\text{g/mL})^{-1}$. They further observed that corresponding shifts in conformer populations with solvent led to changes in both the magnitude and sign of the intrinsic rotation. In CH₂Cl₂, for example, the *g-I* conformer was found to be dominant with a mole fraction of 0.554 vs. 0.345 for the *g-II* conformer, while in CCl₄ these values were reversed to 0.352 and 0.559, respectively. The changes in conformer populations with solvent explain the dramatic difference in intrinsic rotation: $-22.4 \pm 0.1 \text{ deg dm}^{-1} (\text{g/mL})^{-1}$ in CH₂Cl₂ versus $+38.4 \pm 0.3 \text{ deg dm}^{-1} (\text{g/mL})^{-1}$ in CCl₄. Furthermore, the B3LYP values of $[\alpha]_D$ agreed reasonably well with experiment for each

liquid-phase environment, in spite of the fact that solvation effects were included only in the free energy and conformer population analysis and were ignored in the specific rotation calculations themselves.

The study by Polavarapu¹⁷⁰ left open two fundamental questions: (1) Are comparisons between the experimental condensed-phase data and (implicitly) gas-phase theoretical calculations robust? (2) How reliable is the time-dependent DFT (TD-DFT) B3LYP approach for optical rotation? That is, is the apparent success of DFT in the case of epichlorohydrin based on accurate rotations of the individual conformers or a providential averaging of inaccurate rotations?

Müller, Wiberg, and Vaccaro recently reported significant progress towards the answer to the first question with the development of the ultrasensitive cavity ring-down polarimetry (CRDP) technique, which has provided the first quantitative measurements of *gas-phase* optical rotation.^{102,103} Since their initial publication of the details of such measurements, they have applied the CRDP approach to a number of small molecules, including epichlorohydrin, thus allowing more systematic comparisons between experiment and state-of-the-art theoretical models.^{174,175} For the (*S*) enantiomer of epichlorohydrin, Wilson *et al.* recently reported specific rotations of $-238.7 \pm 2.3 \text{ deg dm}^{-1} (\text{g/mL})^{-1}$ at 355 nm and $-55.0 \pm 1.7 \text{ deg dm}^{-1} (\text{g/mL})^{-1}$ at 633 for a sample with 97% enantiomeric excess.¹⁷⁵ In addition, they carried out B3LYP-level DFT calculations in agreement with those reported earlier by Polavarapu,¹⁷⁰ and explained the shifts in conformer populations in polar solvents such as acetonitrile on the basis of the widely differing dipole moments of the three conformers.

The purpose of this work is to address the second question regarding the reliability and accuracy of theoretical models of optical rotation when applied to conformationally flexible molecules. Specifically, we compare the new gas-phase CRDP data of Wilson *et al.* with results from both DFT and

recently developed linear-response coupled cluster methods.^{53,56,160,162} Coupled cluster theory is widely considered the most robust quantum chemical method for small molecules and has been used for hyperaccurate predictions of a variety of properties including geometrical structures, thermochemical data, vibrational spectra, UV/vis spectra, NMR spin-spin coupling constants, etc.^{110–112} However, the overall dependability of coupled cluster theory for response properties such as optical rotation remains an open question. Epichlorohydrin is an excellent test case for such questions, because it is small (with only five non-hydrogen atoms) and therefore allows the application of state-of-the-art computational methods.

5.2 Computational Details

In 1928, Rosenfeld developed the quantum mechanical foundations for first-principles calculations of optical rotation, and demonstrated that, for a non-absorbing field of plane-polarized light of frequency ω , angle of rotation, $[\alpha]_\omega$, of the light is related to the trace of the β tensor:^{5,85,176}

$$\beta(\omega) = \frac{2}{\hbar} \text{Im} \sum_{n \neq 0} \frac{\langle 0 | \boldsymbol{\mu} | n \rangle \langle n | \mathbf{m} | 0 \rangle}{\omega_{n0}^2 - \omega^2} \quad (5.1)$$

where $\boldsymbol{\mu}$ and \mathbf{m} represent the electric and magnetic dipole operators, respectively, and the summation runs over all excited electronic (unperturbed) wave functions. In this work, we have computed β using the coupled cluster singles and doubles (CCSD) linear response approach^{115,160} in order to predict the optical rotation of the conformationally flexible chiral molecule (*R*)-epichlorohydrin. For comparison, time-dependent density functional theory (B3LYP)^{137–139} with gauge invariant atomic orbitals (GIAOs)¹³⁴ was also used to calculate the optical rotation.^{49,55,82,159} CCSD and B3LYP optical rotation calculations were carried out using several different basis sets: (1) the

split valence basis sets 6-31++G* and 6-311++G(2*d*,2*p*);¹⁷⁷ and (2) the correlation-consistent basis sets: aug-cc-pVDZ, aug-cc-pVTZ, and a mixed basis set denoted as “mixed-cc-pVTZ” which used the aug-cc-pVTZ basis set for carbon, oxygen, and chlorine and the cc-pVDZ basis set for hydrogen^{106,149,150,178} using wavelengths of 355, 589, and 633 nm for each conformer. The coupled cluster optical rotation calculations used both the length gauge (using the center of mass as the origin) and the “modified velocity gauge” (independent of origin) approach of Pedersen *et al.*¹⁶¹ for the electric-dipole operator.

To account for conformational flexibility, we assume that the specific rotation can be expressed as a sum of the products of each individual conformer’s optical rotation α_i and its corresponding mole fraction X_i :

$$\alpha_{\text{AVG}} = \alpha_A X_A + \alpha_B X_B + \alpha_C X_C + \dots \quad (5.2)$$

where *A* refers to the lowest energy conformation and *B*, *C*, etc. refer to higher energy conformations. The X_i s for each conformation of (*R*)-epichlorohydrin are dependent upon the Gibbs free energies of the conformations

$$X_i = X_A \exp\left(\frac{-(G_i - G_A)}{RT}\right) \quad (5.3)$$

and X_A may be determined from $X_A + X_B + X_C + \dots = 1$.

The individual conformations were identified using density functional theory with the B3LYP functional. Each geometry was optimized and harmonic vibrational frequencies were computed for the *cis*, *g*-I, and *g*-II conformations of (*R*)-epichlorohydrin using Dunning’s correlation-consistent cc-pVTZ basis set.¹⁰⁶

Because the conformationally averaged theoretical optical rotation is highly dependent on the accuracy of the corresponding free energies, we employed several methods for a systematic com-

parison: B3LYP/cc-pVQZ, CCSD/cc-pVDZ, the composite methods, Gaussian-2 (G2)^{179,180} and Gaussian-3 (G3)^{181,182} theory, as well as complete basis set (CBS) extrapolations of coupled cluster energies.^{183,184} CBS extrapolations of the Hartree-Fock energy were carried out using the following equation,

$$E_X^{\text{HF}} = E_\infty^{\text{HF}} + Ae^{-BX}, \quad (5.4)$$

where X is the cardinal number of the cc-pVXZ basis sets ($X=2$ for cc-pVDZ, 3 for cc-pVTZ, etc.). The extrapolations of the correlation components of the frozen-core coupled cluster energies were calculated using

$$E_X^{\text{CC}} = E_\infty^{\text{CC}} + AX^{-3}. \quad (5.5)$$

The Hartree-Fock CBS extrapolations were carried out using the cc-pVDZ, cc-pVTZ, and cc-pVQZ basis sets while the coupled cluster extrapolations used the cc-pVTZ and cc-pVQZ basis sets, the latter of which contains a total of 429 functions. The extrapolations were performed at the B3LYP/cc-pVTZ optimized geometry of each minimum-energy conformation. Harmonic vibrational frequencies were computed at the CCSD(T)/6-31G* level (using the corresponding optimized structure) to correct for zero point energy and thermal effects (assuming the ideal gas/rigid rotor model).¹⁸⁵ Liquid-phase conformer populations were also obtained for several solvents (CH₂Cl₂, CHCl₃, CCl₄, and cyclohexane) at the B3LYP/cc-pVQZ level of theory using the polarizable continuum model (PCM)¹⁸⁶ to obtain internal energies, with the same CCSD(T)/6-31G* vibrational/thermal corrections used for the CBS-CC gas-phase populations.

Vertical electronic transition energies were computed using both equation-of-motion CCSD (EOM-CCSD)¹²⁴ and TD-DFT/B3LYP^{147,148,187} approaches. All electrons were correlated for the geometry and vibrational frequency calculations, while core electrons (1s for C and Cl) were frozen

for single point energies, excitation energies, and CCSD optical rotation calculations (except for the CCSD/mixed-cc-pVTZ optical rotation calculations where the core electrons, 1s for C and 1s2s2p for Cl, were frozen due to memory constraints). Both length gauge and velocity gauge CCSD optical rotation calculations were carried out in order to test the significance of freezing the core electrons. For each wavelength, our results indicate that freezing the 1s2s2p electrons for Cl has little impact on the computed rotation. At the CCSD/aug-cc-pVDZ level of theory, the specific rotations computed when freezing only the 1s electrons for Cl differ less than $0.5 \text{ deg dm}^{-1} (\text{g/mL})^{-1}$ from values computed at the same level of theory where the 1s2s2p core electrons of Cl were frozen. Gaussian03¹⁵² was used for all B3LYP optimized geometries and optical rotation calculations. All coupled cluster single point energies and optical rotation calculations were performed using the PSI3 program package.¹²⁷ CCSD(T) geometry optimizations and vibrational frequency calculations were carried out using Aces2.¹⁵³

5.3 Results and Discussion

The B3LYP/cc-pVTZ optimized geometries of the three minimum-energy conformations of (*R*)-epichlorohydrin are reported in Fig. 5.1. Apart from the C–C–C–Cl dihedral angle, most of the structural parameters of the three conformations vary only slightly. The conformations are denoted as *cis*, *g*-I, and *g*-II with dihedral angles of -20.6° , -151.1° , and 94.0° , respectively, in agreement with earlier studies.¹⁷³ The lowest energy gas-phase conformation is the *g*-II structure, with the *g*-I and *cis* conformers somewhat higher in energy, at approximately 0.5 kcal/mol and 1.6 kcal/mol, respectively.

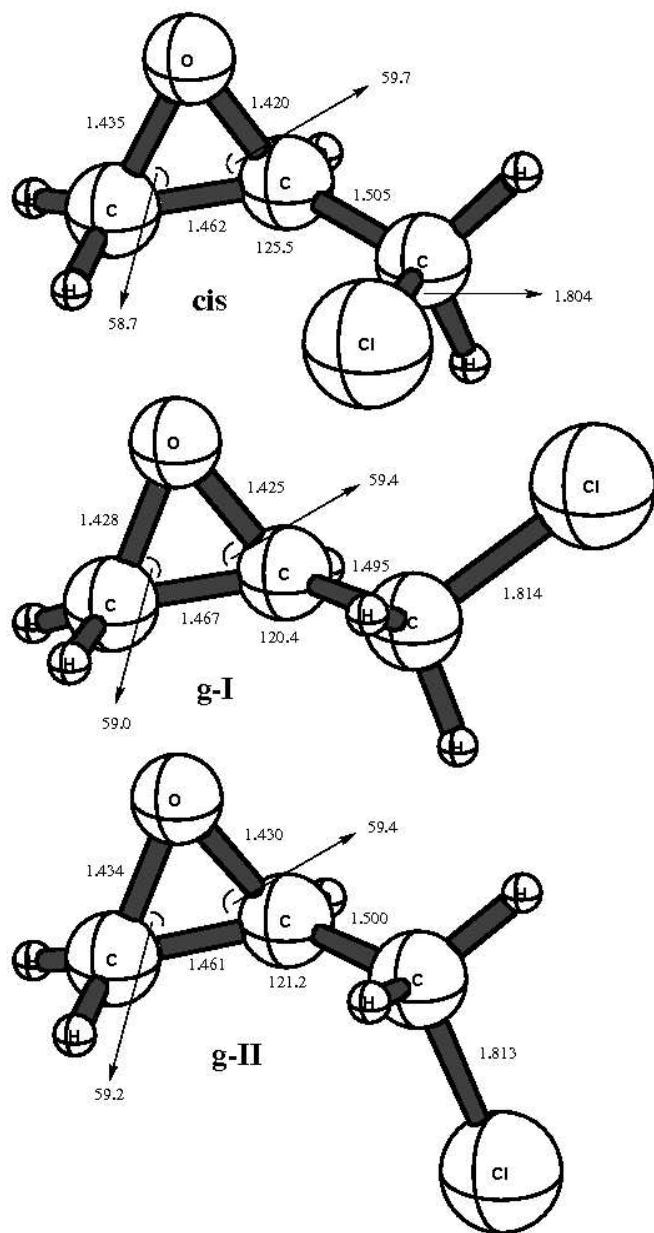


Figure 5.1: Optimized geometries of the three minimum-energy conformers — *cis*, *gauche*-I, and *gauche*-II — of (*R*)-epichlorohydrin at the B3LYP/cc-pVTZ level of theory. Bond lengths are given in Å and bond angles in degrees.

Tables 5.1, 5.2, and 5.3 summarize the computed values of individual conformer specific rotations in $\text{deg dm}^{-1} (\text{g/mL})^{-1}$ using a variety of basis sets at the B3LYP and CCSD levels of theory, using wavelengths of plane-polarized light of 355, 589, and 633 nm, respectively. For each wavelength, the *cis* and *g*-II conformations give positive values of $[\alpha]_{\lambda}$, while the *g*-I conformer gives a negative rotation. The specific rotation of the *cis* conformer is the least dependent on the choice of basis set, while the $[\alpha]_{\lambda}$ s for the *g*-I and *g*-II conformers show significant variation, especially between the split valence and correlation consistent basis sets. We also see that the variation between basis sets decreases for each individual conformation as the choice of wavelength increases. For each of the conformers, $[\alpha]_{\lambda}$ deviates very little between the aug-cc-pVDZ and mixed-cc-pVTZ basis sets for each method, suggesting that the smaller correlation consistent basis set is reasonably well converged for this property. Also, the B3LYP calculations show almost no variation of $[\alpha]_{\lambda}$ between the mixed-cc-pVTZ and aug-cc-pVTZ basis sets, which suggests that the lack of diffuse functions on hydrogen has a negligible effect on the computed optical rotation. It can also be seen from Tables 5.1, 5.2, and 5.3, that B3LYP consistently predicts optical rotation values which are much larger in magnitude than their CCSD counterparts for all of the basis sets and wavelengths used in this study and that the value of $[\alpha]_{\lambda}$ increases with decreasing wavelength.

Tables 5.1-5.3 report CCSD-level specific rotations for two choices of gauge for the electric-dipole operator: the origin-dependent length-gauge representation and the origin-independent modified velocity-gauge representation of Pedersen *et al.*¹⁶¹ For the latter, we have shifted the raw velocity-gauge rotation by its zero-frequency counterpart to account for the fact that this choice of gauge does not lead to the physically realistic result of $[\alpha]_{\lambda} = 0$ as $\lambda \rightarrow \infty$. As can be seen from the Tables, the choice of length- vs. velocity-gauge has a significant impact on the coupled cluster

Table 5.1: Specific rotations (in deg/[dm (g/cm³)]) of (*R*)-epichlorohydrin conformers at 355 nm. Computed at the B3LYP/cc-pVTZ optimized geometry.

Conformation	6-31++G*	6-311++G(2d,2p)	aug-cc-pVDZ	mixed-cc-pVTZ	aug-cc-pVTZ
B3LYP					
cis	301.7	282.3	277.0	279.2	278.8
g-II	625.5	633.1	608.4	608.5	600.3
g-I	-659.7	-574.3	-513.6	-491.9	-493.2
CCSD (Length Gauge)					
cis	123.8	177.6	165.5	164.8	-
g-II	520.0	559.4	499.6	508.3	-
g-I	-563.5	-493.0	-436.1	-442.8	-
CCSD (Modified Velocity Gauge)					
cis	203.6	176.7	171.0	177.1	-
g-II	422.5	504.5	438.0	473.3	-
g-I	-481.7	-484.4	-392.3	-412.9	-

Table 5.2: Specific rotations (in deg/[dm (g/cm³)]) of (*R*)-epichlorohydrin conformers at 589 nm. Computed at the B3LYP/cc-pVTZ optimized geometry.

Conformation	6-31++G*	6-311++G(2d,2p)	aug-cc-pVDZ	mixed-cc-pVTZ	aug-cc-pVTZ
B3LYP					
cis	72.5	66.5	63.0	64.9	64.7
g-II	177.9	179.3	172.1	171.5	169.5
g-I	-216.9	-187.3	-167.8	-159.7	-160.2
CCSD (Length Gauge)					
cis	25.1	44.7	38.9	40.6	-
g-II	153.2	167.2	146.5	149.9	-
g-I	-187.1	-163.9	-145.0	-146.0	-
CCSD (Modified Velocity Gauge)					
cis	52.4	44.6	41.0	43.2	-
g-II	124.1	149.9	127.2	139.2	-
g-I	-162.1	-162.4	-131.8	-137.3	-

Table 5.3: Specific rotations (in deg/[dm (g/cm³)]) of (*R*)-epichlorohydrin conformers at 633 nm. Computed at the B3LYP/cc-pVTZ optimized geometry.

Conformation	6-31++G*	6-311++G(2d,2p)	aug-cc-pVDZ	mixed-cc-pVTZ	aug-cc-pVTZ
B3LYP					
cis	60.9	55.8	52.7	54.4	54.2
g-II	151.2	152.5	146.4	145.9	144.1
g-I	-186.4	-160.8	-144.0	-137.1	-137.5
CCSD (Length Gauge)					
cis	20.7	37.7	32.5	34.2	-
g-II	130.8	142.7	124.9	127.9	-
g-I	-160.9	-141.0	-124.6	-125.5	-
CCSD (Modified Velocity Gauge)					
cis	44.2	37.6	34.4	36.3	-
g-II	105.8	128.0	108.4	118.7	-
g-I	-139.6	-139.8	-113.4	-118.1	-

specific rotations, particularly for shorter wavelengths. At 355 nm, the mixed-cc-pVTZ basis CCSD rotation for *g*-II, for example, varies from 508.3 deg dm⁻¹ (g/mL)⁻¹ in the length gauge to 473.3 deg dm⁻¹ (g/mL)⁻¹ in the velocity gauge. This variation is much smaller for longer wavelengths, but is nevertheless significant. The likely reason for this variation is the expected slower basis-set convergence of the velocity-gauge representation of the electric-dipole operator, though we note that, for coupled cluster methods, the two representations will not give identical results even in the limit of a complete basis set.^{131,158} Though both length- and velocity-gauge CCSD specific rotations are in semi-quantitative agreement with each other, both are significantly lower than the corresponding B3LYP rotations. Further study of the comparative behavior of the length- and velocity-gauge representations is clearly needed.

The differences between the B3LYP and CCSD specific rotations can be understood in terms of the relative abilities of the two methods to predict accurately the lowest-lying excitation energies that implicitly influence the computed optical rotation *via* Eq. (1). Table 5.4 summarizes the lowest vertical excitation energies for each of the three minimum-energy conformers of (*R*)-epichlorohydrin using equation-of-motion CCSD (EOM-CCSD) and TD-DFT/B3LYP. The energies vary only slightly among the individual conformers, but comparison between the EOM-CCSD and TD-DFT methods show more dramatic differences, with the latter falling below the former by approximately 0.7 eV. According to the gas-phase electronic circular dichroism (CD) spectrum measured by Basil *et al.* in 1991,¹⁸⁸ the lowest electronic excitation produces a positive CD band peaked at *ca.* 171.0 nm (7.25 eV), corresponding to a *n*(O) → 3s Rydberg excitation.

Table 5.4: EOM-CCSD and B3LYP-TDDFT excitation energies for (*R*)-epichlorohydrin computed with various basis sets at the B3LYP/cc-pVTZ optimized geometry.

Conformation	Individual Conformer Vertical Excitation Energies											
	EOM-CCSD						B3LYP/TDDFT					
	cc-pVTZ		aug-cc-pVDZ		6-311++G(2d,2p)		cc-pVTZ		aug-cc-pVDZ		6-311++G(2d,2p)	
	eV	nm	eV	nm	eV	nm	eV	nm	eV	nm	eV	nm
cis	7.55	164	7.38	168	7.34	169	6.91	179	6.63	187	6.62	187
g-II	7.53	167	7.35	169	7.33	169	6.90	180	6.68	186	6.66	186
g-I	7.46	166	7.30	170	7.28	170	6.85	181	6.84	181	6.57	189

This peak falls 0.03-0.13 eV below the corresponding EOM-CCSD vertical excitation energy (depending on the conformer and using the aug-cc-pVDZ and 6-311++G(2*d*,2*p*) basis-sets), but 0.41-0.68 eV above the B3LYP results (again depending on the conformer and with the same basis sets). Given that the computed optical rotation is inversely proportional to the difference in the squares of the excitation energy and chosen frequency of plane polarized light [*cf.* Eq. (1)], the consistent underestimation of vertical excitation energies by the B3LYP method leads to a concomitant overestimation of each conformer's $[\alpha]_{\lambda}$. (In addition, we note that B3LYP/aug-cc-pVDZ calculations indicate that this state is likely the major contributor to the measured gas-phase specific rotation with a rotational strength of *ca.* 11.3×10^{-40} cgs units.) This effect was also observed in (*S*)-methyloxirane¹⁶⁰ and (*P*)-[4]triangulane.¹⁶² On the other hand, the agreement between the EOM-CCSD excitation energies and experiment suggests greater reliability of the CCSD optical rotation values. We note, however, the theoretical specific rotations reported here are not yet converged in that the level of electron correlation remains limited to double-excitations at most, and other effects such as zero-point vibrational motion have been ignored.^{166,167}

An opposing example, however, is given by (*1S,4S*)-norbornenone, for which CCSD (length-gauge) and B3LYP specific rotations differ dramatically at -741 and -1216 deg dm⁻¹ (g/mL)⁻¹, respectively, with only the latter in reasonable agreement with the liquid-phase experimental value of *ca.* -1150 deg dm⁻¹ (g/mL)⁻¹. As Ruud *et al.* demonstrated, the B3LYP values of both the lowest excitation energy and its rotational strength agree well with experiment in this case, while the corresponding CCSD values are too large and too small, respectively.⁵⁶ However, the norbornenone case differs from that of epichlorohydrin in that its lowest excited state arises from a valence $n \rightarrow \pi^*$ excitation, a type of transition often well-reproduced by the B3LYP functional, as opposed to the

low-lying Rydberg transitions in epichlorohydrin. In addition, the comparison between theoretical gas-phase and experimental liquid-phase specific rotations is problematic, as demonstrated below.

Table 5.5 reports conformer populations for the gas phase using B3LYP, G2, G3, and CBS-extrapolated CC methods. In the gas phase the *g*-II conformation clearly dominates at 67-70%, followed by the *g*-I conformer at 24-27%, and finally the *cis* conformer at only about 5-7%. Note, however, that the gas-phase mole fractions vary only slightly with the level of theory, $\pm 3\%$ at most. Table 5.6 reports conformer populations for liquid-phase environments, including the neat state, methylenechloride, chloroform, carbon tetrachloride, and cyclohexane. The experimental data from Polavarapu *et al.*¹⁷⁰ were determined using comparisons between experimental infrared absorption spectra in several solvent environments with their theoretical counterparts (B3LYP/aug-cc-pVTZ). The theoretical liquid-phase populations were obtained at the B3LYP/cc-pVQZ level of theory, including PCM-based solvent corrections. For each solvent in Table 5.6, the *g*-I conformation clearly dominates with the exception of CCl₄ and cyclohexane, for which conformer *g*-II lies lower in energy, as in the gas phase. These data are also consistent with the more recent results of Wilson *et al.*, who observed a reversal of the sign of $[\alpha]_D$ in acetonitrile relative to the gas phase.¹⁷⁵ Clearly the solvent introduces significant perturbations to the system. However, the theoretical (B3LYP) populations are shifted significantly from the experimentally inferred values of Polavarapu *et al.*:¹⁷⁰ B3LYP tends to underestimate the population of the *cis* conformer relative to experiment (up to 6.8% for methylene chloride), and simultaneously overestimate that of the *g*-I conformer (up to 9.3% for chloroform).

Tables 5.7, 5.8, and 5.9 summarize the B3LYP and CCSD specific rotations for (*R*)-epichlorohydrin at 355, 589, and 633 nm, respectively, averaged using the populations reported in Tables 5.5 and

Table 5.5: Gas-phase conformer populations of (*R*)-epichlorohydrin.

Conformation	G2	G3	B3LYP/cc-pVQZ	CBS CCSD	CBS CCSD(T)
cis	0.055	0.073	0.034	0.059	0.064
g-II	0.708	0.682	0.648	0.670	0.676
g-I	0.237	0.245	0.318	0.271	0.259

Table 5.6: Liquid-phase conformer populations for (*R*)-epichlorohydrin.

Conformation	neat		CH ₂ Cl ₂		CHCl ₃		CCl ₄		cyclohexane
	Expt.	B3LYP	Expt.	B3LYP	Expt.	B3LYP	Expt.	B3LYP	
cis	0.114	0.043	0.111	0.041	0.108	0.044	0.089	0.038	
g-II	0.330	0.342	0.345	0.406	0.432	0.515	0.559	0.529	
g-I	0.556	0.615	0.544	0.553	0.460	0.441	0.352	0.433	

5.6. The gas-phase average $[\alpha]_{\lambda}$ values exhibit the same trend as seen for the individual conformer optical rotation results, with the B3LYP values always significantly larger than the CCSD values (using both length- and velocity-gauge). For the liquid-phase results, however, this is no longer the case. In fact, at 355 nm, CCSD predicts $[\alpha]_s$ which are larger in magnitude than those of B3LYP, and at 589 nm and 633 nm, B3LYP and CCSD give similar rotations. These data also indicate that, at all wavelengths and basis sets used in this study, the CCSD length-gauge values for $[\alpha]_{\lambda}$ are somewhat larger than the CCSD velocity gauge values.

Just as for the individual conformer rotations in Tables 5.1-5.3, correlation-consistent basis sets provide much more rapidly convergent rotations than the split-valence sets, suggesting that the latter may not be well-suited to describe this property. Also, our calculations do not show significant differences in $[\alpha]_{\lambda}$ between the aug-cc-pVDZ and mixed-cc-pVTZ basis sets for the B3LYP and CCSD (length gauge) methods individually. The velocity-gauge CCSD $[\alpha]_{\lambda}$ s appears to be somewhat more sensitive to the choice of basis set than its length-gauge counterpart, especially at 355 nm, where the difference in specific rotation between the two basis sets is approximately 20 $\text{deg dm}^{-1} (\text{g/mL})^{-1}$ for each of the methods used to compute the free energy. At all wavelengths, the conformationally averaged B3LYP $[\alpha]_{\lambda}$ determined using the mixed-cc-pVTZ and aug-cc-pVTZ basis sets for both the gas and liquid phases are not significantly different, indicating that the use of the larger basis set on the hydrogen atoms is not necessary in this case.

The best comparisons with experiment for all wavelengths in the gas phase are given by the CCSD length-gauge data. At 355 nm, Wilson *et al.*'s gas phase experimental value¹⁷⁵ of $-238.7 \pm 2.3 \text{ deg dm}^{-1} (\text{g/mL})^{-1}$ for the (*S*) enantiomer agrees extremely well with the length-gauge CCSD/mixed-cc-pVTZ specific rotation of $+240.0 \text{ deg dm}^{-1} (\text{g/mL})^{-1}$ for the (*R*) enantiomer,

computed with the populations obtained from complete basis set extrapolations of the CCSD(T) correlation energy. B3LYP optical rotations at 355 nm do not agree as well with the experimental value for any of the methods used, giving results that are too large by about 25%. The CCSD modified velocity-gauge gives values of $[\alpha]_{\lambda}$ that are closer to the experimental value than B3LYP, but are still too low by about $15 \text{ deg dm}^{-1} (\text{g/mL})^{-1}$ (6%). The same trend is found at 633 nm, where the length-gauge CCSD/mixed-cc-pVTZ specific rotation of $+56.3 \text{ deg dm}^{-1} (\text{g/mL})^{-1}$ for (*R*) compares well with the gas phase optical rotation of $-55.0 \pm 1.7 \text{ deg dm}^{-1} (\text{g/mL})^{-1}$ of Wilson *et al.* for (*S*).¹⁷⁵

At 589 nm, the experimental specific rotation for (*R*)-epichlorohydrin is $-41.94 \text{ deg dm}^{-1} (\text{g/mL})^{-1}$ in neat liquid.¹⁷⁵ The conformationally averaged results calculated using the theoretical gas-phase conformer populations for every method and basis set fail to produce the correct sign of the rotation and drastically overestimate its magnitude by a factor of more than two. Although this is clearly an apples-to-oranges comparison of the experimental and theoretical optical rotation data because of the lack of solvation modeling in the latter, the difference between the two serves to emphasize the need to include the effect of the solvent at least in the determination of conformer populations in order to obtain reasonable comparison with conventional polarimetry data in many cases. In addition, it may be necessary to explicitly include the effect of the solvent on the response function itself, though that does not appear to be the case for epichlorohydrin.

The conformationally averaged B3LYP and CCSD optical rotation values for the various liquid-phase environments shown in Tables 5.7-5.9 were calculated using the theoretical individual conformer optical rotations and the conformer populations given in Table 5.6, as determined both by PCM-corrected theoretical calculations and by Polavarapu *et al.*¹⁷⁰ Polavarapu *et al.* reported

Table 5.7: Specific rotations (in deg/[dm (g/cm³)]) for (*R*)-epichlorohydrin at 355 nm in gas- and liquid-phase environments. Computed at the B3LYP/cc-pVTZ optimized geometry.

		6-31++G*	6-311++G(2d,2p)	aug-cc-pVDZ	mixed-cc-pVTZ	aug-cc-pVTZ	
		B3LYP					
Gas-Phase	G2	303.0	327.5	324.1	329.5	323.3	
	G3	286.8	311.5	309.1	314.7	308.7	
	CBS CCSD(T)	272.1	298.0	296.7	302.5	296.6	
neat		-126.0	-78.2	-53.2	-40.9	-44.4	
Liquid-Phase	CH ₂ Cl ₂	Expt.	-109.6	-62.7	-38.8	-26.7	-30.3
		B3LYP	-179.2	-124.9	-96.2	-86.4	-82.7
	CHCl ₃	Expt.	-0.65	39.8	56.5	66.8	62.5
		B3LYP	-98.0	-48.5	-25.2	-17.2	-13.1
	CCl ₄	Expt.	144.3	176.9	184.0	191.9	186.8
		B3LYP	44.5	85.2	99.0	103.9	108.7
	cyclohexane		56.1	96.4	109.4	114.0	119.0
	CCSD (Length Gauge)						
	Gas-Phase	G2	241.3	288.8	259.4	263.9	-
		G3	225.4	273.4	245.8	250.0	-
CBS CCSD(T)		214.0	262.3	235.9	240.0	-	
neat		-127.6	-76.1	-58.7	-59.7	-	
Liquid-Phase	CH ₂ Cl ₂	Expt.	-113.4	-62.2	-46.5	-47.2	-
		B3LYP	-163.7	-104.6	-90.5	-91.7	-
	CHCl ₃	Expt.	-21.2	27.6	33.1	33.7	-
		B3LYP	-95.0	-37.9	-31.2	-31.3	-
	CCl ₄	Expt.	103.3	149.6	140.5	143.0	-
		B3LYP	24.7	78.4	72.2	73.7	-
	cyclohexane		35.2	88.7	81.3	83.0	-
	CCSD (Modified Velocity Gauge)						
	Gas-Phase	G2	196.0	251.7	226.4	246.9	-
		G3	184.8	237.8	214.9	234.4	-
CBS CCSD(T)		174.4	227.2	205.9	224.8	-	
neat		-105.2	-82.8	-54.1	-53.2	-	
Liquid-Phase	CH ₂ Cl ₂	Expt.	-93.7	-70.0	-43.3	-41.7	-
		B3LYP	-143.3	-118.2	-84.3	-84.7	-
	CHCl ₃	Expt.	-17.1	14.0	27.2	33.7	-
		B3LYP	-86.1	-55.6	-31.8	-28.6	-
	CCl ₄	Expt.	84.7	127.0	122.0	135.0	-
		B3LYP	14.1	53.7	60.1	69.4	-
	cyclohexane		22.2	63.2	67.9	77.9	-

Table 5.8: Specific rotations (in deg/[dm (g/cm³)]) for (*R*)-epichlorohydrin at 589 nm in gas- and liquid-phase environments. Computed at the B3LYP/cc-pVTZ optimized geometry.

		6-31++G*	6-311++G(2d,2p)	aug-cc-pVDZ	mixed-cc-pVTZ	aug-cc-pVTZ	
		B3LYP					
Gas-Phase	G2	78.5	86.1	85.5	87.1	85.5	
	G3	73.4	81.1	80.8	82.5	81.0	
	CBS CCSD(T)	68.9	77.1	77.1	78.9	77.4	
neat		-53.6	-37.4	-29.3	-24.8	-25.8	
Liquid-Phase	CH ₂ Cl ₂	Expt.	-48.6	-32.7	-24.9	-20.5	-21.5
		B3LYP	-69.6	-51.2	-41.7	-37.9	-36.9
	CHCl ₃	Expt.	-15.1	-1.6	4.0	7.6	6.5
		B3LYP	-44.6	-27.9	-20.2	-17.0	-15.9
	CCl ₄	Expt.	29.5	40.2	42.7	45.4	44.1
		B3LYP	-0.9	12.6	17.4	19.4	20.7
	cyclohexane		2.7	16.1	20.6	22.6	23.9
	CCSD (Length Gauge)						
Gas-Phase	G2	65.5	81.9	71.4	73.8	-	
	G3	60.4	77.0	67.1	69.4	-	
	CBS CCSD(T)	56.9	73.6	64.1	66.3	-	
neat		-50.6	-30.9	-27.8	-27.1	-	
Liquid-Phase	CH ₂ Cl ₂	Expt.	-46.1	-26.5	-24.0	-23.2	-
		B3LYP	-61.7	-41.8	-37.5	-36.9	-
	CHCl ₃	Expt.	-17.2	1.7	0.8	2.0	-
		B3LYP	-40.1	-20.8	-19.0	-18.1	-
	CCl ₄	Expt.	22.0	39.7	34.3	36.0	-
		B3LYP	-2.5	15.8	13.2	14.6	-
	cyclohexane		0.8	19.0	16.0	17.5	-
	CCSD (Modified Velocity Gauge)						
Gas-Phase	G2	52.3	70.0	61.0	68.4	-	
	G3	48.7	65.6	57.4	64.4	-	
	CBS CCSD(T)	45.4	62.3	54.6	61.5	-	
neat		-43.2	-35.8	-26.6	-25.5	-	
Liquid-Phase	CH ₂ Cl ₂	Expt.	-39.6	-31.7	-23.3	-21.9	-
		B3LYP	-55.1	-46.8	-35.9	-35.0	-
	CHCl ₃	Expt.	-15.3	-5.1	-1.3	1.7	-
		B3LYP	-37.0	-27.0	-19.5	-17.5	-
	CCl ₄	Expt.	16.9	30.6	28.4	33.4	-
		B3LYP	-5.3	7.5	9.2	13.1	-
	cyclohexane		-2.7	10.5	11.6	15.7	-

Table 5.9: Specific rotations (in deg/[dm (g/cm³)]) for (*R*)-epichlorohydrin at 633 nm in gas- and liquid-phase environments. Computed at the B3LYP/cc-pVTZ optimized geometry.

		6-31++G*	6-311++G(2d,2p)	aug-cc-pVDZ	mixed-cc-pVTZ	aug-cc-pVTZ	
		B3LYP					
Gas-Phase	G2	66.2	72.9	72.4	73.6	72.4	
	G3	61.9	68.6	68.3	69.6	68.5	
	CBS CCSD(T)	58.0	65.2	65.2	66.6	65.4	
neat		-46.8	-32.7	-25.8	-22.3	-22.7	
Liquid-Phase	CH ₂ Cl ₂	Expt.	-42.4	-28.7	-22.0	-18.6	-19.1
		B3LYP	-60.4	-44.4	-36.3	-33.0	-32.7
	CHCl ₃	Expt.	-13.8	-2.1	2.7	5.5	4.9
		B3LYP	-39.0	-24.6	-18.0	-15.2	-14.7
	CCl ₄	Expt.	24.4	33.6	35.8	37.9	37.0
		B3LYP	-1.6	10.1	14.2	16.0	16.7
	cyclohexane		1.5	13.0	16.9	18.6	19.4
	CCSD (Length Gauge)						
	Gas-Phase	G2	55.6	69.7	60.6	62.7	-
		G3	51.3	65.5	57.0	58.9	-
CBS CCSD(T)		48.2	62.5	54.3	56.3	-	
neat		-43.9	-27.0	-24.4	-23.7	-	
Liquid-Phase	CH ₂ Cl ₂	Expt.	-40.1	-23.3	-21.1	-20.4	-
		B3LYP	-53.4	-36.3	-32.6	-32.1	-
	CHCl ₃	Expt.	-15.3	0.9	0.1	1.2	-
		B3LYP	-34.9	-18.3	-16.8	-16.0	-
	CCl ₄	Expt.	18.43	33.5	28.8	30.4	-
		B3LYP	-2.7	13.0	10.8	12.0	-
	cyclohexane		0.2	15.8	13.2	14.5	-
	CCSD (Modified Velocity Gauge)						
	Gas-Phase	G2	44.3	59.5	51.7	58.1	-
		G3	41.2	55.7	48.6	54.7	-
CBS CCSD(T)		38.4	52.8	46.2	52.1	-	
neat		-37.6	-31.2	-23.4	-22.3	-	
Liquid-Phase	CH ₂ Cl ₂	Expt.	-34.5	-27.7	-20.5	-19.2	-
		B3LYP	-47.8	-40.7	-31.3	-30.5	-
	CHCl ₃	Expt.	-13.7	-5.0	-1.6	0.9	-
		B3LYP	-32.3	-23.7	-17.2	-15.5	-
	CCl ₄	Expt.	14.0	25.7	23.7	28.0	-
		B3LYP	-5.1	5.9	7.3	10.7	-
	cyclohexane		-2.9	8.5	9.4	12.9	-

intrinsic optical rotations of (*R*)-epichlorohydrin of $-22.4 \text{ deg dm}^{-1} (\text{g/mL})^{-1}$ in CH_2Cl_2 , $+3.2 \text{ deg dm}^{-1} (\text{g/mL})^{-1}$ in CHCl_3 , and $+38.5 \text{ deg dm}^{-1} (\text{g/mL})^{-1}$ in CCl_4 at 589 nm for the (*R*) enantiomer.¹⁷⁰ Using the experimentally inferred populations, the length-gauge CCSD results from Table 5.8 reproduce these values to within $\pm 2.0 \text{ deg dm}^{-1} (\text{g/mL})^{-1}$. The velocity-gauge CCSD results are similar in quality, while B3LYP brackets the experimental results vs. CCSD, but nevertheless gives a reasonable comparison. This indicates that, although the B3LYP specific rotations for the individual conformers may, in fact, be too large, the statistically averaged rotations can still agree well with experiment. In spite of the fact that the solvent was not considered in the calculation of the Rosenfeld tensors for the individual conformers, the averaged specific rotations compare extremely well to experiment.

On the other hand, conformer populations based on the PCM-corrected B3LYP/cc-pVQZ Gibbs free energies compare very poorly to experiment. In every case, the PCM-based average rotations are shifted towards more negative values, leading to underestimation of the positive CCl_4 rotation (*e.g.*, by approximately a factor of two at 355 nm with CCSD), overestimation of the negative CH_2Cl_2 rotation (again, by approximately a factor of two at 355 nm with CCSD), and the incorrect sign of the CHCl_3 rotation. This failure appears to result primarily from the overestimation of the *g-I* conformer population by the PCM-based free energies in Table 5.6 noted above.

Wilson *et al.* have also reported extrapolated cyclohexane solution phase data — obtained from the experimental optical rotatory dispersion curve ranging from 365 nm to 589 nm and then extrapolating to 355 nm and 633 nm — giving specific rotations of $-167.7 \text{ deg dm}^{-1} (\text{g/mL})^{-1}$ at 355 nm and $-30.4 \text{ deg dm}^{-1} (\text{g/mL})^{-1}$ at 633 nm for the (*S*) enantiomer of epichlorohydrin. The PCM-based rotations of the (*R*) enantiomer in cyclohexane given in Tables 5.1 and 5.3 are

too small by a factor of two at the CCSD/mix-cc-pVTZ level of theory. By comparison to the chlorine-based solvents above, this most likely occurs because of overestimation of the contribution of the *g*-*I* conformer’s negative rotation.

5.4 Conclusions

In this study, we have reported theoretical conformationally averaged values of the optical rotation at several polarized-field wavelengths for (*R*)-epichlorohydrin using coupled cluster and density functional theory. At 355 and 633 nm, the CCSD/aug-cc-pVTZ level of theory (using the length-gauge representation of the electric dipole operator and the cc-pVDZ basis set for hydrogen) does a remarkable job reproducing the gas-phase specific rotation reported by Wilson *et al.*¹⁷⁵ The corresponding velocity-gauge values underestimate the experimental gas-phase results at 355 and 633 nm by approximately 14 deg dm⁻¹ (g/mL)⁻¹ (6%) and 3 deg dm⁻¹ (g/mL)⁻¹ (5%), respectively. It remains unclear whether this is an intrinsic shortcoming of the “modified” velocity-gauge formulation¹⁶¹ or simply the result of slower basis-set convergence relative to the length-gauge approach. The B3LYP method overestimates the specific rotation for both wavelengths: approximately 58 deg dm⁻¹ (g/mL)⁻¹ (24%) at 355 nm and 10 deg dm⁻¹ (g/mL)⁻¹ (19%) at 633 nm. As for our earlier studies of the conformationally rigid molecules (*S*)-methyloxirane and (*P*)-[4]triangulane, we have rationalized these errors based on the concomitant underestimation of the lowest excitation energies of (*R*)-epichlorohydrin by the TD-DFT/B3LYP approach.

Comparison to the solution-phase experimental data of Polavarapu *et al.*¹⁷⁰ requires that solvent effects be considered in the Boltzmann averaging of the individual conformers. If this

factor is ignored, then both B3LYP and coupled cluster theories overestimate the magnitude of the conformationally averaged optical rotation by more than a factor of two, and even fail to reproduce the correct sign at 589 nm. However, when solvent effects are incorporated via experimental estimates of the conformer populations, both CCSD and B3LYP give reasonable comparison to experimental sodium D-line specific (intrinsic) rotations, in spite of the rather large differences in rotations for each conformer between the two methods. On the other hand, PCM-based estimates of the conformer populations compare poorly to experiment in this case.

Chapter 6

Coupled Cluster and Density

Functional Theory Optical Rotatory

Dispersion of the Conformationally

Flexible Molecules

(*R*)-3-chloro-1-butene and

(*R*)-2-chlorobutane

6.1 Introduction

In the last several years, correctly predicting the optical rotation of chiral molecules has proven to be a challenge to computational chemists. Although the theoretical background for calculating optical rotation has been known since 1928,⁸⁵ it was more than 50 years later when Amos developed the static limit electric-dipole magnetic-dipole linear response polarizability tensor,⁶³ that marked the pathway for calculations of this property. Only recently has it been implemented in density functional theory^{49–54} and in coupled cluster theory.^{53,56–60}

Because of the limited number of small rigid chiral molecules, this work focuses on benchmarking the calculated optical rotation of conformationally flexible molecules. When the optical rotation is experimentally determined, several conformations may be present in the sample at the experimental temperature. When predicting a theoretical value that is directly comparable to that of experiment, the optical rotation of each conformer must be computed and then statistically weighed to determine an averaged optical rotation.

Wiberg *et al.* addressed this issue by examining several different 3-substituted 1-butene using density functional theory (DFT) and demonstrated that, although replacing the substituent had little impact, the calculated specific rotation values varied significantly as a function of the dihedral angle of the carbon backbone.¹⁸⁹ For one specific case, 3-chloro-1-butene, the 0° dihedral angle conformation had a specific rotation value, $[\alpha]_D$, of +244 deg dm⁻¹ (g/mL)⁻¹ whereas the 180° conformation had an $[\alpha]_D$ value of -526 deg dm⁻¹ (g/mL)⁻¹. Their conformationally averaged results for this molecule, -112 deg dm⁻¹ (g/mL)⁻¹, overestimated the (liquid-phase) experimental value of -57.3 deg dm⁻¹ (g/mL)⁻¹ by a factor of two. In an effort to reconcile this discrepancy, they

also considered the impact of vibrational motion on the calculated rotations. After excluding the torsional motion of the carbon backbone, they reported a room-temperature vibrational correction of $+7.95 \text{ deg dm}^{-1} (\text{g/mL})^{-1}$, not enough to account for the difference between the experimental and theoretical optical rotation.

In 2005, Wiberg *et al.* continued with a similar study, in which the specific rotation of several 2-substituted butanes was addressed.¹⁹⁰ Their results indicated that even though each molecule exhibits significantly different electronic transitions, they have similar specific rotations. Since their results for 2-chlorobutane were similar to those previously described for 3-chloro-1-butene, they concluded that the double bond does not have a significant effect on the $[\alpha]_D$. However, unlike their earlier results for 3-chloro-1-butene,¹⁸⁹ the DFT specific rotation of $-37.1 \text{ deg dm}^{-1} (\text{g/mL})^{-1}$ agreed fairly well with the experimental value $-33.8 \text{ deg dm}^{-1} (\text{g/mL})^{-1}$.

The discrepancies in the the specific rotation for these two structurally similar molecules poses the question: Why is the B3LYP method capable of correctly predicting the specific rotation of (*R*)-2-chlorobutane and why does it overestimate the value for (*R*)-3-chloro-1-butene by a factor of two? It is also curious to compare density functional theory results to that of coupled cluster theory and see if this method is able to predict specific rotations which agree with the experimental values.

Previously, we reported theoretical conformationally averaged values of optical rotation for (*R*)-epichlorohydrin using coupled cluster theory and density functional theory.¹⁹¹ When comparing to experimental gas phase data at 355 and 633 nm, coupled cluster theory (length gauge) does a remarkable job reproducing the specific rotation, giving values which agree superbly with experimental CRDP gas phase results. Since it has been shown that coupled cluster theory is capable

of correctly predicting the specific rotation of conformationally flexible molecules at several wavelengths, it is hopeful that this method will succeed when applied to both (*R*)-3-chloro-1-butene and (*R*)-2-chlorobutane.

Most experimental optical rotation data is obtained using a specific solvent while theoretical predictions of this property refers to the gas phase. Previously, it has been shown that solvation effects can drastically influence the experimental optical rotation, making comparison with theory unreliable. Recently, Müller, Wiberg, and Vaccaro developed a new technique, cavity ring-down polarimetry (CRDP), which has eliminated this problem.^{103,192} This method allows direct comparison between theory and experiment by providing ultrasensitive measurements of optical rotation in the gas phase. CRDP gas phase data provided by Wilson, Vaccaro and Wiberg for (*S*)-3-chloro-1-butene gives optical rotation values of $+259.4 \pm 1.0 \text{ deg dm}^{-1} (\text{g/mL})^{-1}$ at 355 nm and $+53.3 \pm 1.0 \text{ deg dm}^{-1} (\text{g/mL})^{-1}$ at 633 nm.¹⁷⁵ For (*R*)-2-chlorobutane, the experimental gas phase specific rotation is $-121.4 \pm 1.2 \text{ deg dm}^{-1} (\text{g/mL})^{-1}$ at 355 nm and $-32.3 \pm 1.0 \text{ deg dm}^{-1} (\text{g/mL})^{-1}$ at 633 nm.¹⁷⁵ They also report neat liquid sodium D-line (589 nm) specific rotation values of $+51.6 \text{ deg dm}^{-1} (\text{g/mL})^{-1}$ and $-31.5 \text{ deg dm}^{-1} (\text{g/mL})^{-1}$ for (*S*)-3-chloro-1-butene and (*R*)-2-chlorobutane, respectively.

Since the previously published data indicate that the value of the theoretical optical rotation for the conformationally flexible molecules, (*R*)-3-chloro-1-butene and (*R*)-2-chlorobutane, is largely dependent on their respective dihedral angles along the carbon backbone, an effort has been made to assess these conformational effects on optical rotation using the coupled cluster level of theory, along with density functional theory (B3LYP) for comparison. Concomitantly, we have also calculated the differences in free energy among the three conformers of using several high levels of theory,

including complete-basis-set extrapolations. Since this pair of molecules are structurally similar (same heavy atoms, same connectivity, only differing by hydrogen saturation of double bond), they are an excellent test case to establish how conformational flexibility and structure affect the theoretical calculation of optical rotation.

6.2 Computational Details

Rosenfeld set the foundation for computing optical rotation when he showed that at a non-absorbing frequency, the angle of rotation, $[\alpha]_{\omega}$, can be computed using the β tensor:⁸⁵

$$\beta(\omega) = \frac{2}{\hbar} \text{Im} \sum_{n \neq 0} \frac{\langle 0 | \boldsymbol{\mu} | n \rangle \langle n | \mathbf{m} | 0 \rangle}{\omega_{n0}^2 - \omega^2} \quad (6.1)$$

where ω is the frequency of plane-polarized light, $\boldsymbol{\mu}$ and \mathbf{m} represent the electric and magnetic dipole operators, respectively, and the summation runs over the excited electronic (unperturbed) wave functions. For this research, the β tensor was implemented using the coupled cluster singles and doubles (CCSD) linear response theory.^{57,193} CCSD specific rotations for both (*R*)-3-chloro-1-butene and (*R*)-2-chlorobutane were computed, along with time-dependent density functional theory (B3LYP)^{36,194,195} values using gauge invariant atomic orbitals (GIAOs).^{49,52,55,82} Optical rotation calculations were carried out at 355, 589, and 633 nm wavelengths, using the following basis sets: (1) the split valence basis set 6-311++G(2d,2p)¹⁷⁷ and (2) the correlation consistent basis sets: aug-cc-pVDZ, aug-cc-pVTZ, and a mixed basis set denoted as “mixed-cc-pVTZ” which used the aug-cc-pVTZ basis set for carbon and chlorine, and the cc-pVDZ basis set for hydrogen.^{106,196,197} The coupled cluster optical rotation calculations used both the length gauge (using the center of mass as the origin) and the modified velocity gauge (independent of origin) for the electric dipole

operator.⁵⁸

Earlier work on (*R*)-epichlorohydrin¹⁹¹ describes in detail how the specific rotation is computed for conformationally flexible molecules. The observed specific rotation can be expressed as the sum of the products of the optical rotation for each individual conformer and its corresponding mole fraction. This paper also describes the methods used in this work to compute the free energies of each conformer, the Gaussian-2 (G2)^{198–200} and Gaussian-3 (G3)^{201,202} composite methods, along with complete basis set (CBS) extrapolations of Hartree-Fock and coupled cluster energies.^{203,204} The Hartree-Fock CBS extrapolations were carried out using the cc-pVDZ, cc-pVTZ, and cc-pVQZ basis sets while the coupled cluster extrapolations used only the cc-pVDZ and cc-pVTZ basis sets. (Earlier work for (*R*)-epichlorohydrin¹⁹¹ showed that the averaged optical rotation computed using CBS coupled cluster extrapolations carried out with the cc-pVDZ and cc-pVTZ basis sets were only slightly different (less than two deg dm⁻¹ (g/mL)⁻¹ at 355, 589 and 633 nm wavelengths) than the averaged optical rotation computed using extrapolated free energies computed with the cc-pVTZ and cc-pVQZ basis sets.)

The individual conformers for (*R*)-3-chloro-1-butene and (*R*)-2-chlorobutane were identified using density functional theory with the B3LYP functional^{36,194,195} and Dunning's correlation-consistent cc-pVTZ basis set.¹⁰⁶ In order to correct for zero point energy and thermal effects (assuming the ideal gas/rigid rotor model), vibrational frequencies were computed at the CCSD(T)/6-31G* level of theory. Vertical electronic transition energies were computed using the EOM-CCSD¹²⁴ and TD-DFT/B3LYP^{75,76} methods. All electrons were correlated for the geometry and vibrational frequency calculations, while core electrons (1s for C and Cl) were frozen for single point energies, excitation energies, and CCSD optical rotation calculations (except for the CCSD/mixed-cc-pVTZ

optical rotation calculations where the core electrons, 1s for C and 1s2s2p for Cl, were frozen due to memory constraints). All calculations were carried out using the B3LYP/cc-pVTZ optimized structure for each conformer using the (*R*)-enantiomer for both 3-chloro-1-butene and 2-chlorobutane. Gaussian03²⁰⁵ was used for all B3LYP optimized geometries, TD-DFT/B3LYP excitation energies, and optical rotation calculations. All coupled cluster single point energies, EOM/CCSD excitation energies, and optical rotation calculations were performed using the PSI3 program package.¹²⁷

6.3 Results and Discussion

6.3.1 (*R*) – 3 – chloro – 1 – butene

The B3LYP/cc-pVTZ optimized geometries of the three minimum-energy conformers of (*R*)-3-chloro-1-butene are reported in Fig. 6.1. Most of the structural parameters of each conformation, such as the bond angles and bond lengths, vary only slightly, but each conformer has a different C=C-C-C dihedral angle. The conformations are labeled as 0°, 120°, and 240°, in reference to their dihedral angle. The lowest energy conformation is the 120° structure, with the 0° and 240° conformers approximately 0.9 kcal/mole and 1.4 kcal/mole higher in energy, respectively.

Tables 6.1, 6.2, and 6.3 report the CCSD and B3LYP computed values of individual conformer specific rotations in $\text{deg dm}^{-1} (\text{g/mL})^{-1}$ using several basis sets at 355, 589, and 633 nm wavelengths. For each wavelength, the 120° and 240° conformers both have negative values of $[\alpha]_{\lambda}$, while the 0° conformer gives a positive specific rotation. With respect to basis set, the B3LYP method predicts consistent optical rotations values at 589 and 633 nm for each of the conformers. There

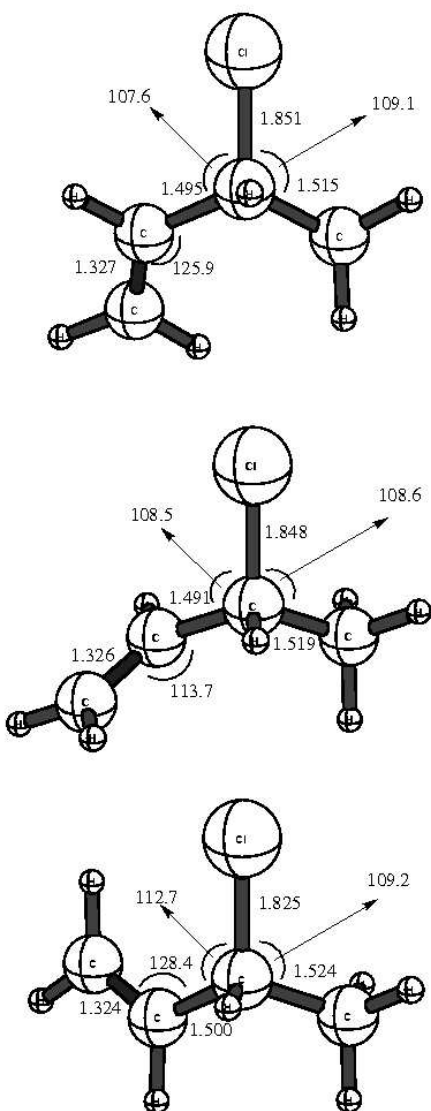


Figure 6.1: Optimized geometries of the three minimum-energy conformers of (*R*)-3-chloro-1-butene at the B3LYP/cc-pVTZ level of theory. Bond lengths are given in Å and bond angles in degrees.

is very little variation with its prediction at 355 nm. The B3LYP optical rotation results for the mixed-cc-pVTZ and aug-cc-pVTZ are not significantly different, indicating that the lack of augmented basis functions for hydrogen does not effect the computed rotation. On the other hand, both the CCSD length gauge and CCSD modified velocity gauge show somewhat significant variation between the split valence and correlation consistent basis sets, but the two correlation consistent basis sets, aug-cc-pVDZ and mixed-cc-pVTZ predict very similar results. These CCSD variants differ significantly when predicting the optical rotation of each individual conformer, with the length gauge always predicting larger $[\alpha]_{\lambda}$ s than the modified velocity gauge. The large difference between the two methods is especially emphasized at 355 nm, for the 0° and 120° conformations. For all the methods, the variation between basis sets decreases for each conformer as the wavelength increases. Also, B3LYP consistently predicts optical rotation values which are larger than those of CCSD, both length and modified velocity gauge.

Table 6.4 reports the gas-phase conformer populations computed using G2, G3, and complete basis set extrapolated CCSD and CCSD(T) energies. The 120° conformer dominates, while the other two conformers are present in almost equal amounts. The conformer populations vary only slightly with regards to the level of theory, with the exception of the Gaussian-2 method.

Tables 6.5, 6.6, and 6.7 report the B3LYP and CCSD specific rotations for (*R*)-3-chloro-1-butene averaged using the populations given in Table 6.4. Just like the results for the individual conformers, the B3LYP method consistently predicts larger $[\alpha]_{\lambda}$ s than both length gauge and modified velocity gauge CCSD methods for 355, 589, and 633 nm. Also, the CCSD modified velocity gauge results are always significantly smaller than those of CCSD length gauge. These trends, along with the fact that the correlation consistent basis sets are much more stable than the

Table 6.1: Specific Rotations (in deg/[dm (g/cm³)]) of the individual conformers of (*R*)-3-chloro-1-butene at 355 nm. Computed at the B3LYP/cc-pVTZ optimized geometry.

Dihedral Angle	6-311++G(2d,2p)	aug-cc-pVDZ	mixed-cc-pVTZ	aug-cc-pVTZ
B3LYP				
0	1356.2	1330.0	1342.6	1352.3
120	-874.9	-853.2	-862.9	-859.8
240	-485.9	-477.9	-481.6	-484.0
CCSD (Length Gauge)				
0	929.6	933.7	935.3	-
120	-649.5	-609.6	-614.9	-
240	-230.4	-330.4	-328.3	-
CCSD (Modified Velocity Gauge)				
0	808.2	769.5	783.3	-
120	-497.1	-445.2	-453.3	-
240	-328.9	-348.6	-346.9	-

Table 6.2: Specific Rotations (in deg/[dm (g/cm³)]) of the individual conformers of (*R*)-3-chloro-1-butene at 589 nm. Computed at the B3LYP/cc-pVTZ optimized geometry.

Dihedral Angle	6-311++G(2d,2p)	aug-cc-pVDZ	mixed-cc-pVTZ	aug-cc-pVTZ
B3LYP				
0	316.5	315.2	316.8	319.5
120	-190.5	-189.4	-190.1	-189.1
240	-130.0	-127.0	-128.4	-129.1
CCSD (Length Gauge)				
0	241.3	245.6	246.1	-
120	-165.8	-155.3	-157.0	-
240	-85.8	-92.4	-92.3	-
CCSD (Modified Velocity Gauge)				
0	209.5	199.7	203.9	-
120	-122.3	-108.6	-110.8	-
240	-91.3	-97.9	-97.9	-

Table 6.3: Specific Rotations (in deg/[dm (g/cm³)]) of the individual conformers of (*R*)-3-chloro-1-butene at 633 nm. Computed at the B3LYP/cc-pVTZ optimized geometry.

Dihedral Angle	6-311++G(2d,2p)	aug-cc-pVDZ	mixed-cc-pVTZ	aug-cc-pVTZ
B3LYP				
0	265.9	265.1	266.3	268.6
120	-159.1	-158.5	-159.0	-158.1
240	-110.2	-107.6	-108.7	-109.4
CCSD (Length Gauge)				
0	204.0	207.9	208.3	-
120	-140.0	-131.2	-132.6	-
240	-72.4	-78.5	-78.4	-
CCSD (Modified Velocity Gauge)				
0	177.2	168.8	172.5	-
120	-103.0	-91.4	-93.3	-
240	-77.5	-83.2	-83.2	-

Table 6.4: Gas-Phase Conformer Populations

Conformation	Computational Method			
	G2	G3	CBS CCSD	CBS CCSD(T)
(<i>R</i>)-3-chloro-1-butene				
0	0.129	0.148	0.142	0.154
120	0.754	0.698	0.718	0.705
240	0.117	0.154	0.140	0.141
(<i>R</i>)-2-chlorobutane				
60	0.245	0.209	0.222	0.218
180	0.597	0.632	0.622	0.618
300	0.157	0.159	0.156	0.164

split valence basis sets, are similar to the ones previously discussed for the individual conformers of (*R*)-3-chloro-1-butene. There is little difference between the B3LYP results for the aug-cc-pVTZ and the mixed-cc-pVTZ basis sets, indicating that the augmented functions for hydrogen are not necessary for proper prediction of specific rotation values. The difference between the aug-cc-pVDZ and mixed-cc-pVTZ is more interesting: B3LYP predicts averaged $[\alpha]_{\lambda}$ s which are similar for both basis sets, and the same for the CCSD length gauge results. However, the CCSD modified velocity gauge variant is much more sensitive, especially at 355 nm, where the difference between averaged $[\alpha]_{\lambda}$ s for the aug-cc-pVDZ and mixed-cc-pVTZ basis sets is approximately $25 \text{ deg dm}^{-1} (\text{g/mL})^{-1}$ or more for each of the energy methods.

These basic trends for both the individual conformers and the averaged $[\alpha]_{\lambda}$ s for (*R*)-3-chloro-1-butene are consistent with a previous study on the conformationally flexible molecule, (*R*)-epichlorohydrin.¹⁹¹ While the predicted averaged specific rotation for epichlorohydrin matched spot on with experimental gas-phase results at 355 and 633 nm, this is not the case for 3-chloro-1-butene. As mentioned previously, Wiberg *et al.* used density functional theory (B3LYP/6-311++G**) to predict a specific rotation for (*R*)-3-chloro-1-butene of $-112 \text{ deg dm}^{-1} (\text{g/mL})^{-1}$ which overestimated the experimental value by more than a factor of two, for 589 nm. Using the same wavelength, our best B3LYP value is $-102.4 \text{ deg dm}^{-1} (\text{g/mL})^{-1}$ computed using the aug-cc-pVTZ basis set and the CBS CCSD(T) energetic method; a value which still overestimates the experimental solution phase result. Even with better basis set and energetics, we were still unable to predict an accurate averaged specific rotation using density functional theory. However, CCSD length gauge does a much better job, coming in at $-85.9 \text{ deg dm}^{-1} (\text{g/mL})^{-1}$, while the modified velocity gauge variant produces the best result of $-60.6 \text{ deg dm}^{-1} (\text{g/mL})^{-1}$. Even though CCSD modified velocity gauge

Table 6.5: Specific Rotations (in deg/[dm (g/cm³)]) for (*R*)-3-chloro-1-butene at 355 nm.

Computed at the B3LYP/cc-pVTZ optimized geometry.

Method	6-311++G(2d,2p)	aug-cc-pVDZ	mixed-cc-pVTZ	aug-cc-pVTZ
B3LYP				
G2	-541.8	-527.9	-534.0	-530.7
G3	-484.3	-471.9	-477.3	-474.1
CBS CCSD	-503.8	-490.9	-496.5	-493.3
CBS CCSD(T)	-476.9	-464.5	-469.9	-466.6
CCSD (Length Gauge)				
G2	-396.9	-378.0	-381.6	-
G3	-351.0	-337.9	-341.1	-
CBS CCSD	-366.7	-351.5	-354.8	-
CBS CCSD(T)	-347.5	-332.9	-336.1	-
CCSD (Modified Velocity Gauge)				
G2	-309.2	-277.4	-281.5	-
G3	-277.8	-250.3	-253.6	-
CBS CCSD	-288.3	-259.3	-262.9	-
CBS CCSD(T)	-272.7	-244.8	-248.1	-

Table 6.6: Specific Rotations (in deg/[dm (g/cm³)]) for (*R*)-3-chloro-1-butene at 589 nm.

Computed at the B3LYP/cc-pVTZ optimized geometry.

Method	6-311++G(2d,2p)	aug-cc-pVDZ	mixed-cc-pVTZ	aug-cc-pVTZ
B3LYP				
G2	-118.1	-117.1	-117.6	-116.5
G3	-106.0	-105.0	-105.5	-104.5
CBS CCSD	-110.1	-109.1	-109.6	-108.5
CBS CCSD(T)	-104.0	-103.0	-103.5	-102.4
CCSD (Length Gauge)				
G2	-91.1	-96.3	-97.5	-
G3	-78.3	-86.2	-87.3	-
CBS CCSD	-82.6	-89.6	-90.7	-
CBS CCSD(T)	-76.5	-84.8	-85.9	-
CCSD (Modified Velocity Gauge)				
G2	-75.9	-61.7	-68.8	-
G3	-68.4	-61.3	-62.2	-
CBS CCSD	-70.9	-63.4	-64.4	-
CBS CCSD(T)	-66.9	-59.7	-60.6	-

Table 6.7: Specific Rotations (in deg/[dm (g/cm³)]) for (*R*)-3-chloro-1-butene at 633 nm.

Computed at the B3LYP/cc-pVTZ optimized geometry.

Method	6-311++G(2d,2p)	aug-cc-pVDZ	mixed-cc-pVTZ	aug-cc-pVTZ
B3LYP				
G2	-98.6	-97.9	-98.3	-97.4
G3	-88.6	-87.9	-88.2	-87.4
CBS CCSD	-92.0	-91.2	-91.6	-90.7
CBS CCSD(T)	-86.9	-86.2	-86.5	-85.6
CCSD (Length Gauge)				
G2	-87.8	-81.3	-82.3	-
G3	-78.6	-72.8	-73.7	-
CBS CCSD	-81.7	-75.7	-76.6	-
CBS CCSD(T)	-77.6	-71.6	-72.5	-
CCSD (Modified Velocity Gauge)				
G2	-63.9	-56.9	-57.9	-
G3	-57.6	-51.6	-52.3	-
CBS CCSD	-59.7	-53.3	-54.2	-
CBS CCSD(T)	-56.3	-50.2	-51.0	-

does better than B3LYP or CCSD length gauge, it is still off by approximately 17%, a factor which could be attributed to unaccounted solvent perturbations.

The best comparison with experimental data for 355 and 633 nm in the gas phase is given by the CCSD modified velocity gauge calculations. The B3LYP predicted values that are extremely overestimated by 80%, while the CCSD length gauge $[\alpha]_{355}$ is a little better, off by 30%, still not acceptable. Wilson *et al.*'s gas phase experimental value of $+259.4 \pm 1.0 \text{ deg dm}^{-1} (\text{g/mL})^{-1}$ agrees reasonable well with the CCSD/mixed-cc-pVTZ (modified velocity gauge) specific rotation of $-248.1 \text{ deg dm}^{-1} (\text{g/mL})^{-1}$, only off by approximately 4%. Comparing the experimental gas phase result of $+53.3 \pm 1.0 \text{ deg dm}^{-1} (\text{g/mL})^{-1}$ at 633 nm with the results from this study, we see that the trend is similar to that of 355 nm. The B3LYP values are significantly overestimated, along with the CCSD length gauge results. The best comparison is with the CCSD modified velocity gauge results of $-51.0 \text{ deg dm}^{-1} (\text{g/mL})^{-1}$.

The overestimation of the B3LYP method can be attributed to its poor prediction of the excited energies which are inherently related to the computed specific rotation. The vertical excitation energies for each of the conformers of (*R*)-3-chloro-1-butene and averaged excitations are given in Table 6.8. The results only vary slightly between basis set and conformer among each method. From Equation 6.1, we see that the computed optical rotation is inversely proportional to the difference in the squares of the excitation energy and chosen frequency of plane polarized light. Since the B3LYP method consistently predicts vertical excitation energies which are underestimated by approximately 0.7 eV, there is an inherent increase in $[\alpha]_{\lambda}$ for all wavelengths, therefore causing B3LYP to predict optical rotation values which are significantly larger in magnitude than coupled cluster theory.

Table 6.8: EOM-CCSD and B3LYP-TDDFT Excitation Energies Computed with Various Basis Sets at the B3LYP/cc-pVTZ Optimized Geometry.

individual conformer vertical excitation energies: (<i>R</i>)-3-chloro-1-butene								
Conformation	EOM-CCSD				B3LYP/TDDFT			
	aug-cc-pVDZ		6-311++G(2d,2p)		aug-cc-pVDZ		6-311++G(2d,2p)	
	eV	nm	eV	nm	eV	nm	eV	nm
120	6.93	179	6.82	182	6.14	202	6.11	203
0	6.87	180	6.88	180	6.11	203	6.08	204
240	7.13	174	7.20	172	6.38	194	6.41	194
conformationally averaged vertical excitation energies: (<i>R</i>)-3-chloro-1-butene								
G2	6.94	179	6.87	180	6.16	201	6.14	202
G3	6.95	178	6.89	180	6.17	201	6.15	202
CBS CCSD	6.95	178	6.88	180	6.17	201	6.15	202
CBS CCSD(T)	6.95	178	6.88	180	6.17	201	6.15	202
individual conformer vertical excitation energies: (<i>R</i>)-2-chlorobutane								
Conformation	EOM-CCSD				B3LYP/TDDFT			
	aug-cc-pVDZ		6-311++G(2d,2p)		aug-cc-pVDZ		6-311++G(2d,2p)	
	eV	nm	eV	nm	eV	nm	eV	nm
180	7.37	168	7.32	170	6.92	179	6.86	181
60	7.35	169	7.28	170	6.78	183	6.74	184
300	7.37	168	7.31	170	6.89	180	6.85	181
conformationally averaged vertical excitation energies: (<i>R</i>)-2-chlorobutane								
G2	7.37	168	7.31	170	6.88	180	6.83	182
G3	7.37	168	7.31	170	6.89	180	6.83	182
CBS CCSD	7.37	168	7.31	170	6.89	180	6.83	182
CBS CCSD(T)	7.37	168	7.31	170	6.89	180	6.83	182

6.3.2 (*R*) – 2 – chlorobutane

Fig. 6.2 gives the three minimum-energy B3LYP/cc-pVTZ optimized geometries of (*R*)-2-chlorobutane. The dihedral angle of the carbon backbone is the only structure parameter of significant difference between each conformer. The three conformations of 2-chlorobutane are denoted as 60°, 180°, and 300°, according to the appropriate dihedral angle. The lowest energy conformation is the 180° structure, with the 60° and 300° conformers approximately 0.6 kcal/mole and 0.9 kcal/mole higher in energy, respectively.

The CCSD and B3LYP specific rotation values at 355, 589, and 633 nm are reported in $\text{deg dm}^{-1} (\text{g/mL})^{-1}$ in Tables 6.9, 6.10, and 6.11. Just like our results for (*R*)-3-chloro-1-butene, at 589 and 633 nm, the B3LYP method for (*R*)-2-chlorobutane predicts consistent optical rotation values with regard to basis set, while the results for 355 nm are much more sensitive. Again, the insignificance of augmented basis functions for hydrogen is confirmed because the B3LYP mixed-cc-pVTZ and aug-cc-pVTZ results differ only slightly. The basis set dependence between the split-valence and the correlation consistent basis sets is much more pronounced in both the CCSD length and modified velocity gauge methods, especially at 355 nm where the difference between $[\alpha]_{\lambda\text{s}}$ can be larger than $20 \text{ deg dm}^{-1} (\text{g/mL})^{-1}$. Furthermore, the difference between the aug-cc-pVDZ and mixed-aug-cc-pVTZ basis sets is much more pronounced for (*R*)-2-chlorobutane especially for the CCSD method at 355 nm. For example, the CCSD length gauge predicts $[\alpha]_{355\text{s}}$ which vary by approximately $20 \text{ deg dm}^{-1} (\text{g/mL})^{-1}$ between the two basis sets for the 180° conformation.

The gas-phase conformer populations can be found in Table 6.4. Values were computed using the G2, G3, and CBS CCSD and CBS CCSD(T) energies. Results show that for all methods, the 180° dominates, while the 60° and 300° conformers are only present in small amounts. The

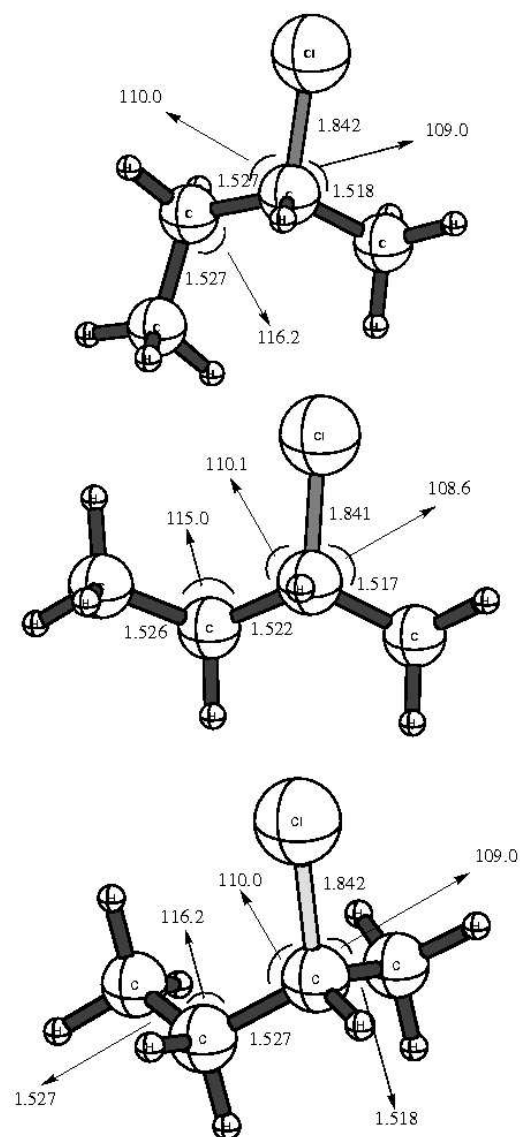


Figure 6.2: Optimized geometries of the three minimum-energy conformers of (*R*)-2-chlorobutane at the B3LYP/cc-pVTZ level of theory. Bond lengths are given in Å and bond angles in degrees.

Table 6.9: Specific Rotations (in deg/[dm (g/cm³)]) of the individual conformers of (*R*)-2-chlorobutane at 355 nm. Computed at the B3LYP/cc-pVTZ optimized geometry.

Dihedral Angle	6-311++G(2d,2p)	aug-cc-pVDZ	mixed-cc-pVTZ	aug-cc-pVTZ
B3LYP				
60	48.1	51.6	43.1	46.4
180	-290.8	-284.3	-273.5	-274.4
300	176.5	157.4	167.5	169.0
CCSD (Length Gauge)				
60	25.9	41.6	30.1	-
180	-248.1	-222.4	-242.8	-
300	148.6	129.1	144.4	-
CCSD (Modified Velocity Gauge)				
60	20.4	41.0	44.7	-
180	-234.5	-212.0	-231.2	-
300	169.1	124.2	152.2	-

Table 6.10: Specific Rotations (in deg/[dm (g/cm³)]) of the individual conformers of (*R*)-2-chlorobutane at 589 nm. Computed at the B3LYP/cc-pVTZ optimized geometry.

Dihedral Angle	6-311++G(2d,2p)	aug-cc-pVDZ	mixed-cc-pVTZ	aug-cc-pVTZ
B3LYP				
60	16.5	17.5	14.9	15.8
180	-90.8	-88.8	-85.0	-85.2
300	58.2	52.2	55.6	55.2
CCSD (Length Gauge)				
60	9.6	14.6	10.5	-
180	-80.0	-70.9	-77.4	-
300	49.8	43.2	47.2	-
CCSD (Modified Velocity Gauge)				
60	7.8	14.3	15.3	-
180	-75.8	-67.8	-63.3	-
300	57.1	41.9	49.9	-

Table 6.11: Specific Rotations (in deg/[dm (g/cm³)] of the individual conformers of (*R*)-2-chlorobutane at 633 nm. Computed at the B3LYP/cc-pVTZ optimized geometry.

Dihedral Angle	6-311++G(2d,2p)	aug-cc-pVDZ	mixed-cc-pVTZ	aug-cc-pVTZ
B3LYP				
60	14.3	15.1	13.6	12.9
180	-77.7	-76.1	-72.9	-72.8
300	50.0	44.9	47.4	47.8
CCSD (Length Gauge)				
60	8.4	12.6	9.0	-
180	-68.0	-60.8	-66.4	-
300	42.8	37.1	40.5	-
CCSD (Modified Velocity Gauge)				
60	6.8	12.3	13.2	-
180	-65.0	-58.2	-63.3	-
300	49.2	36.0	42.9	-

conformer populations are consistent throughout each method used, except for the G2 method.

Using the conformer populations given in Table 6.4, we then predicted averaged specific rotation values for (*R*)-2-chlorobutane. The B3LYP and CCSD computed averaged rotations are reported in Tables 6.12, 6.13, and 6.14. The results are similar to those previously discussed for (*R*)-3-chloro-1-butene: the correlation consistent basis sets are again more stable than the split-valence basis sets, and the B3LYP method predicts averaged $[\alpha]_{DS}$ that are larger in magnitude than both of the CCSD methods. The vertical excitation energies for each conformer of (*R*)-2-chlorobutane and the corresponding averaged values are reported in Table 6.8. Again we see that B3LYP predicts smaller excitation energies than the EOM-CCSD method, by approximately 0.5 eV, causing B3LYPs overestimation of specific rotation.

When comparing to the gas experimental data, both CCSD and B3LYP do a reasonable job predicting the specific rotation of (*R*)-2-chlorobutane. At 355 nm, the most sensitive wavelength, the CCSD length gauge variant predicts a value of $-119.9 \text{ deg dm}^{-1} (\text{g/mL})^{-1}$, which agrees remarkably well with the CRDP gas phase result of $-121.4 \pm 1.2 \text{ deg dm}^{-1} (\text{g/mL})^{-1}$. The B3LYP values of $-132.1 \text{ deg dm}^{-1} (\text{g/mL})^{-1}$ only overestimates the experimental value by 9%. The CCSD modified velocity gauge does the poorest job at 355 nm, underestimating by 11%.

At 633 nm, predicted specific rotation values are in much better agreement for each method used in this study. Averaged B3LYP and CCSD length gauge $[\alpha]_{633}$ are only overestimated by 2 $\text{deg dm}^{-1} (\text{g/mL})^{-1}$ from the gas phase experimental value of $-32.3 \pm 1.0 \text{ deg dm}^{-1} (\text{g/mL})^{-1}$. CCSD modified velocity gauge also does a remarkable job predicting an $[\alpha]_{633}$ of $-29.2 \text{ deg dm}^{-1} (\text{g/mL})^{-1}$, which is under the gas phase number by only 4 $\text{deg dm}^{-1} (\text{g/mL})^{-1}$. At 589 nm, the $[\alpha]_D$ for (*R*)-2-chlorobutane is $-31.5 \text{ deg dm}^{-1} (\text{g/mL})^{-1}$ in neat liquid. Although comparison between theory

Table 6.12: Specific Rotations (in deg/[dm (g/cm³)]) for (*R*)-2-chlorobutane at 355 nm.

Computed at the B3LYP/cc-pVTZ optimized geometry.

Method	6-311++G(2d,2p)	aug-cc-pVDZ	mixed-cc-pVTZ	aug-cc-pVTZ
B3LYP				
G2	-134.0	-132.3	-126.1	-126.1
G3	-145.5	-143.7	-136.8	-136.9
CBS CCSD	-142.7	-140.9	-134.3	-134.2
CBS CCSD(T)	-140.3	-138.7	-132.1	-132.0
CCSD (Length Gauge)				
G2	-118.4	-102.3	-114.9	-
G3	-127.6	-111.2	-124.1	-
CBS CCSD	-125.5	-109.0	-121.9	-
CBS CCSD(T)	-123.4	-107.2	-119.9	-
CCSD (Modified Velocity Gauge)				
G2	-108.4	-97.0	-103.1	-
G3	-116.9	-105.6	-112.4	-
CBS CCSD	-115.0	-103.5	-110.2	-
CBS CCSD(T)	-112.8	-101.8	-108.2	-

Table 6.13: Specific Rotations (in deg/[dm (g/cm³)]) for (*R*)-2-chlorobutane at 589 nm.

Computed at the B3LYP/cc-pVTZ optimized geometry.

Method	6-311++G(2d,2p)	aug-cc-pVDZ	mixed-cc-pVTZ	aug-cc-pVTZ
B3LYP				
G2	-41.0	-40.5	-38.3	-38.3
G3	-44.6	-44.1	-41.7	-41.7
CBS CCSD	-43.8	-43.2	-40.9	-40.9
CBS CCSD(T)	-43.0	-42.5	-40.2	-40.2
CCSD (Length Gauge)				
G2	-37.6	-32.0	-36.2	-
G3	-40.6	-34.9	-39.2	-
CBS CCSD	-39.9	-34.2	-38.5	-
CBS CCSD(T)	-39.2	-33.6	-37.9	-
CCSD (Modified Velocity Gauge)				
G2	-34.4	-30.4	-26.2	-
G3	-37.1	-33.2	-28.8	-
CBS CCSD	-36.5	-32.5	-28.2	-
CBS CCSD(T)	-35.8	-31.9	-27.6	-

Table 6.14: Specific Rotations (in deg/[dm (g/cm³)]) for (*R*)-2-chlorobutane at 633 nm.

Computed at the B3LYP/cc-pVTZ optimized geometry.

Method	6-311++G(2d,2p)	aug-cc-pVDZ	mixed-cc-pVTZ	aug-cc-pVTZ
B3LYP				
G2	-35.1	-34.7	-32.8	-32.8
G3	-38.2	-37.7	-35.7	-35.7
CBS CCSD	-37.4	-37.0	-35.0	-35.0
CBS CCSD(T)	-36.8	-36.4	-34.3	-34.4
CCSD (Length Gauge)				
G2	-31.8	-27.4	-31.1	-
G3	-34.4	-29.9	-33.6	-
CBS CCSD	-33.8	-29.3	-33.0	-
CBS CCSD(T)	-33.2	-28.8	-32.4	-
CCSD (Modified Velocity Gauge)				
G2	-29.4	-26.0	-27.8	-
G3	-31.8	-28.4	-30.4	-
CBS CCSD	-31.3	-27.8	-29.8	-
CBS CCSD(T)	-30.7	-27.4	-29.2	-

and experiment is unfair at this wavelength because there is no consideration of solvent effects, the CCSD method for both length and modified velocity gauges correctly predicts the specific rotation. B3LYP's averaged specific rotation is comparable to experiment but still slightly overestimated.

6.3.3 Comparison

One of the purposes of this research was to see if coupled cluster theory was capable of predicting the specific rotation of the structurally similar molecules (*R*)-3-chloro-1-butene and (*R*)-2-chlorobutane. From our calculations, we see that for both molecules, overall, coupled cluster theory predicts values which are comparable with gas-phase experimental data. Specifically for the butene, it is the coupled cluster modified velocity gauge that does the best job, underestimating the magnitude by only 4%, for both the 355 and 633 nm. On the other hand, the coupled cluster length gauge variant performs the best for (*R*)-2-chlorobutane matching spot on with experimental specific rotations in the gas-phase. Like Wiberg *et al.*, we see the same discrepancies in the B3LYP method, which overestimates the rotations by 80% (355 nm) and 61% (633 nm) for the butene, but does a reasonably good job for the butane, only overestimating by 9% (355 nm) and 7% (633 nm). Why does this occur? The answer lies in the calculated rotations of the individual conformers. The B3LYP method predicts values which are significantly larger than both CCSD variants for the individual conformers of (*R*)-3-chloro-1-butene. Although the same trend is seen with (*R*)-2-chlorobutane, B3LYP's overestimation of the individual conformers' specific rotations is not as apparent. In fact, there is only a slight variation in the conformers' calculated rotations for all the methods.

6.4 Conclusions

In this study, we have reported theoretical values of optical rotation for the conformationally flexible molecules (*R*)-3-chloro-1-butene and (*R*)-2-chlorobutane at 355, 589, and 633 nm. Our results indicate that for (*R*)-3-chlorobutene, at all wavelengths, the CCSD modified velocity gauge variant does the best job reproducing experimental values, especially at 355 nm, where our CCSD/mixed-cc-pVTZ results are only off by approximately 4%. As the wavelength increases, so does the overestimation of all theoretical results. Also, our results show that the B3LYP method consistently predicts specific rotation values that are significantly greater in magnitude than their coupled cluster counterparts. This method fails to correctly predict $[\alpha]_D$ at all wavelengths, drastically overestimating by 80% and 61%, for 355 nm and 633 nm, respectively. The same trends with regard to basis set and method are reproduced for (*R*)-2-chlorobutane, but in this case, each method predicts the averaged rotation for each wavelength reasonably well. These results are comparable to gas phase value at 355 nm and 633 nm, and also with 589 nm neat liquid experimental data.

Since (*R*)-3-chloro-1-butene and (*R*)-2-chlorobutane are both conformationally flexible and very similar in structure, it is very interesting to compare the averaged specific rotation results for the two molecules. We see the same types of errors when computing specific rotation using both the CCSD and B3LYP methods for the individual conformations, and the same trends for basis set and wavelength dependence. After averaging the individual rotations, the CCSD method is the most comparable with experiment of all the methods studied for both molecules. Even though B3LYP does a better job for (*R*)-2-chlorobutane, this is not the case for (*R*)-3-chloro-1-butene. Its success with (*R*)-2-chlorobutane results from a cancellation of errors.

Chapter 7

Coupled Cluster and Density

Functional Theory Calculations of

Optical Rotation for

(*R*)-Methylthiirane

7.1 Introduction

Accurately predicting the optical rotation (OR) of a chiral molecule allows for the determination of its absolute configuration, a task that is experimentally difficult to accomplish through total molecular synthesis and x-ray crystallography. Using *ab initio* calculations of optical rotation as a pathway to determine the absolute configuration has recently become a popular focus of computational chemistry. Since its implementation in density functional theory^{49–55} and in coupled cluster theory,^{53,56–60} this computational technique has been used to successfully determine the absolute configuration for a variety of molecules.^{54,61,62}

Recently, there has been a considerable focus in this area surrounding the difficulties in calculating the optical rotation of the small, conformationally rigid molecule, (*S*)-methyloxirane.^{57,60,166,206,207} In 2004, coupled cluster and density functional theory calculations of optical rotation for this molecule were computed at 355, 589, and 633 nm, and compared to experimental gas-phase cavity ringdown polarimetry values.⁵⁷ The results of this study showed that B3LYP values of $[\alpha]_{355}$ agreed reasonably well with the experimental, while CCSD predicted qualitatively incorrect results. The success of the B3LYP method was attributed to density functional theory's underestimation of the lowest excitation energy of (*S*)-methyloxirane which causes a fortuitous shift in the computed rotation. Kongsted *et al.* reported coupled cluster specific rotations, including those computed with the highly correlated CC3 method.⁶⁰ Still, they were unable to predict the correct sign of the gas-phase experimental rotation, and attributed this failure to significant vibrational effects which are not taken into account in their *ab initio* calculations.

Ruud and Zanasi focused on the importance of molecular vibrations to the calculation of optical

rotation in their 2005 study of (*S*)-methyloxirane.¹⁶⁶ At 355 nm, they presented B3LYP zero-point vibrational corrections of 18.6 and 48.1 deg dm⁻¹ (g/mL)⁻¹ using the aug-cc-pVDZ and aug-cc-pVTZ basis sets, respectively, which led to a vibrationally averaged optical rotation that correctly predicted the sign of the experimental value. The most recent study on the optical rotation of this molecule was presented by Kongsted *et al.* in which coupled cluster and density functional theory vibrational contributions were addressed at 355, 589, and 633 nm.²⁰⁷ They showed that there is a large dependence of optical rotation on the torsional motion of the methyl group and that at 355 nm, zero-point vibrational corrections substantially improve the CCSD results,⁶⁰ predicting the correct sign of rotation for (*S*)-methyloxirane and a magnitude which agrees remarkably well with experiment.

Although the story of methyloxirane is a great testament to the difficulties surrounding the calculations of optical rotation, the focus has only surrounded this particular molecule. It has yet to be determined whether other molecules behave in the same manner. (*R*)-methylthiirane is a great test case for investigation of this. It is a small, rigid molecule, similar in structure to methyloxirane, but there has been little focus on its theoretical specific rotation. In 2005, Wilson *et al.* experimentally determined the specific rotation of (*R*)-methylthiirane in the gas phase using the ultrasensitive cavity ring-down polarimetry method.¹⁷⁵ They reported an $[\alpha]_{355}$ and $[\alpha]_{633}$ of 64.7 ± 2.3 deg dm⁻¹ (g/mL)⁻¹ and 36.5 ± 1.7 deg dm⁻¹ (g/mL)⁻¹, respectively. They also determined a 48.79 deg dm⁻¹ (g/mL)⁻¹ rotation in neat liquid at 589 nm. The circular dichroism spectrum of this molecule was studied experimentally,²⁰⁸ and theoretically with multireference configuration interaction²⁰⁹ in 1994, but since then, this molecule has received little attention. Because of the shortage of high level calculations of optical rotation for (*R*)-methylthiirane, we

have computed these values using coupled cluster and density functional theory. The purpose of this work is to address the case of methylthiirane and compare our results for this molecule with those previously discussed for (*S*)-methyloxirane.^{57,60,166,206,207} It is particularly interesting to see whether the effects of molecular vibrations are as apparent for methylthiirane as it was for methyloxirane, and also to assess the effects that sulfur may have on the computed rotation.

7.2 Computational Details

Rosenfeld set the foundation for computing optical rotation when he showed that at a non-absorbing frequency, the angle of rotation, $[\alpha]_\omega$, can be computed using the β tensor:⁸⁵

$$\beta(\omega) = \frac{2}{\hbar} \text{Im} \sum_{n \neq 0} \frac{\langle 0 | \boldsymbol{\mu} | n \rangle \langle n | \mathbf{m} | 0 \rangle}{\omega_{n0}^2 - \omega^2} \quad (7.1)$$

where ω is the frequency of plane-polarized light, $\boldsymbol{\mu}$ and \mathbf{m} represent the electric and magnetic dipole operators, respectively, and the summation runs over the excited electronic (unperturbed) wave functions. For this research, the β tensor was implemented using the coupled cluster singles and doubles (CCSD) linear response theory.^{57,193} CCSD specific rotations for (*R*)-methylthiirane were computed, along with time-dependent density functional theory (B3LYP)^{36,194,195} values using gauge invariant atomic orbitals (GIAOs).^{49,52,55,82} Optical rotation calculations were carried out at 355, 589, and 633 nm wavelengths, using the following basis sets: (1) the split valence basis set 6-311++G(2d,2p)¹⁷⁷ and (2) the correlation consistent basis sets: aug-cc-pVDZ, d-aug-cc-pVDZ, aug-cc-pVTZ, d-aug-cc-pVTZ, aug-cc-pVQZ, and d-aug-cc-pVQZ..^{106,196,197} In order to account for the errors in the standard correlation consistent basis sets for sulfur, the aug-cc-pV(D+d)Z, d-aug-cc-pV(D+d)Z, aug-cc-pV(T+d)Z, d-aug-cc-pV(T+d)Z, and aug-cc-pV(Q+d)Z were also used

to compute the optical rotation. These basis sets contain high exponent functions in addition to the standard correlation consistent basis functions which allow for a reduction in basis set error. The coupled cluster optical rotation calculations used both the length gauge (using the center of mass as the origin) and the modified-velocity gauge (independent of origin) for the electric dipole operator.⁵⁸

The optimized structure of (*R*)-methylthiirane was identified using density functional theory, with the B3LYP functional^{36,194,195} and Dunning's correlation-consistent cc-pVTZ basis set.¹⁰⁶ Vertical electronic transition energies were computed using the EOM-CCSD¹²⁴ and TD-DFT/B3LYP^{75,76} methods. All electrons were correlated for the geometry calculations, while core electrons (1s for C and S) were frozen for excitation energies and CCSD optical rotation calculations (except for the CCSD/aug-cc-pVTZ and CCSD/aug-cc-pV(T+d)Z optical rotation calculations where the core electrons, 1s for C and 1s2s2p for S, were frozed due to memory constraints). All calculations were carried out using the B3LYP/cc-pVTZ optimized structure of (*R*)-enantiomer for methylthiirane. Gaussian03²⁰⁵ was used for the B3LYP optimized geometry, TD-DFT/B3LYP excitation energies, and B3LYP optical rotation calculations. All EOM/CCSD excitation energies, and CCSD optical rotation calculations were performed using the PSI3 program package.¹²⁷

7.3 Results and Discussion

Fig 7.1 gives the B3LYP/cc-pVTZ optimized geometry of (*R*)- methylthiirane. In Table 7.1, we report the B3LYP and CCSD specific rotations in $\text{deg dm}^{-1} (\text{g/mL})^{-1}$ computed with various basis sets at 355, 589, and 633 nm. From this data, we see that there is a tremendous amount

of basis set dependence at all levels of theory, but especially for the B3LYP method. At 355 nm, the most sensitive wavelength, the B3LYP values vary by $23 \text{ deg dm}^{-1} (\text{g/mL})^{-1}$, when using the aug-cc-pVDZ and aug-cc-pV(D+d)Z basis sets, indicating that the five extra diffuse functions for sulfur have a significant effect on the computed rotation. There is an even larger variation in $[\alpha]_{355}$ when comparing the B3LYP values for aug-cc-pVDZ and d-aug-cc-pVDZ. The doubly augmented functions added in the bigger basis set, account for an approximate $100 \text{ deg dm}^{-1} (\text{g/mL})^{-1}$ shift. At 355 nm, the B3LYP method only seems to converge when the incredibly large basis sets, aug-cc-pVQZ (600 basis functions) and d-aug-cc-pVQZ (771 basis functions) are used. At 589 and 633 nm, the basis set dependence is not as emphasized, the +d functions for sulfur are negligible where the variation between aug-cc-pTZ and aug-cc-pV(T+d)Z is approximately $1 \text{ deg dm}^{-1} (\text{g/mL})^{-1}$. Also, there is a more rapid basis set convergence at these two wavelengths.

Both CCSD length gauge and CCSD modified-velocity gauge specific rotations also show the extreme basis set dependence that was seen with B3LYP, especially at 355 nm. For the length gauge variant, there is a $92 \text{ deg dm}^{-1} (\text{g/mL})^{-1}$ difference between the aug-cc-pVDZ and d-aug-cc-pVDZ basis sets. The effect of the +d basis functions for sulfur is not as pronounced for the CCSD method, as it was for B3LYP. At 355 nm, the difference between the aug-cc-pVDZ and aug-cc-pV(D+d)Z basis sets is $14 \text{ deg dm}^{-1} (\text{g/mL})^{-1}$ for CCSD length gauge and $18 \text{ deg dm}^{-1} (\text{g/mL})^{-1}$ for CCSD modified-velocity gauge. As the wavelength increases, the variation between these two basis sets decreases dramatically for both CCSD variants. With the exception of Pople's split-valence basis set, both CCSD length and modified-velocity gauge predict similar values of $[\alpha]_{\lambda}$ when the same basis set is used. It is also interesting to note that at 589 nm and 633 nm, both CCSD variants are consistently predicting specific rotations that are larger than those of B3LYP.

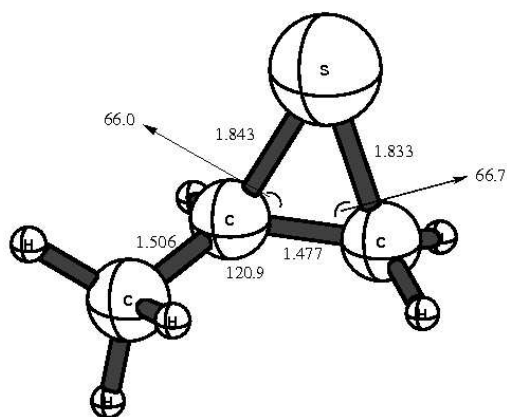


Figure 7.1: Optimized geometry of (*R*)-methylthiirane at the B3LYP/cc-pVTZ level of theory. Bond lengths are given in Å and bond angles in degrees.

This is not the case at 355 nm; the B3LYP and CCSD methods predict opposite signs for $[\alpha]_{\lambda}$ for (*R*)-methylthiirane.

At 355 nm, the experimental CRDP gas phase result is $64.7 \pm 2.3 \text{ deg dm}^{-1} (\text{g/mL})^{-1}$ for (*R*)-methylthiirane. The best theoretical comparison is with the CCSD length gauge result (using the aug-cc-pV(T+d)Z basis set), which is underestimating the gas phase value by just $3 \text{ deg dm}^{-1} (\text{g/mL})^{-1}$. The B3LYP method fails to predict the correct sign of $[\alpha]_{355}$ with all basis sets. In this case, the predicted B3LYP specific rotation underestimates the experimental value by about a factor of three. Also, as the size of the basis set grows, B3LYP predicts values which are increasingly overestimated in magnitude. The largest B3LYP calculation was computed with the d-aug-cc-pVQZ (771 basis functions) and gave a $[\alpha]_{355}$ of $-158.9 \text{ deg dm}^{-1} (\text{g/mL})^{-1}$, a result that is incorrect in sign and overestimated by a factor of 2.5.

For the 633 nm results, again we see that both CCSD variants are predicting the specific rotation of (*R*)-methylthiirane remarkable well, giving results that are only slightly off of the experimental value when using the the d-aug-cc-pVDZ and aug-cc-pVTZ basis sets. The aug-cc-pVDZ and aug-cc-pV(D+d)Z basis sets do not seem to contain significant diffuse functions; both CCSD methods predict $[\alpha]_{633}$ s which are overestimated by approximately $20 \text{ deg dm}^{-1} (\text{g/mL})^{-1}$. When using the B3LYP functional, our best comparison with the experimental gas phase data of $36.5 \pm 1.7 \text{ deg dm}^{-1} (\text{g/mL})^{-1}$, is a specific rotation of $45.4 \text{ deg dm}^{-1} (\text{g/mL})^{-1}$, computed with the aug-cc-pVDZ basis set. For this wavelength, B3LYP is able to correctly predict the sign of the rotation, but as the size of the basis set increases, there is a larger deviation from the experimental value.

At 589 nm, there is no gas phase experimental data, but in neat liquid, the $[\alpha]_D$ is $48.79 \text{ deg dm}^{-1} (\text{g/mL})^{-1}$. Although comparison between theory and experiment is unfair at this wavelength,

Table 7.1: Specific Rotations (in deg/[dm (g/cm³)]) for (*R*)-Methylthiirane at 355, 589, and 633 nm.

basis set	B3LYP			CCSD (length)			CCSD (velocity)		
	355	589	633	355	589	633	355	589	633
6-311++G(2d,2p)	-73.0	49.8	44.7	119.1	65.2	56.8	153.1	76.3	66.4
aug-cc-pVDZ	-57.0	50.7	45.4	139.1	67.3	58.4	138.9	68.3	59.3
aug-cc-pV(D+d)Z	-80.4	49.0	44.1	125.6	64.5	56.1	120.3	63.9	55.6
d-aug-cc-pVDZ	-158.8	19.5	18.8	47.0	39.0	34.3	48.4	39.2	34.4
d-aug-cc-pV(D+d)Z	-183.3	17.6	17.3	32.8	36.0	31.7	30.0	34.8	30.7
aug-cc-pVTZ	-140.8	25.5	23.9	77.6	45.3	39.4	90.2	48.4	42.1
aug-cc-pV(T+d)Z	-157.0	24.4	23.0	68.0	43.4	37.9	80.5	46.1	40.2
d-aug-cc-pVTZ	-149.8	24.3	22.9	-	-	-	-	-	-
d-aug-cc-pV(T+d)Z	-166.5	23.0	22.0	-	-	-	-	-	-
aug-cc-pVQZ	-160.5	21.7	20.8	-	-	-	-	-	-
aug-cc-pV(Q+d)Z	-170.5	21.0	20.2	-	-	-	-	-	-
d-aug-cc-pVQZ	-158.9	22.7	21.7	-	-	-	-	-	-

it is interesting to note that the B3LYP method correctly predicts this value when using the 6-311++G(2d,2p), aug-cc-pVDZ, and aug-cc-pV(D+d)Z basis sets. On the other hand, both CCSD length and modified-velocity gauge methods do good jobs predicting the $[\alpha]_D$ with only the aug-cc-pVTZ and aug-cc-pV(T+d)Z basis sets.

It has been previously shown with many chiral molecules that B3LYP usually predicts specific rotations that are much larger in magnitude than those of coupled cluster theory.^{57,59,191} This trend, which is not seen with (*R*)-methylthiirane, has been attributed to B3LYP's poor ability to accurately calculate excitation energies which are inherently related to the calculation of optical rotation (Equ. 7.1). The TD-DFT and EOM-CCSD vertical excitation energy for the lowest-lying excited state for (*R*)-methylthiirane are reported in Table 7.2. There is little variation for each method with regard to basis set, but there are dramatic differences between the two methods. B3LYP/TD-DFT predicts excitations which are significantly lower than those of EOM-CCSD by more than 0.5 eV. The experimentally determined excitation energy is 5.85 eV (212.1 nm),²⁰⁸ which coincides extremely well with our EOM-CCSD calculations. Since B3LYP predicts vertical excitation energies which are underestimated, we would expect an inherent increase in $[\alpha]_\lambda$, which is surprisingly not seen in this case.

7.4 Conclusions

In this study, we have reported CC and DFT theoretical values of optical rotation for (*R*)-methylthiirane, computed with various basis sets at 355, 589, and 633 nm. All methods show significant basis set dependence, especially at 355 nm. Coupled cluster theory predicts similar

Table 7.2: EOM-CCSD and B3LYP-TDDFT excitation energies for (*R*)-methylthiirane computed with various basis sets at the B3LYP/cc-pVTZ optimized geometry.

	6-311++G(2d,2p)		aug-cc-pVDZ		aug-cc-pV(D+d)Z	
	eV	nm	eV	nm	eV	nm
EOM-CCSD	5.88	211	5.83	213	5.85	212
TD-DFT	5.29	234	5.27	235	5.26	236

rotations when using the length and modified-velocity gauges, and these $[\alpha]_{\lambda}$ s are larger in magnitude than those of B3LYP. At 355 nm, B3LYP fails to predict the correct sign of rotation and significantly overestimates the experimental value. Coupled cluster theory does a better job, but still underestimates by approximately 24% when the d-aug-cc-pVDZ basis set is used. With the aug-cc-pV(T+d)Z basis set, coupled cluster length gauge values match spot on with the experimental results. At 633 nm, both variants of coupled cluster theory do a remarkable job predicting the specific rotation, giving values which agree superbly with gas-phase results, while B3LYP significantly underestimates the observed optical rotation with most basis sets.

Chapter 8

Conclusions

8.1 General Comments

Coupled cluster and density functional theory calculations of optical rotation have been presented for five small chiral molecules including (*S*)-methyloxirane, (*R*)-epichlorohydrin, (*R*)-3-chloro-1-butene, (*R*)-2-chlorobutane, and (*R*)-methylthiirane. These calculations have been carried out using either the coupled cluster linear response formalism with both the length- and velocity- gauge, or with time-dependent density functional theory. Our predicted results have been compared to published ultrasensitive gas-phase cavity ringdown polarimetry data.

8.2 (*S*)-Methyloxirane

Theoretical optical rotation calculations, $[\alpha]_{\lambda}$, have been carried out for the difficult case of (*S*)-methyloxirane for comparison to recently published gas-phase cavity ring-down polarimetry data. Both coupled cluster and density functional theoretical methods are exquisitely sensitive to the choice of one-electron basis set, and diffuse functions have a particularly large impact on the computed values of $[\alpha]_{\lambda}$. Furthermore, both methods show a surprising sensitivity to the choice of optimized geometry, with $[\alpha]_{355}$ values varying by as much as $15 \text{ deg dm}^{-1} (\text{g/mL})^{-1}$ among molecular structures that differ only negligibly. Although at first glance the DFT/B3LYP values of $[\alpha]_{355}$ appear to be superior to those from CC theory, the success of DFT in this case appears to stem from a significant underestimation of the lowest (Rydberg) excitation energy in methyloxirane, resulting in a shift of the first-order pole in $[\alpha]_{\lambda}$ (the Cotton effect) towards the experimentally chosen incident radiation lines. This leads to a fortuitous positive shift in the value of $[\alpha]_{355}$ towards the experimental result. The coupled cluster singles and doubles (CCSD) model, on the other hand, correctly predicts the position of the absorption pole (to within 0.05 eV of the experimental result), but fails to describe correctly the shape/curvature of the ORD region $\lambda = 355$, resulting in an incorrect prediction of both the magnitude and the *sign* of the optical rotation.

8.3 (*R*)-Epichlorohydrin

Ab initio optical rotation data from linear-response coupled cluster and density-functional methods were compared to both gas-phase and liquid-phase polarimetry data for the small, conformationally flexible molecule epichlorohydrin. Three energy minima exist along the C–C–C–Cl

dihedral angle, each with strong, antagonistic specific rotations ranging from *ca.* -450 to +500 deg dm⁻¹ (g/mL)⁻¹ at 355 nm. Density-functional theory (specifically the B3LYP functional) consistently overestimates the optical rotations of each conformer relative to coupled cluster theory (in agreement with our earlier observations for conformationally rigid species), and we attribute this to density-functional theory's underestimation of the lowest-lying excitation energies of epichlorohydrin. Length- and velocity-gauge formulations of the coupled cluster response function lead to slightly different specific rotations (*ca.* 7% at short wavelengths). We have determined well-converged Gibbs free energy differences among the conformers using complete-basis-set extrapolations of coupled cluster energies including triple excitations in order to obtain Boltzmann-averaged specific rotations for comparison to the gas-phase results. The length-gauge coupled cluster data agree remarkably well with experiment, with the velocity-gauge coupled-cluster and density-functional data bracketing the experimental results from below and above, respectively. Liquid-phase conformer populations reported earlier by Polavarapu and co-workers from combined infrared absorption and theoretical analyses differ markedly from the gas-phase populations, particularly for polar solvents. Nevertheless, Boltzmann-averaged specific rotations from both coupled cluster and density-functional calculations agree well with the corresponding experimental intrinsic rotations, in spite of the fact that the theoretical specific rotations for the individual conformers do not take solvent effects into account. PCM-based estimates of conformer populations lead to poor agreement with experiment.

8.4 (*R*)-3-chloro-1-butene and (*R*)-2-chlorobutane

Coupled cluster (CC) and density functional theory (B3LYP) optical rotation calculations have been carried out for two structurally similar conformationally flexible molecules, (*R*)-3-chloro-1-butene and (*R*)-2-chlorobutane. Since previously published data indicate that the specific rotations for both molecules are largely dependent on the dihedral angle of the carbon chain, an effort has been made to assess the conformational effects on optical rotation. The difference in free energy between the conformations of each molecule was investigated using several high level theories, including G2 and G3 methods, and coupled cluster energies extrapolated to the complete basis set limit. Averaged rotations have been compared to experimental gas-phase cavity ring-down polarimetry values. Our results indicate that even though the two molecules are structurally similar, they produce drastically different specific rotations. Of the methods used, the CCSD modified velocity gauge variant does the best job predicting the $[\alpha]_D$ for (*R*)-3-chloro-1-butene, while the B3LYP method fails to predict comparable results with that of experiment, overestimating by 80% and 61%, for 355 nm and 633 nm. Although the trends with regard to basis set and method for (*R*)-2-chlorobutane are similar to those of (*R*)-3-chloro-1-butene, each method is able to predict values which are comparable to those of gas-phase data. For 2-chlorobutane, the CCSD length gauge $[\alpha]_{\lambda S}$ compare extremely well with experimental gas-phase values, while the B3LYP method overestimates by no more than 9% for each wavelength. These results indicate that since B3LYP does a terrible job predicting the specific rotation for (*R*)-3-chloro-1-butene, but yet compares well for the case of (*R*)-2-chlorobutane, the success of this method can only be contributed to a cancellation of errors and is unreliable.

8.5 (*R*)-Methylthiirane

Because of the recent popularity surrounding the difficulties in calculating the optical rotation of (*S*)-methyloxirane, (*R*)-methylthiirane, a small, rigid molecule, similar in structure to the oxirane is studied using coupled cluster (CC) and density functional theory (DFT/B3LYP). Theoretical specific rotation values have been compared with recently published gas-phase cavity ringdown polarimetry experimental data. Both DFT and CC theory are extremely dependent on choice of basis set, especially at 355 nm. For this most sensitive wavelength, the B3LYP method only seems to converge when incredibly large basis sets, such as aug-cc-pVQZ and d-aug-cc-pVQZ are used. Although the results at 589 nm and 633 nm are dependent on basis set, the effects are not as pronounced. Surprisingly, both CCSD length and modified-velocity gauge variants predict similar specific rotations, which are larger in magnitude larger than those of B3LYP. At 355 nm, B3LYP is unable to predict the correct sign of the rotation and significantly underestimates the experimental value by a factor of three, while the CCSD length gauge method is only $3 \text{ deg dm}^{-1} (\text{g/mL})^{-1}$ higher than the gas-phase value. At 633 nm, CCSD/d-aug-cc-pVDZ calculations compare extremely well with experiment, while B3LYP with the same basis set underestimates by $9 \text{ deg dm}^{-1} (\text{g/mL})^{-1}$.

8.6 Concluding Remarks

Ab initio calculations of optical rotation provide a route for the assignment of the absolute configuration of chiral systems. For this technique to be reliable, the calculated result must correctly predict both the sign and magnitude of the specific rotation. The research presented here focused on this particular point. By benchmarking the optical rotation of several small chiral molecules,

our overall results indicate that theoretical specific rotations are highly dependent on the method used for computation along with gauge selection, and the choice of optimized geometry and basis set. We have shown that there is a large difference between coupled cluster specific rotations and density functional theory's counterparts, with the latter predicting magnitudes that are usually larger than the former.

Of the methods used, the coupled cluster length gauge variant predicts results that are in good agreement for most of the molecules studied. The velocity gauge variant predicts values which are slightly underestimated relative to the length gauge results. This study shows that the B3LYP method predicts values that are significantly larger than either variant of the coupled cluster method, due to its underestimation of the excited state energies. Although one might be more inclined to use the velocity gauge variant over length gauge because of its origin invariance, even in the limit of a complete basis set, when a truncated form of the coupled cluster method is used, the length gauge variant is not expected to give equivalent results to its velocity gauge counterpart. This arises because of the lack of variational optimization of the underlying molecular orbitals. In the future, the optimized orbital coupled cluster (OCC) approach may be implemented to allow for origin independent results.

The conclusions and trends taken from this research are only based on a small sampling of chiral molecules. Before the ultimate predictive power of *ab initio* determination of optical rotation can be reached, more widespread studies on larger chiral systems must be completed. Also, in some cases where the effects of molecular vibrations on optical rotation are substantial, it may be necessary to account for these vibrational effects in order to achieve qualitative agreement between theory and experiment. With the development of more sophisticated theoretical techniques comes the

possibility of a better understanding of optical rotation and its relationship to molecular structure. Therefore, with continued research, the reliable determination of absolute configuration through theoretical prediction of optical rotation is within reach.

Bibliography

- [1] L. G. Wade, J. *Organic Chemistry, 4th Ed.*; Printice-Hall, Inc., New Jersey, 1999.
- [2] Friedman, L.; Miller, J. G. *Science* **1971**, page 1044.
- [3] Evans, A. M.; Nation, R. L.; Sansom, L. N.; Bochner, F.; Somogyi, A. A. *Biopharm. Drug Dispo.* **1990**, *6*, 507–518.
- [4] Mason, S. F. *Molecular Optical Activity and the Chiral Discriminations*; Cambridge University Press: Cambridge, 1982.
- [5] Barron, L. D. *Molecular Light Scattering and Optical Activity*; Cambridge University Press: Cambridge, U.K., 2nd edition ed., 2004.
- [6] Charney, E. *The Molecular Basis of Optical Activity: Optical Rotatory Dispersion and Circular Dichroism*; John Wiley and Sons: New York, 1979.
- [7] Griffiths, D. J. *Introduction to Electrodynamics, 3rd ed.*; Prentice Hall, New Jersey, 1999.
- [8] Atkins, P. W.; Friedman, R. S. *Molecular Quantum Mechanics, 3rd Edition*; Oxford University Press Inc., New York, 1997.
- [9] Born, M.; Oppenheimer, J. R. *Ann. d. Phys.* **1927**, *84*, 457–484.

- [10] Szasz, L. *Phys. Rev.* **1962**, *126*, 169–181.
- [11] Hartree, D. R. *Proc. Camb. Phil. Soc.* **1928**, *24*, 111–133.
- [12] v. V. Fock. *Physik* **1930**, *61*, 126–148.
- [13] Szabo, A.; Ostlund, N. S. *Modern Quantum Chemistry, Introduction to Advanced Electronic Structure Theory*; Dover Publications, Inc., Mineola, 1996.
- [14] Roothaan, C. C. J. *Rev. Mod. Phys.* **1951**, *23*, 69–69.
- [15] Pople, J. A. *Rev. Mod. Phys.* **1998**, *71*, 1267–1274.
- [16] Bartlett, R. J.; Stanton, J. F. *Reviews in Computational Chemistry, Vol. 5*; VCH Publishers, Inc., New York, 1994.
- [17] Cory, M. G.; Zerner, M. *J. Chem. Phys.* **1999**, *103*, 7287–7293.
- [18] Slater, J. C. *Rev. Mod. Phys.* **1963**, *35*, 484–487.
- [19] Harriss, F. E.; Monkhorst, H.; Freeman, D. L. *Algebraic and Diagrammatic Methods in Many-Fermion Theory*; Oxford University Press, Inc., New York, 1992.
- [20] Čížek, J. *J. Chem. Phys.* **1966**, *45*, 4256–4266.
- [21] Čížek, J. *Adv. Quant. Chem.* **1969**, *14*, 35.
- [22] Crawford, R. D.; Shaefer, H. F. *Reviews in Computational Chemistry, Vol. 14*; Wiley-VCH, John Wiley and Sons, Inc., New York, 2000.
- [23] Corson, E. M. *Phys. Rev.* **1946**, *70*, 728–748.

- [24] Wick, G. C. *Phys. Rev.* **1950**, *80*, 268–272.
- [25] Stanton, J. F.; Gauss, J.; Watts, J. D.; Bartlett, R. J. *J. Chem. Phys.* **1991**, *94*, 4334–4345.
- [26] Kucharski, S. A.; Bartlett, R. J. *J. Chem. Phys.* **1992**, *97*, 4282–4288.
- [27] Kucharski, S. A.; Bartlett, R. J. *Adv. Quant. Chem.* **1986**, *18*, 281–344.
- [28] Kvasnička, V.; Laurinc, V.; Biskupič, S. *Adv. Quant. Chem.* **1983**, *53*, 181–262.
- [29] Stanton, J. F.; Gauss, J. *J. Chem. Phys.* **1995**, *103*, 1064–1076.
- [30] Raghavachari, K.; Trucks, G. W.; Pople, J. A.; Head-Gordon, M. *Chem. Phys. Lett* **1989**, *157*, 479–483.
- [31] Stanton, J. F. *Chem. Phys. Lett.* **1997**, *281*, 130–134.
- [32] Kohn, W. *Rev. Mod. Phys.* **1999**, *71*, 1253–1266.
- [33] Hohenberg, P.; Kohn, W. *Phys. Rev.* **1964**, *136*, B864.
- [34] Kohn, W.; Sham, L. J. *Phys. Rev.* **1965**, *A140*, 1133.
- [35] Jensen, F. *Introduction to Computational Chemistry*; John Wiley & Sons, Inc., New York, 2002.
- [36] Parr, R. G.; Yang, W. *Density-Functional Theory of Atoms and Molecules*; Oxford University Press, New York, 1989.
- [37] Koch, W.; Holthausen, M. C. *A Chemist's Guide to Density Functional Theory*; Wiley-VCH, New York, 2001.

- [38] Cramer, C. J. *Essentials of Computational Chemistry: Theories and Models*; John Wiley & Sons, Inc., New Jersey, 2003.
- [39] Becke, A. D. *Phys. Rev. A* **1988**, *38*, 3098–3100.
- [40] Becke, A. D. *J. Chem. Phys.* **1993**, *98*, 5648–5651.
- [41] Pople, J. A.; Head-Gordon, M.; Fox, D. J.; Raghavachari, K.; Curtiss, L. A. *J. Chem. Phys.* **1989**, *90*(10), 5622.
- [42] Curtiss, L. A.; Jones, C.; Trucks, G. W.; Raghavachari, K.; Pople, J. A. *J. Chem. Phys.* **1990**, *93*(4), 2537.
- [43] Lee, C.; Yang, W.; Parr, R. G. *Phys. Rev. B* **1988**, *37*, 785–789.
- [44] Colle, R.; Salvetti, O. *Theor. Chim. Acta* **1975**, *37*, 329.
- [45] Handy, N. C.; Cohen, A. J. *J. Chem. Phys.* **2002**, *116*, 5411–5418.
- [46] Davidson, E. R.; Feller, D. *Chem. Rev.* **1986**, *86*, 681–696.
- [47] Almlöf, J.; Helgaker, T.; Taylor, P. *J. Phys. Chem.* **1988**, *92*, 3029–3033.
- [48] Dunning, T. H. *J. Chem. Phys.* **1989**, *90*, 1007–1023.
- [49] Cheeseman, J. R.; Frisch, M. J.; Devlin, F. J.; Stephens, P. J. *J. Phys. Chem. A* **2000**, *104*, 1039–1046.
- [50] Grimme, S. *Chem. Phys. Lett.* **2001**, *339*, 380–388.
- [51] Stephens, P. J.; Devlin, F. J.; Cheeseman, J. R.; Frisch, M. J. *J. Phys. Chem. A* **2001**, *105*, 5356–5371.

- [52] Autschbach, J.; Patchkovskii, S.; Ziegler, T.; van Gisbergen, S. J. A.; Baerends, E. J. *J. Chem. Phys.* **2002**, *117*, 581–592.
- [53] Ruud, K.; Helgaker, T. *Chem. Phys. Lett.* **2002**, *352*, 533–539.
- [54] McCann, D. M.; Stephens, P. J.; Cheeseman, J. R. *J. Org. Chem.* **2004**, *69*, 8709–8717.
- [55] Stephens, P. J.; McCann, D. M.; Cheeseman, J. R.; Frisch, M. J. *Chirality* **2005**, *17*, S52–S64.
- [56] Ruud, K.; Stephens, P. J.; Devlin, F. J.; Taylor, P. R.; Cheeseman, J. R.; Frisch, M. J. *Chem. Phys. Lett.* **2003**, *373*, 606–614.
- [57] Tam, M. C.; Russ, N. J.; Crawford, T. D. *J. Chem. Phys.* **2004**, *121*, 3550–3557.
- [58] Pedersen, T. B.; Koch, H.; Boman, L.; de Merás, A. M. *J. S. Chem. Phys. Lett.* **2004**, *393*, 319–326.
- [59] Crawford, T. D.; Owens, L. S.; Tam, M. C.; Schreiner, P. R.; Koch, H. *J. Am. Chem. Soc.* **2005**, *127*, 1368–1369.
- [60] Kongsted, J.; Pedersen, T. B.; Strange, M.; Osted, A.; Hansen, A. E.; Mikkelsen, K. V.; Pawłowski, F.; Jørgensen, P.; Hättig, C. *Chem. Phys. Lett.* **2005**, *401*, 385–392.
- [61] Stephens, P. J.; Devlin, F. J.; Cheeseman, J. R.; Frisch, M. J.; Rosini, C. *Org. Lett.* **2002**, *4*, 4595–4598.
- [62] Giorgio, E.; Viglione, R. G.; Zanasi, R.; Rosini, C. *J. Am. Chem. Soc.* **2004**, *126*, 12968–12976.
- [63] Amos, R. D. *Chem. Phys. Lett.* **1982**, *87*(1), 23–26.

- [64] Polavarapu, P. L. *Mol. Phys.* **1997**, *91*(3), 551–554.
- [65] Polavarapu, P. L.; Chakraborty, D. K. *J. Am. Chem. Soc.* **1998**, *120*, 6160–6164.
- [66] Kondru, R. K.; Wipf, P.; Bertan, D. N. *J. Phys. Chem. A* **1999**, *103*, 6603–6611.
- [67] Caldwell, D. J.; Eyring, H. *The Theory of Optical Activity*; Wiley-Interscience; John Wiley & Sons, Inc., New York, 1971.
- [68] Linderberg, J.; Öhrn, Y. *Propagators in Quantum Chemistry*; Academic Press Inc., London, 1973.
- [69] Jørgensen, P.; Simons, J. *Second Quantization-Based Methods in Quantum Chemistry*; Academic Press, Inc., New York, 1981.
- [70] Koch, H.; Jørgensen, P. *J. Chem. Phys.* **1990**, *93*, 3333–3344.
- [71] Kobayashi, R.; Koch, H.; Jørgensen, P. *Chem. Phys. Lett.* **1994**, *219*, 30–35.
- [72] Christiansen, O.; Jørgensen, P.; Haetiig, C. *Int. J. Quant. Chem.* **1998**, *68*, 1–52.
- [73] Christiansen, O.; Halkier, A.; Koch, H.; Jørgensen, P. *J. Chem. Phys.* **1999**, *108*, 2801–2816.
- [74] Crawford, T. D. *Theor. Chem. Acta* **2006**.
- [75] Jamorski, C.; Casida, M. E.; Salahub, D. R. *J. Chem. Phys.* **1996**, *104*, 5134.
- [76] Bauernschmitt, R.; Ahlrichs, R. *Chem. Phys. Lett.* **1996**, *256*, 454.
- [77] Marques, M. A. L.; Gross, E. K. U. *Annu. Rev. Phys. Chem.* **2004**, *55*, 427–455.
- [78] Diedrich, C.; Kausemann, S.; Grimme, S. *J. Comp. Meth. Sci. Eng.* **2004**, *4*, 1–8.

- [79] Furche, F. *J. Chem. Phys.* **2001**, *114*, 5982–.
- [80] Eliel, E. L.; Wilen, S. H. *Stereochemistry of Organic Compounds*; John Wiley and Sons: New York, 1994.
- [81] Polavarapu, P. L.; Chakraborty, D. K. *Chem. Phys.* **1999**, *240*, 1–8.
- [82] Stephens, P. J.; Devlin, F. J. *Chirality* **2000**, *12*, 172–179.
- [83] Furche, F.; Ahlrichs, R.; Wachsmann, C.; Weber, E.; Sobanski, A.; Vögtle, F.; Grimme, S. *J. Am. Chem. Soc.* **2000**, *122*(8), 1717–1724.
- [84] Stephens, P. J.; Devlin, F. J.; Cheeseman, J. R.; Frisch, M. J. *J. Phys. Chem. A* **2001**, *105*(22), 5356–5371.
- [85] Rosenfeld, L. *Z. Physik* **1928**, *52*, 161.
- [86] Pao, Y. H.; Santry, D. P. *J. Am. Chem. Soc.* **1966**, *88*, 4157–.
- [87] Bouman, T. D.; Lightner, D. A. *J. Am. Chem. Soc.* **1976**, *98*, 3145–3154.
- [88] Volosov, A. *Int. J. Quantum Chem.* **1989**, *36*, 473–486.
- [89] Helgaker, T.; Ruud, K.; Bak, K. L.; Jørgensen, P.; Olsen, J. *Faraday Discuss.* **1994**, *99*, 165–180.
- [90] Ruud, K.; Taylor, P. R.; Åstrand, P.-O. *Chem. Phys. Lett.* **2001**, *337*, 217–223.
- [91] Grimme, S. *Chem. Phys. Lett.* **2001**, *339*, 380–388.
- [92] Grimme, S.; Furche, F.; Ahlrichs, R. *Chem. Phys. Lett.* **2002**, *361*, 321–328.

- [93] Pedersen, T. B.; Koch, H.; Ruud, K. *J. Chem. Phys.* **1999**, *110*(6), 2883–2892.
- [94] Kondru, R. K.; Wipf, P.; Beratan, D. N. *Science* **1998**, *282*, 2247–2250.
- [95] Kondru, R. K.; Wipf, P.; Beratan, D. N. *J. Am. Chem. Soc.* **1998**, *120*, 2204–2205.
- [96] Ribe, S.; Kondru, R. K.; Beratan, D. N.; Wipf, P. *J. Am. Chem. Soc.* **2000**, *122*, 4608–4617.
- [97] Perry, T. L.; Dickerson, A.; Kahn, A. A.; Kondru, R. K.; Beratan, D. N.; Wipf, P.; Kelly, M.; Hamann, M. T. *Tetrahedron* **2001**, *57*, 1483–1487.
- [98] Diedrich, C.; Grimme, S. *J. Phys. Chem. A* **2003**, *107*, 2524–2539.
- [99] Wiberg, K. B.; Vaccaro, P. H.; Cheeseman, J. R. *J. Am. Chem. Soc.* **2003**, *125*, 1888–1896.
- [100] Wiberg, K. B.; Wang, Y. G.; Vaccaro, P. H.; Cheeseman, J. R.; Trucks, G.; Frisch, M. J. *J. Phys. Chem. A* **2004**, *108*(1), 32–38.
- [101] Rinderspacher, B. C.; Schreiner, P. R. *J. Phys. Chem. A* **2004**, *108*(15), 2867–2870.
- [102] Müller, T.; Wiberg, K. B.; Vaccaro, P. H. *J. Phys. Chem. A* **2000**, *104*, 5959–5968.
- [103] Müller, T.; Wiberg, K. B.; Vaccaro, P. H.; Cheeseman, J. R.; Frisch, M. J. *J. Opt. Soc. Am. B* **2002**, *19*, 125–141.
- [104] Kumata, Y.; Furukawa, J.; Fueno, T. *Bull. Chem. Soc. Japan* **1970**, *43*(12), 3920–3921.
- [105] Giorgio, E.; Rosini, C.; Viglione, R. G.; Zanasi, R. *Chem. Phys. Lett.* **2003**, *376*, 452–456.
- [106] Dunning, T. H. *J. Chem. Phys.* **1989**, *90*(2), 1007.
- [107] Sadlej, A. J. *Coll. Czech. Chem. Commun.* **1988**, *53*, 1995.

- [108] Sadlej, A. J. *Theor. Chim. Acta* **1991**, *79*, 123–140.
- [109] Cohen, D.; Levi, M.; Basch, H.; Gedanken, A. *J. Am. Chem. Soc.* **1983**, *105*, 1738–1742.
- [110] Crawford, T. D.; Schaefer, H. F. In *Reviews in Computational Chemistry*; Lipkowitz, K. B., Boyd, D. B., Eds., Vol. 14; VCH Publishers: New York, 2000; chapter 2, pages 33–136.
- [111] Bartlett, R. J. In *Modern Electronic Structure Theory*; Yarkony, D. R., Ed., Vol. 2 of *Advanced Series in Physical Chemistry*; World Scientific: Singapore, 1995; chapter 16, pages 1047–1131.
- [112] Lee, T. J.; Scuseria, G. E. In *Quantum Mechanical Electronic Structure Calculations with Chemical Accuracy*; Langhoff, S. R., Ed.; Kluwer Academic Publishers: Dordrecht, 1995; pages 47–108.
- [113] Gauss, J. In *Encyclopedia of Computational Chemistry*; Schleyer, P., Allinger, N. L., Clark, T., Gasteiger, J., Kollman, P. A., Schaefer III, H. F., Schreiner, P. R., Eds.; John Wiley and Sons: Chichester, 1998; pages 615–636.
- [114] Monkhorst, H. J. *Int. J. Quantum Chem., Symp.* **1977**, *11*, 421–432.
- [115] Koch, H.; Jørgensen, P. *J. Chem. Phys.* **1990**, *93*(5), 3333–3344.
- [116] Olsen, J.; Jørgensen, P. In *Modern Electronic Structure Theory*; Yarkony, D., Ed., Vol. 2 of *Advanced Series in Physical Chemistry*; World Scientific: Singapore, 1995; chapter 13, pages 857–990.
- [117] Christiansen, O.; Jørgensen, P.; Hättig, C. *Int. J. Quantum Chem.* **1998**, *68*, 1–52.
- [118] Christiansen, O.; Halkier, A.; Koch, H.; Jørgensen, P.; Helgaker, T. *J. Chem. Phys.* **1998**, *108*(7), 2801–2816.

- [119] Adamowicz, L.; Laidig, W. D.; Bartlett, R. J. *Int. J. Quantum Chem. Symp.* **1984**, *18*, 245.
- [120] Fitzgerald, G.; Harrison, R.; Laidig, W. D.; Bartlett, R. J. *Chem. Phys. Lett.* **1985**, *117*(5), 433.
- [121] Bartlett, R. J. In *Geometrical Derivatives of Energy Surfaces and Molecular Properties*; Jørgensen, P., Simons, J., Eds.; D. Reidel: Dordrecht, 1986; pages 35–61.
- [122] Scheiner, A. C.; Scuseria, G. E.; Rice, J. E.; Lee, T. J.; Schaefer, H. F. *J. Chem. Phys.* **1987**, *87*(9), 5361.
- [123] Gauss, J.; Lauderdale, W. J.; Stanton, J. F.; Watts, J. D.; Bartlett, R. J. *Chem. Phys. Lett.* **1991**, *182*(3,4), 207.
- [124] Stanton, J. F.; Bartlett, R. J. *J. Chem. Phys.* **1993**, *98*(9), 7029.
- [125] Purvis, G. D.; Bartlett, R. J. *J. Chem. Phys.* **1982**, *76*, 1910–1918.
- [126] Rittby, M.; Bartlett, R. J. *J. Phys. Chem.* **1988**, *92*, 3033.
- [127] Psi 3.2. Crawford, T. D.; Sherrill, C. D.; Valeev, E. F.; Fermann, J. T.; King, R. A.; Leininger, M. L.; Brown, S. T.; Janssen, C. L.; Seidl, E. T.; Kenny, J. P.; Allen, W. D. **2003**.
- [128] Stanton, J. F.; Gauss, J.; Watts, J. D.; Bartlett, R. J. *J. Chem. Phys.* **1991**, *94*(6), 4334.
- [129] Gauss, J.; Stanton, J. F.; Bartlett, R. J. *J. Chem. Phys.* **1991**, *95*(4), 2623.
- [130] Pedersen, T. B.; Koch, H. *Chem. Phys. Lett.* **1998**, *293*, 251–260.
- [131] Pedersen, T. B.; Koch, H.; Hättig, C. *J. Chem. Phys.* **1999**, *110*(17), 8318–8327.
- [132] Pedersen, T. B.; Fernández, B.; Koch, H. *J. Chem. Phys.* **2001**, *114*(16), 6983–6993.

- [133] London, F. *J. Phys. Radium* **1937**, *8*, 397.
- [134] Ditchfield, R. *Mol. Phys.* **1974**, *27*(4), 789–807.
- [135] Helgaker, T.; Jørgensen, P. *J. Chem. Phys.* **1991**, *95*(4), 2595–2601.
- [136] Helgaker, T.; Taylor, P. R. In *Modern Electronic Structure Theory*; Yarkony, D., Ed., Vol. 2 of *Advanced Series in Physical Chemistry*; World Scientific: Singapore, 1995; chapter 12, pages 725–856.
- [137] Parr, R. G.; Yang, W. *Density-Functional Theory of Atoms and Molecules*; Oxford University: New York, 1989.
- [138] Lee, C.; Yang, W.; Parr, R. G. *Phys. Rev. B.* **1988**, *37*, 785–789.
- [139] Becke, A. D. *J. Chem. Phys.* **1993**, *98*, 5648–5652.
- [140] Raghavachari, K.; Trucks, G. W.; Pople, J. A.; Head-Gordon, M. *Chem. Phys. Lett.* **1989**, *157*, 479.
- [141] Bartlett, R. J.; Watts, J. D.; Kucharski, S. A.; Noga, J. *Chem. Phys. Lett.* **1990**, *165*, 513; erratum: **167**, 609 (1990).
- [142] Lee, T. J.; Rendell, A. P. *J. Chem. Phys.* **1991**, *94*(9), 6229.
- [143] Scuseria, G. E. *J. Chem. Phys.* **1991**, *94*(1), 442.
- [144] Hariharan, P. C.; Pople, J. A. *Theor. Chim. Acta* **1973**, *28*, 213–222.
- [145] Stanton, J. F.; Gauss, J. In *Recent Advances in Coupled-Cluster Methods*; Bartlett, R. J., Ed.; World Scientific Publishing: Singapore, 1997; pages 49–79.

- [146] Gauss, J.; Stanton, J. F. *Chem. Phys. Lett.* **1997**, *276*, 70.
- [147] Bauernschmitt, R.; Ahlrichs, R. *Chem. Phys. Lett.* **1996**, *256*(4-5), 454–464.
- [148] Jamorski, C.; Casida, M. E.; Salahub, D. R. *J. Chem. Phys.* **1996**, *104*(13), 5134–5147.
- [149] Kendall, R. A.; Dunning, T. H.; Harrison, R. J. *J. Chem. Phys.* **1992**, *96*(9), 6796–6806.
- [150] Woon, D. E.; Dunning, T. H. *J. Chem. Phys.* **1994**, *100*(4), 2975.
- [151] Basis sets were obtained from the Extensible Computational Chemistry Environment Basis Set Database, Version 02/25/04, as developed and distributed by the Molecular Science Computing Facility, Environmental and Molecular Sciences Laboratory which is part of the Pacific Northwest Laboratory, P.O. Box 999, Richland, Washington 99352, USA, and funded by the U.S. Department of Energy. The Pacific Northwest Laboratory is a multi-program laboratory operated by Battelle Memorial Institute for the U.S. Department of Energy under contract DE-AC06-76RLO 1830. Contact Karen Schuchardt for further information.
- [152] GAUSSIAN-03. Frisch, M. J.; Trucks, G. W.; Schlegel, H. B.; Scuseria, G. E.; Robb, M. A.; Cheeseman, J. R.; Montgomery, J. A., Jr.; Vreven, T.; Kudin, K. N.; Burant, J. C.; Millam, J. M.; Iyengar, S. S.; Tomasi, J.; Barone, V.; Mennucci, B.; Cossi, M.; Scalmani, G.; Rega, N.; Petersson, G. A.; Nakatsuji, H.; Hada, M.; Ehara, M.; Toyota, K.; Fukuda, R.; Hasegawa, J.; Ishida, M.; Nakajima, T.; Honda, Y.; Kitao, O.; Nakai, H.; Klene, M.; Li, X.; Knox, J. E.; Hratchian, H. P.; Cross, J. B.; Adamo, C.; Jaramillo, J.; Gomperts, R.; Stratmann, R. E.; Yazyev, O.; Austin, A. J.; Cammi, R.; Pomelli, C.; Ochterski, J. W.; Ayala, P. Y.; Morokuma, K.; Voth, G. A.; Salvador, P.; Dannenberg, J. J.; Zakrzewski, V. G.; Dapprich, S.; Daniels, A. D.; Strain, M. C.; Farkas, O.; Malick, D. K.; Rabuck, A. D.; Raghavachari, K.; Foresman,

- J. B.; Ortiz, J. V.; Cui, Q.; Baboul, A. G.; Clifford, S.; Cioslowski, J.; Stefanov, B. B.; Liu, G.; Liashenko, A.; Piskorz, P.; Komaromi, I.; Martin, R. L.; Fox, D. J.; Keith, T.; Al-Laham, M. A.; Peng, C. Y.; Nanayakkara, A.; Challacombe, M.; Gill, P. M. W.; Johnson, B.; Chen, W.; Wong, M. W.; Gonzalez, C.; Pople, J. A. Gaussian, Inc., Pittsburg, PA U. S. A., **2003**.
- [153] ACES II. Stanton, J. F.; Gauss, J.; Watts, J. D.; Lauderdale, W. J.; Bartlett, R. J. **1993**.
The package also contains modified versions of the MOLECULE Gaussian integral program of J. Almlöf and P. R. Taylor, the ABACUS integral derivative program written by T. U. Helgaker, H. J. Aa. Jensen, P. Jørgensen and P. R. Taylor, and the PROPS property evaluation integral code of P. R. Taylor.
- [154] Creswell, R. A.; Schwendeman, R. H. *J. Mol. Spectrosc.* **1977**, *64*, 295.
- [155] Crawford, T. D.; Stanton, J. F.; Allen, W. D.; Schaefer, H. F. *J. Chem. Phys.* **1997**, *107*(24), 10626.
- [156] Stanton, J. F. *J. Chem. Phys.* **2001**, *115*(22), 10382–10393.
- [157] Russ, N. J.; Crawford, T. D. *J. Chem. Phys.* **2004**, *120*, 7298–7306.
- [158] Crawford, T. D. *Theor. Chem. Acc.* **2005**; in press.
- [159] Autschbach, J.; Patchkovskii, S.; Ziegler, T.; van Gisbergen, S.; Baerends, E. J. *J. Chem. Phys.* **2002**, *117*(2), 581–592.
- [160] Tam, M. C.; Russ, N. J.; Crawford, T. D. *J. Chem. Phys.* **2004**, *121*, 3550–3557.
- [161] Pedersen, T. B.; Koch, H.; Boman, L.; de Meras, A. M. *J. S. Chem. Phys. Lett.* **2004**, *393*(4-6), 319–326.

- [162] Crawford, T. D.; Owens, L. S.; Tam, M. C.; Schreiner, P. R.; Koch, H. *J. Am. Chem. Soc.* **2005**, *127*, 1368–1369.
- [163] Kongsted, J.; Pedersen, T. B.; Strange, M.; Osted, A.; Hansen, A. E.; Mikkelsen, K. V.; Pawlowski, F.; Jørgensen, P.; Hättig, C. *Chem. Phys. Lett.* **2005**, *401*, 385–392.
- [164] Polavarapu, P. L. *Chirality* **2002**, *14*, 768–781.
- [165] Stephens, P. J.; Devlin, F. J.; Cheeseman, J. R.; Drisch, M. J.; Bortolini, O.; Besse, P. *Chirality* **2003**, *15*, S57–S64.
- [166] Ruud, K.; Zanasi, R. *Angew. Chem. Int. Ed. Engl.* **2005**, *44*(23), 3594–3596.
- [167] Kongsted, J.; Pedersen, T. B.; Jensen, L.; Hansen, A. E.; Mikkelsen, K. V. *J. Phys. Chem. A* **2005**; submitted.
- [168] Mort, B. C.; Autschbach, J. *J. Phys. Chem. A* **2005**, *109*(38), 8617–8623.
- [169] Wiberg, K. B.; Wang, Y.-G.; Vaccaro, P. H.; Cheeseman, J. R.; Luderer, M. R. *J. Phys. Chem. A* **2005**, *109*(15), 3405–3410.
- [170] Polavarapu, P. L.; Petrovic, A.; Wang, F. *Chirality* **2003**, *15*, S143–S149.
- [171] Pecul, M.; Ruud, K.; Rizzo, A.; Helgaker, T. *J. Phys. Chem. A* **2004**, *108*, 4269–4276.
- [172] Marchesan, D.; Coriani, S.; Forzato, C.; Nitti, P.; Pitacco, G.; Rudd, K. *J. Phys. Chem. A* **2005**, *109*, 1449–1453.
- [173] Wang, F.; Polavarapu, P. L. *J. Phys. Chem. A* **2000**, *104*, 6189–6196.

- [174] Wiberg, K. B.; Wang, Y.; Wilson, S. M.; Vaccaro, P. H.; Cheeseman, J. R. *J. Phys. Chem. A* **2005**, *109*(15), 3448–3453.
- [175] Wilson, S. M.; Wiberg, K. B.; Cheeseman, J. R.; Frisch, M. J.; Vaccaro, P. H. *J. Phys. Chem. A* **2005**, *109*(51), 11752–11764.
- [176] Caldwell, D. J.; Eyring, H. *The Theory of Optical Activity*; Wiley: New York, 1971.
- [177] Pople, J. A. In *Energy, Structure, and Reactivity*; Smith, D. W., McRae, W. B., Eds.; John Wiley: New York, 1973; pages 51–61.
- [178] Woon, D. E.; Dunning, T. H. *J. Chem. Phys.* **1993**, *98*(2), 1358.
- [179] Curtiss, L. A.; Raghavachari, K.; Trucks, G. W.; Pople, J. A. *J. Chem. Phys.* **1991**, *94*(11), 7221.
- [180] Curtiss, L. A.; Raghavachari, K.; Pople, J. A. *J. Chem. Phys.* **1995**, *103*(10), 4192.
- [181] Curtiss, L. A.; Raghavachari, K.; Redfern, P. C.; Rassolov, V.; Pople, J. A. *J. Chem. Phys.* **1998**, *109*, 7764–7776.
- [182] Curtiss, L. A.; Raghavachari, K. *Theor. Chem. Acc.* **2002**, *108*, 61–70.
- [183] Feller, D. *J. Chem. Phys.* **1992**, *96*(8), 6104.
- [184] Halkier, A.; Helgaker, T.; Jørgensen, P.; Klopper, W.; Koch, H.; Olsen, J.; Wilson, A. K. *Chem. Phys. Lett.* **1998**, *286*(3-4), 243.
- [185] McQuarrie, D. A. *Statistical Thermodynamics*; University Science Books: Mill Valley, California, 1973.

- [186] Tomasi, J.; Cammi, R.; Mennucci, B.; Cappelli, C.; Corni, S. *Phys. Chem. Chem. Phys.* **2002**, *4*, 5697–5712.
- [187] Casida, M. E.; World Scientific: Singapore, 1995; Vol. 1.
- [188] Basil, A.; Ben-Tzur, S.; Gedanken, A.; Rodger, A. *Chem. Phys. Lett.* **1991**, *180*, 482–484.
- [189] Wiberg, K. B.; Vaccaro, P. H.; Cheeseman, J. R. *J. Am. Chem. Soc.* **2003**, *125*, 1888–1896.
- [190] Wiberg, K. B.; Wang, Y.; Vaccaro, P. H.; Cheeseman, J. R.; Luderer, M. R. *J. Phys. Chem. A* **2005**, *109*, 3405–3410.
- [191] Tam, M. C.; Crawford, T. D. *J. Phys. Chem. A* **2006**, *100*, 2290–2298.
- [192] Müller, T.; Wiberg, K. B.; Vaccaro, P. H. *J. Phys. Chem. A* **2000**, *104*, 5959–5968.
- [193] Koch, H.; Jørgensen, P. *J. Chem. Phys.* **1990**, *93*, 3333–3344.
- [194] Lee, C.; Yang, W.; Parr, R. G. *Phys. Rev. B* **1988**, *37*, 785.
- [195] Becke, A. D. *J. Chem. Phys.* **1993**, *98*, 5648.
- [196] Kendall, R. A.; Dunning, T. H. *J. Chem. Phys.* **1992**, *96*, 6796.
- [197] Woon, D. E.; Dunning, T. H. *J. Chem. Phys.* **1994**, *100*, 2975.
- [198] Curtiss, L. A.; Raghavachari, K.; Trucks, G. W.; Pople, J. A. *J. Chem. Phys.* **1991**, *94*, 7221–7230.
- [199] Curtiss, L. A.; Carpenter, J. E.; Raghavachari, K.; Pople, J. A. *J. Chem. Phys.* **1992**, *96*, 9030–9034.

- [200] Curtiss, L. A.; Raghavachari, K.; Pople, J. A. *J. Chem. Phys.* **1995**, *103*, 4192–4200.
- [201] Curtiss, L. A.; Raghavachari, K.; Redfern, P. C.; Rassolov, V.; Pople, J. A. *J. Chem. Phys.* **1998**, *109*, 7764–7776.
- [202] Curtiss, L. A.; Raghavachari, K. *Theor. Chem. Acc.* **2002**, *108*, 61–70.
- [203] Feller, D. *J. Chem. Phys.* **1992**, *96*, 6104–6114.
- [204] Halkier, A.; Helgaker, T.; Jørgensen, P.; Klopper, W.; Koch, H.; Olsen, J.; Wilson, A. K. *Chem. Phys. Lett.* **1998**, *286*, 243.
- [205] GAUSSIAN. Frisch, M. J.; Trucks, G. W.; Schlegel, H. B.; Scuseria, G. E.; Robb, M. A.; Cheeseman, J. R.; Zakrzewski, V. G.; Montgomery, J. A.; Stratmann, R. E.; Burant, J. C.; Dapprich, S.; et al. **2003**.
- [206] Giorgio, E.; Rosini, C.; Viglione, R. G.; Zanasi, R. *Chem. Phys. Lett.* **2003**, *376*, 452–456.
- [207] Kongsted, J.; Pedersen, T. B.; Jensen, L.; Hansen, A. E.; Mikkelsen, K. V. *J. Am. Chem. Soc.* **2006**, *128*, 976–982.
- [208] Breest, A.; Ochmann, P.; Pulm, F.; Godderz, K. H.; Carnell, M.; Hormes, J. *Mol. Phys.* **1994**, *82*, 539–551.
- [209] Carnell, M.; Peyerimhoff, S. D. *Chem. Phys.* **1994**, *183*, 37–44.

Vita

Mary Christina Tam was born on September 9, 1979 to Francis and Margaret Tam, in Cumberland, MD. She was raised with two brothers, Peter and Matthew, in Frostburg, MD. Mary graduated from Bishop Walsh High School in 1997, and attended Frostburg State University from which she received Bachelor of Science degrees in Physics and Chemistry. After graduation, Mary moved to Blacksburg, VA where she continued her studies in physical chemistry under the advisement of Dr. T. Daniel Crawford in pursuit of a Ph.D. Upon completion of her degree, Mary plans to marry Brent Cunningham and live happily ever after.